2017

THE DEFAULT MODE NETWORK AND EXECUTIVE FUNCTION: INFLUENCE OF AGE, WHITE MATTER CONNECTIVITY, AND ALZHEIMER'S PATHOLOGY

Christopher A. Brown
University of Kentucky, cabr237@uky.edu
Author ORCID Identifier:
 https://orcid.org/0000-0003-2057-3976
Digital Object Identifier: https://doi.org/10.13023/ETD.2017.367

THE DEFAULT MODE NETWORK AND EXECUTIVE FUNCTION:
INFLUENCE OF AGE, WHITE MATTER CONNECTIVITY, AND
ALZHEIMER'S PATHOLOGY

_____

DISSERTATION

_____

A dissertation submitted in partial fulfillment of the
requirements for the degree of Doctor of Philosophy in the
College of Medicine at the University of Kentucky

By
Christopher Alan Brown

Lexington, Kentucky

Director: Dr. Brian Gold, Professor of Neuroscience

Lexington, Kentucky

2017

ABSTRACT OF DISSERTATION

THE DEFAULT MODE NETWORK AND EXECUTIVE FUNCTION: INFLUENCE OF AGE, WHITE MATTER CONNECTIVITY, AND ALZHEIMER'S PATHOLOGY

The default mode network (DMN) consists of a set of interconnected brain regions supporting autobiographical memory, our concept of the self, and the internal monologue. These processes must be maintained at all times and consume the highest amount of the brain's energy during its baseline state. However, when faced with an active, externally-directed cognitive task, the DMN shows a small, but significant, decrease in activity. The reduction in DMN activity during the performance of an active, externally-directed task compared to a baseline state is termed task-induced deactivation (TID), which is thought to 'free-up' resources required to respond to external demands. However, older adults show a reduced level of TID in the DMN. Recently, it has begun to be appreciated that this decrease in TID may be associated with poorer cognitive performance, especially during tasks placing high demands on executive function (EF). Diminished DMN TID has not only been associated with increasing age but also with multiple age-related neurobiological correlates such as accumulating Alzheimer's disease (AD) pathology and reductions in white matter (WM) connectivity. However, these biological factors—age, WM connectivity reductions and increasing AD pathology—are themselves related. Based on the literature, we hypothesized that declining WM connectivity may represent a common pathway by which both age and AD pathology contribute to diminished DMN TID. Further, we hypothesized that declines in DMN function and WM connectivity would predict poorer in EF. Three experiments were carried out to test these hypotheses. Experiment 1 tested whether WM connectivity predicted the level of DMN TID during a task requiring a high level of EF. Results from 117 adults (ages 25-83) showed that WM connectivity declined with increasing age, and that this decline in WM connectivity was directly associated with reduced DMN TID during the task. Experiment 2 tested whether declines in WM connectivity explained both age-related and AD pathology-related declines in DMN TID. Results from 29 younger adults and 35 older adults showed that declining WM connectivity was associated with increasing age and AD pathology, and that this decline in WM connectivity was a common pathway for diminished DMN TID associated with either aging or AD pathology. Experiment 3 investigated whether measures of WM connectivity and DMN TID at baseline could predict EF measured using clinically-used tests. Results from 29 older adults from Experiment 2 showed that less DMN TID predicted poorer EF at baseline and diminished WM connectivity at baseline predicted a greater decline in EF after 3 years. Further, WM connectivity explained reductions in EF predicted by baseline AD pathology, as well as further reductions in EF not predicted by baseline AD pathology. Together the results of these studies suggest that WM connectivity is a key pathway for age-related and AD pathology-related patterns of diminished DMN TID

associated with poorer EF. Further, WM connectivity may represent a potential therapeutic target for interventions attempting to prevent future declines in EF occurring in aging and AD.

Christopher Brown

06/05/2017
Date

THE DEFAULT MODE NETWORK AND EXECUTIVE FUNCTION:
INFLUENCE OF AGE, WHITE MATTER CONNECTIVITY,
AND ALZHEIMER'S PATHOLOGY

By

Christopher Alan Brown

<div align="right">

Brian Gold
Director of Dissertation

Wayne Cass
Director of Graduate Studies

06/05/2017

</div>

ACKNOWLEDGEMENTS

First and foremost, I would like to acknowledge my mentor, Dr. Brian Gold. From the very first meetings I attended when considering joining Dr. Gold's lab, I was immediately drawn to his emphasis on doing the best science and carefully considering every detail of a project. Dr. Gold has challenged me to understand every aspect of my work to the fullest and to carefully consider each choice made during an experiment. He has dedicated countless hours to helping me become a better scientific communicator through careful review and constructive critique of my work. Dr. Gold has provided me with the freedom to pursue my interests and encouraged me to explore my passions through my scientific endeavors. Finally, his patience, dedication, persistence, and rigor have helped me to better understand what it takes to be a great scientist and mentor.

I also would like to thank the members of my graduate committee, Dr. Charles Smith, Dr. Frederick Schmitt, Dr. Ai-Ling Lin, and Dr. David Powell. Each of them has been invaluable in this process. They have pushed me a step outside my comfort zone in order to help me expand my knowledge and encourage my scientific curiosity. I am grateful for all the support they have provided and look forward to continuing to learn from them in the future.

The MD/PhD program has been a source of support since before I enrolled at the University of Kentucky. Their warmth and encouragement has been a crucial key to my progress in the program. I would especially like to thank Therese Stearns for solving any problems, providing advice, and always being there to listen and encourage. I also would like to thank Dr. Susan Smyth for pushing me to set to the bar high and helping me find ways to reach that bar. The Center for Clinical and Translational Science has also been an important source of support through the TL1 fellowship. I would like to especially thank Dr. Victoria King and Dr. Thomas Kelly for all that they do for the TL1 program.

TABLE OF CONTENTS

LIST OF TABLES

LIST OF FIGURES

1. Background and Introduction

Human aging is associated with alterations in brain structure and function, declines in cognition, and increases in various neurological pathologies. Executive function (EF) is among the most vulnerable cognitive domains in aging, with significant declines observed across the lifespan (1–4). Further, EF is negatively impacted in the two most common forms of neurological pathology in older adults: Alzheimer's disease (AD) and cerebrovascular disease (CVD) (5–7). Importantly, these declines are also associated with poorer quality of life and reduced functional independence (8,9). EF underlies the capacity for the flexible and adaptive thought processes that are integral to human cognition (10). These processes include maintenance and manipulation of information, switching between goal sets, and inhibiting interfering stimuli and automated responses (10).

In practice, EF is measured through the use of cognitive tests of specific component processes or through more general neuropsychological assessments. Functional neuroimaging experiments often utilize task-switching, verbal or visual working memory (including *n*-back tasks), and cognitive control tasks (such as the Stroop task) (11–13). Neuropsychological tests of EF typically place demands on multiple EF processes and include tests such as the Trailmaking Tests, Digit Symbol Test, Digits Backward test, and FAS word generation tests (14–16). Through the use of both specific cognitive tests and neuropsychological tests, declines in EF have been observed in aging, AD, and CVD (1,2,7,15,17,18).

Most of the research seeking to understand alterations in brain structure and function associated with EF declines have investigated the frontoparietal control network (FPCN) (19–21). The FPCN consists of portions of the frontal and parietal cortices that are functionally active during tasks placing high demands on EF (22–24). Older adults reliably show altered functional responses in the FPCN compared to younger adults (24). In

particular, older adults often show increased activity in the FPCN compared to younger adults during tasks placing demands on EF, but this increased activity is often associated with poorer performance on EF tasks (25–27). This has led researchers to suggest that increased activity in the FPCN in aging is either a sign of reduced efficiency or a failed attempt at compensation (25,27,28). While these studies have provided valuable insight into functional alterations contributing to EF declines in older adults, other brain networks may also play an important role.

Specifically, diminished functional responses in the default mode network (DMN) are consistently observed in older adults. The DMN is unique in that it shows less activity during nearly all attention-demanding, externally-directed cognitive tasks compared to rest. It is beginning to be understood that failing to decrease activity in the within the DMN during EF tasks may be related to task performance (26,29,30). Nonetheless, the role of the diminished functional response in the DMN in EF declines are relatively understudied, and exactly how this diminished response is associated with cognition is poorly understood (29,31). The current dissertation will explore the relationship between altered functional responses in the DMN and executive function (EF) declines observed in aging. Experiment 1 will assess the specificity of the relationship between DMN function and EF through the use of a low and high EF demand task. Experiments 2 and 3 will seek to extend these findings to new tasks and explore relationships with longitudinal change in EF. By testing the relationship between DMN activity and performance on a variety of tasks placing demands on EF, it will be possible to assess how DMN function relates to EF in older adults.

Due to the potential cognitive consequences of altered DMN function, structural mechanisms contributing to decreased DMN function will be explored. While a multitude of physiological and molecular alterations both inside and outside of the central nervous system may contribute to altered patterns of brain function, the present dissertation will

focus on structural mechanisms that are detectable using neuroimaging or measurement of pathological proteins. Through the use of multivariate analyses processes associated with normal aging, Alzheimer's disease (AD), and cerebrovascular disease (CVD) that may contribute to altered DMN function in older adults will be investigated simultaneously. Experiment 1 will investigate the potential role of a previously unexplored contributor, white matter (WM) microstructure, to DMN functional declines in aging. Experiment 2 will determine the role of altered WM microstructure in both age-related and pathology-related declines in DMN function. Finally, Experiment 3 will investigate the ability of these various age-related and pathology-related mechanisms to predict longitudinal change in EF.

The following sections in this chapter will provide context for the present dissertation by first describing the discovery and characterization of the DMN. Next, the cognitive and physiological consequences of altered DMN function will be discussed, followed by an overview of potential mechanisms contributing to altered DMN function. A detailed description of WM microstructure and multivariate analyses will provide background on the key techniques employed in this dissertation. Finally, these sections will be summarized and placed into the context of the aims of the present dissertation.

1.1. The Discovery of the DMN

In the 1990s, cognitive neuroscience utilized neuroimaging techniques in an attempt to functionally map the human brain. Regions involved in various cognitive tasks could be identified by using functional neuroimaging to locate areas where greater activity was observed during a task compared to a resting or baseline condition. These so-called areas of "activation" were met with great excitement as the brain could be functionally mapped and segregated based on tasks during which a region was activated (32). In addition, to these areas of activation, some brain regions showed a reverse pattern with less activity during the task compared to baseline (33–35). Some of these decreases in activity were thought to

represent inhibition of sensory processes that might interfere with task performance (i.e.

inhibition of auditory stimuli during a visual task) (33,34). However, other regions were not

part of a well understood brain system and appeared to show reduced activity during a

variety of tasks compared to baseline.

In 1997, Shulman and colleagues published a seminal paper in which they

demonstrated that a consistent set of brain regions showed this pattern of "deactivation"

during tasks across multiple cognitive domains, sensory modalities, and difficulty levels (35).

However, it was still unclear if these deactivations simply represented a return to a baseline

level of activity from an activated state during the resting/baseline condition. If this was the

case, it could indicate a major flaw in the design of functional neuroimaging experiments, as

the baseline conditions being used would not represent a true baseline or control state (36).

In an attempt to answer this question, Raichle and colleagues performed a series of

experiments to demonstrate that the oxygen extraction fraction was uniform across the brain

during the baseline conditions of neuroimaging studies. Thus, the baseline condition

represented a homeostatic state with oxygen supply matching oxygen demand (37). Further,

the set of regions consistently showing deactivation were those that were the most active in

the baseline state. Therefore, they hypothesized that these regions were responsible for

functions ongoing during the baseline state, a so-called "default mode" of brain function.

Thus the concept of the DMN was born.

1.2. Anatomy of the DMN

The DMN includes the midline precuneus/posterior cingulate cortex (pC/PCC) and ventral-

medial prefrontal cortex (vMPFC), as well as bilateral portions of the lateral parietal/occipital

cortex (LPC/LOC), lateral temporal cortex (LTC), and dorsal-medial prefrontal cortex

(dMPFC) (Figure 1.1) (35,37,38). In addition, portions of the medial temporal lobe (MTL),

including the hippocampus (HC) and parahippocampal gyrus (PHG), also contribute to the

DMN (38). Comparative anatomy studies have found evidence of a homologous network in non-human primates, rodents, and, to some extent, canines (39–41). Therefore, the DMN appears to be an evolutionarily conserved network in mammals, although differences exist between the DMN in each species. Further, the functions carried out by the DMN in rodents and canines are unclear but may include some overlapping functions with those of the human DMN or different cognitive functions.

More recently, diffusion tensor imaging (DTI) has been used to identify WM pathways connecting DMN regions (see 1.7 for more details on DTI). Initial work by Greicius et. al. (42) provided the first evidence of structural connection between the pC/PCC and vMPFC, as well as between the PCC and HC. Technical limitations at the time limited the ability to detect connections between other DMN regions, but advances in DTI have allowed for mapping of WM pathways connecting the vMPFC and dMPFC, PCC and LOC/LPC, and PCC/LPC/LOC and LTC/MTL (43–45). These connections include portions of the cingulum, genu and splenium of the corpus callosum (CC), superior longitudinal fasciculus (SLF), inferior longitudinal fasciculus (ILF), and inferior fronto-occipital fasciculus (IFOF) (42,44,45). These WM pathways represent cortico-cortical association tracts and are primarily made up of late maturing, lightly myelinated axonal bundles (46–48).
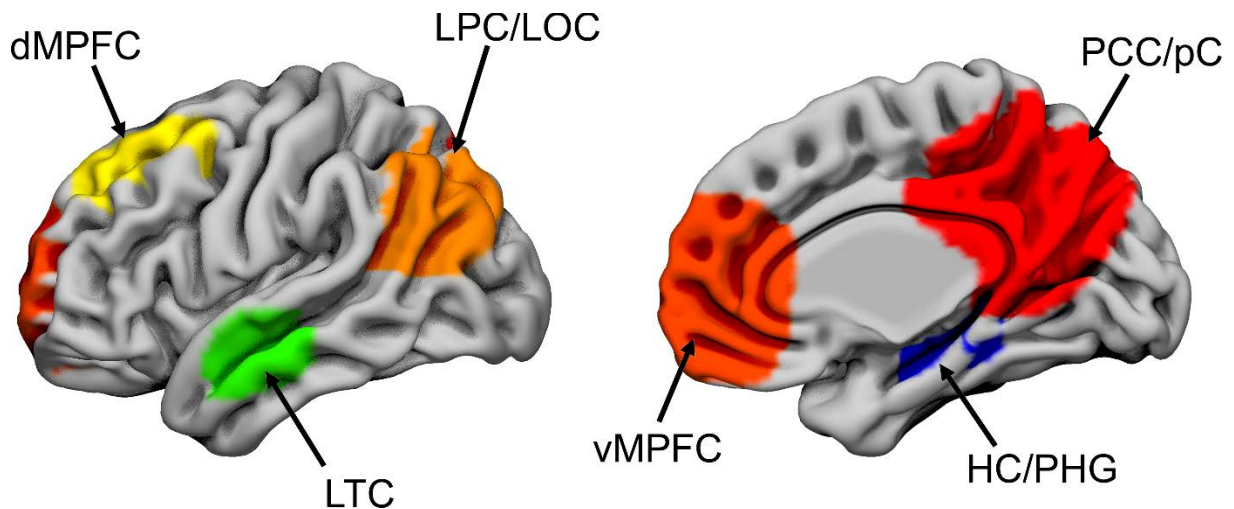
Figure 1.1. Anatomy of the DMN. Views of DMN regions overlaid on the lateral (left) and medial (right) surfaces of the MNI152 2mm^3 brain. The HC/PHG (blue) are roughly labeled although they cannot be directly viewed on these images. dMPFC (yellow): dorsomedial prefrontal cortex; LOC/LPC (light orange): lateral occipital/parietal cortex; LTC (green): lateral temporal cortex; HC/PHG (blue): hippocampus/parahippocampal gyrus; PCC (red): posterior cingulate cortex; vMPFC (dark orange): ventromedial prefrontal cortex.

1.3. Functional neuroimaging of the DMN

Functional neuroimaging of the DMN primarily relies upon ^{15}O-H$_2$O positron emission tomography (PET) and functional magnetic resonance imaging (fMRI). Both measures indirectly assess brain activity via the hemodynamic response (HDR). The principles of the HDR were first described in the late 19th century by Angelo Mosso and were experimentally observed shortly thereafter by Sherrington and Roy (32,49). The Roy-Sherrington principle states that increases in local functional activity lead to an increase in blood flow to that region as a result of signaling pathways related to the "products of cerebral metabolism" (49). ^{15}O-H$_2$O PET utilizes radioactively-labeled water to directly assess alterations in cerebral blood flow (CBF) during a task compared to baseline over a period of several minutes (50,51).

In contrast, fMRI utilizes the blood-oxygen-level-dependent (BOLD) signal to indirectly assess brain activity. Differences in the magnetic properties of oxygenated and deoxygenated hemoglobin produce detectable differences in T2* relaxation rates depending on the ratio of oxy- to deoxy-hemoglobin (52). Following an increase in brain activity, CBF to that region increases, bringing a large supply of oxygenated hemoglobin. However, the increase in oxygen consumption is modest (12-17%) compared to the increase in oxygen delivered to that region as a result of the HDR (~50%) because a majority of the increased metabolism during tasks compared to baseline are in non-oxidative pathways (53,54). This results in a net increase in the ratio of oxy- to deoxy-hemoglobin in regions that are more active during the task, which can be detected via the BOLD signal (55–57).

Importantly, these increases in CBF and BOLD signal appear to most closely reflect alterations in the local field potential (LFP), rather than spiking activity of neurons (58,59). Therefore, brain activations reflect an increase in the overall input to a region during a task, rather than increased output from that region. Conversely, brain deactivations reflect a decrease in the overall input to a region during the task (60). Thus, both brain activation and deactivation can be thought of as an indirect measurement of the degree to which synapses of a given region are more or less active (i.e. an overall measure of neurotransmitter release and recycling, action potentials from pre-synaptic neurons, post-synaptic potentials, and other processes) during the task compared to baseline.

The initial discovery of the DMN was based upon the observation that a consistent set of regions showed a pattern of deactivation in PET and fMRI studies regardless of the cognitive task (35,61). Based on the physiology, these deactivations indicate less synaptic activity in DMN regions during the cognitive tasks compared to baseline. The work by Raichle et. al. demonstrated that these regions have the highest levels of CBF, glucose metabolism, and oxygen consumption during the brain's homeostatic baseline, which

indicates that the DMN is highly metabolically active at rest (37). Up to 80% of the brain's

resting metabolism is devoted to synaptic processes related to neurotransmitter cycling (62–

64). Therefore, the high level of activity in the DMN during the resting state likely indicates

that a large amount of synaptic activity is ongoing during the brain's homeostatic baseline.

Supporting this theory, Greicius et. al. demonstrated that activity in DMN regions at

rest is highly coordinated (65). A technique called resting-state fMRI (rs-fMRI), which was

first demonstrated by Biswal et. al. (66) to show coordinated activity within the motor system,

was used to measure spontaneous fluctuations in BOLD signal around a baseline level of

activity during rest. The time courses of these spontaneous fluctuations in DMN regions are

highly correlated, thus indicating a high level of resting-state connectivity (rsC) (Figure 1.2).

DMN rsC is a sign of highly coordinated signaling at rest, which likely facilitates information

exchange between DMN regions (65–67). Therefore, these findings provided even greater

evidence of important ongoing cognitive processes within the DMN during the brain's
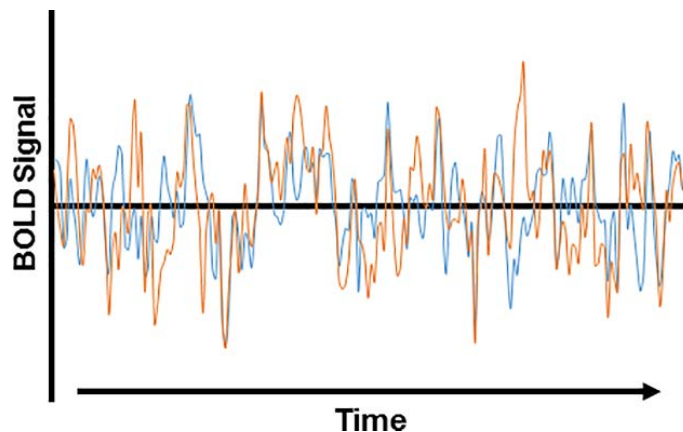
baseline state.

Figure 1.2. DMN resting state connectivity. Coordinated fluctuations in BOLD signal
around baseline between the PCC (blue) and MPFC (orange). Time elapsed is on the x-axis
and BOLD signal on the y-axis. The horizontal line represents average BOLD signal across
the time frame depicted. The high overlap in BOLD signal time series during the resting-
state indicates highly coordinated signaling between regions. The correlation between these
time series is a measure of resting-state connectivity (rsC).

1.4. Default Mode Functions

Shortly after their initial publication hypothesizing a "default mode" of brain function Gusnard and Raichle (68) provided thoughts on the cognitive processes making up this default mode of brain function based on functional neuroanatomy. The pC/PCC are thought to be involved in surveillance of the environment, as well as in emotional processing (69,70), while the vMPFC is thought to integrate emotional and cognitive processes (71,72). In addition, LOC/LPC and LTC are involved in detection of novel stimuli and biological motion (73,74). The dMPFC plays an important role in self-referential cognitive processes, stimulus-independent thoughts, and theory of mind (75–77). While not considered in the original report, the HC and PHG are known to be crucial for encoding and retrieval of episodic memory (78,79).

Together, these functions represent a core set of cognitive processes ongoing during the brain's baseline state. Since this original synthesis, DMN processes have expanded to include visualization of the past, present and future self, internal dialogue, and day-dreaming (38). Further, the DMN is activated during tasks of autobiographical memory and future planning, emotional processing, and maintenance of the self (80,81). Due to these observations, DMN processes are now thought to be primarily responsible for internally-focused, self-referential cognitive processes, including autobiographical knowledge and planning, maintenance and experience of the self, and mind-wandering. These processes require the integration of memory, emotion, and sensory information in order to produce these spontaneously-generated (or stimulus-independent) thought processes (80).

Another field of research has sought to understand how the DMN is impacted in semi-conscious states. These studies have demonstrated that DMN function is reduced during sleep (82,83), anesthesia (39,84), and minimally-conscious states (85,86). However, DMN function is maintained to some extent in all of these states and is correlated with level

of consciousness (87). In contrast, DMN function is lost in persistent vegetative states (85). Further, the functional integrity of the DMN during semi-vegetative states predicts future retention of the self and concept of agency (88). Together, these studies indicate that the DMN plays a role in conscious processing and self-referential cognition. Further, the maintenance of these processes even in minimally-conscious states underscores the importance of maintaining DMN functions.

1.5. Different Measures of DMN Function: TID vs. rsC

Following its initial discovery and description, investigations of the DMN split into those studying function at rest via rsC and those studying function during cognitive tasks via task-induced deactivations (TIDs). Both measures provide important information about DMN function, but studies of rsC have far outpaced those of TID (1947 DMN rsC studies vs. 328 DM TID studies indexed on PubMed). This may be primarily due to the relative ease of performing rs-fMRI compared to task-based fMRI (task-based fMRI requires participants to be trained on a cognitive task and involves less automated data analytic processes), and the greater ease of comparing across studies due to the absence of different cognitive tasks. A large body of research has demonstrated that DMN rsC is negatively impacted by both aging and AD (for reviews see: 56–58). Further, these declines in rsC have been associated with poorer cognition and clinical deterioration (92,93).

Despite being less studied, TID provides a valuable marker of dynamic modulation of DMN function in response to changing cognitive demands. DMN TID is reduced in both normal aging and AD (94,95). These decreases appear to occur linearly across the adult lifespan (96) and gradually across the AD spectrum (97–99). Of particular interest, DMN TID parametrically increases with greater cognitive demands in younger adults until it reaches a plateau (100). This parametric decrease in activity is thought to reflect a mechanism by which DMN processes are maintained at a level that minimizes interference with cognitive

processes involved in the task-at-hand (100). This may be due to interactions between the DMN and networks involved in the task-at-hand.

The DMN is functionally connected with brain networks involved in externally-directed tasks, such as the FPCN and salience (SAL) network. Several studies have indicated that the DMN and SAL network are antagonistic, with increases in one associated with decreases in the other (101,102). Further, some researchers have suggested that the SAL network directly inhibits DMN activity (103). However, experimental evidence using transcranial magnetic stimulation (TMS) to manipulate SAL activity has suggested that the SAL network does not directly modulate DMN activity (104). In contrast, the DMN and FPCN show both agonistic and antagonistic functional patterns depending on whether the task places demands on internally-focused or externally-focused cognitive properties (102). Further, altering activity in the FPCN using TMS appears to impact modulation of DMN activity (104). Thus, DMN TID may reflect a response to signaling from the FPCN following increased demands from the external environment.

Interestingly, older adults fail to parametrically increase DMN TID with greater cognitive demands (29,105,106). Instead, older adults show similar levels of DMN TID as younger adults during low demand tasks but fail to further deactivate the DMN as task demands increase. Thus, older adults have less TID compared to younger adults during high demand conditions (29,105,106). Therefore, older adults are still able to deactivate the DMN during external tasks but have a limited capacity to do so. This may indicate diminished inhibitory signaling from the FPCN that limits the ability to deactivate the DMN or disruption of communication within the DMN that limits the propagation of this inhibitory signal within the DMN. Whether this diminished capacity is the result of intrinsic properties of the DMN or failure of extrinsic inhibition (or a combination of both), this reduced capacity to deactivate the DMN may have important physiological and cognitive implications.

As discussed above, the DMN is primarily responsible for internally-focused cognitive processes. Therefore, many characterized the DMN as a 'task-negative' or 'task-irrelevant' network, believing that the DMN played no role in determining performance on externally-directed tasks (107). However, these theories primarily arose from studies of younger adults, where capacity for DMN TID is high and has minimal relationship with task performance (100,105,106). In contrast, when capacity for DMN TID becomes diminished in older adults, relationships with performance are observed (26,29,30). Interestingly, these relationships are most evident during high demand conditions, once capacity for TID has been reached (29,30). This suggests that activity in the DMN is an important contributor to performance when capacity for TID is diminished.

One explanation for this relationship is that higher levels of ongoing DMN processes interfere with cognitive processes needed for the task-at-hand (29,106). This is supported by the fact that TID-behavior relationships in older adults are commonly observed during tasks placing high demands on EF (29,30). EF is responsible for flexible and adaptive thought processes, such as task-switching, working memory, and inhibitory control (10). These processes allow for information to be maintained and manipulated despite interfering stimuli or processes. Thus, increased DMN activity during externally-directed tasks may require EF resources to be used to prevent interference from these processes (29). However, when EF resources are also needed for the externally-directed task, decreased TID may contribute to poorer task performance.

In addition to these cognitive implications, diminished capacity for DMN TID also may have important physiological implications. As discussed in Section 1.3, BOLD signal is correlated with levels of synaptic metabolism. These metabolic processes include both oxidative and non-oxidative glucose metabolism (Figure 1.3). In neurons, oxidative phosphorylation is the dominant energy source, with 36 ATP generated from a single

glucose molecule (108). In contrast, astrocytes rely heavily on the non-oxidative pathway of

aerobic glycolysis (AG), which produces only 2 ATP from a single glucose molecule (108).

(Note that the term aerobic glycolysis is used to reflect that these non-oxidative pathways

are occurring in the presence of sufficient oxygen supply for oxidative metabolism).

Increases in BOLD signal are primarily driven by increased AG, which produces higher

lactate levels in the blood, triggering hyperemia (54,62,109). However, AG and oxidative

phosphorylation are related (although non-linearly) due to the role of each in

neurotransmitter release and recycling (54,110). Therefore, diminished capacity for DMN

TID likely indicates consistently higher demands on oxidative phosphorylation and AG within

the DMN.
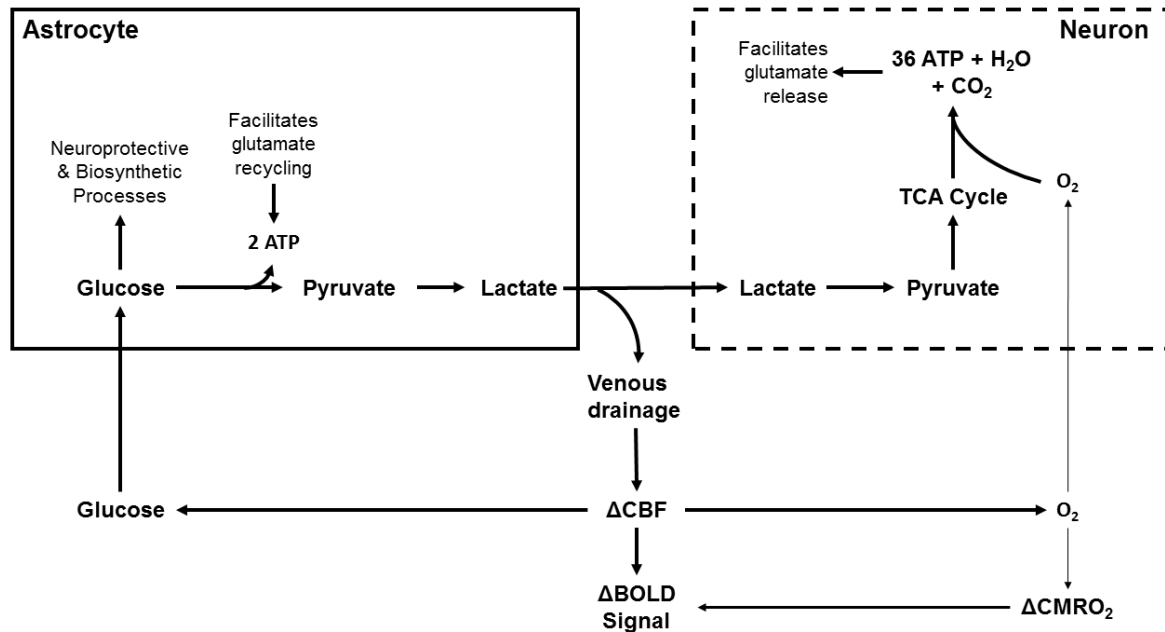
Figure 1.3. Synaptic metabolism related to task-evoked BOLD signal changes. The diagram depicts astrocytic and neuronal changes in metabolism related to BOLD signal alterations during cognitive tasks. Astrocytes uptake glucose, which is used as fuel for aerobic glycolysis, which is responsible for neuroprotective and biosynthetic processes via the pentose phosphate pathway and for neurotransmitter recycling. In order to facilitate neurotransmitter recycling, 2 ATP are generated via the breakdown of glucose to pyruvate and then lactate in order to power Na/K ATPases. Lactate is shuttled to neurons with some loss to the venous circulation. In neurons, lactate is converted to pyruvate and enters the tricarboxylic acid (TCA) cycle as part of oxidative phosphorylation, which requires oxygen. The result of this process is 36 ATP (as well as CO_2 and H_2O), which is used to facilitate neurotransmitter release. Leakage of lactate into the venous drainage alters vasodilation, which impacts change in cerebral blood flow. Change in blood flow leads to altered glucose and O_2 supply to the region. Increased cerebral metabolic rate of oxygen ($CMRO_2$) leads to an increased uptake of O_2 by neurons. However, this change is relatively small compared to the larger shift of glucose uptake by astrocytes occurs. The large change in CBF and smaller change in $CMRO_2$ allows for detection of the BOLD signal. Thus, when BOLD signal decreases during tasks, as is the case in TID, it reflects a decrease in both aerobic glycolysis and oxidative phosphorylation.

Oxidative phosphorylation is carried out by synaptic mitochondria and is crucial for

the processes involved in synthesis and release of neurotransmitters (111,112). Maintaining

mitochondrial function is necessary for cell survival and maintenance of synaptic processes.

However, mitochondrial function is known to decline in aging, and placing increased

14

demands on impaired mitochondria can increase oxidative stress through increased generation of reactive-oxygen species (ROS) (113,114). These ROS may damage mitochondria and synapses, resulting in necrosis (115,116). Further, increased oxidative stress can trigger an imbalance in the mitochondrial redox state, which can result in increased calcium buffering, mitochondrial swelling, and eventual bursting (115,117). As part of mitochondrial bursting, cytochrome c and other pro-apoptotic molecules are released into the synaptic cytosol, triggering programmed cell death (115,117).

AG primarily occurs in glia and is crucial for maintenance of the Na^+/K^+ pumps that generate the necessary Na^+ gradient to take up glutamate from synapses via the glutamate/Na^+ co-transporter (108,118). In addition, AG also serves as important source for biosynthetic and neuroprotective pathways via the pentose-phosphate pathway (119–121). Similar to oxidative phosphorylation, AG appears to decrease in aging (119,122). Therefore, increased demands on AG for synaptic metabolism may divert already diminished resources away from the biosynthetic and anti-inflammatory pathways carried out by AG. Diminished biosynthetic capacity could result in decreased cellular proliferation and reorganization (120), while loss of neuroprotective pathways could lead to greater susceptibility to oxidative stress (121,123).

1.6. Potential structural mechanisms contributing to diminished DMN TID in older adults

Due to the cognitive and physiological implications, it is important to determine the mechanisms contributing to less DMN TID in older adults. Initial research primarily focused on AD-related mechanisms. While diminished capacity for DMN TID is observed in cognitively normal (CN) older adults, autopsy studies indicate that at least 20% of CN adults over the age of 65 have significant AD pathology, while *in vivo* measures have identified that nearly 30% of CN older adults have significant AD pathology despite showing no clinical

signs or symptoms (124–127). This preclinical stage of AD is indistinguishable from normal

aging without direct measurement of AD pathological proteins, thus it was possible that

some alterations in DMN function previously attributed to normal aging may have been

influenced by preclinical AD pathology. The pathological hallmarks of AD are neuritic

plaques made of β-amyloid (Aβ) and neurofibrillary tangles made up of tau (128–131). Both

of these pathological proteins can be found in CN older adults on autopsy (124,125).

Several techniques have been developed to allow for detection of abnormal levels of

AD pathology *in vivo*. Analysis of cerebrospinal fluid provided the first *in vivo* marker of AD

pathology. Abnormally low concentrations of $Aβ_{1-42}$ ($Aβ_{42}$) are observed in individuals with

AD (127,132,133). In addition, individuals with AD have a non-specific increase in tau, which

differentiates them from healthy older adults but not those with other neurodegenerative

disease (134,135). Abnormally phosphorylated tau (p-tau) provides a more specific marker

of tau pathology in AD but suffers from low sensitivity (127,136,137). While initial studies

focused on using these markers to distinguish those with AD dementia from healthy elderly

and individuals with other neurological diseases, these markers also provide a valuable tool

for assessing AD pathology in those without dementia.

CN older adults can show similar CSF concentrations of $Aβ_{42}$ and tau species as

individuals with AD (138–140). Further, using autopsy confirmed cut-off values, both $Aβ_{42}$

and the tau/$Aβ_{42}$ ratio are predictive of future development of AD (139,141). In addition to

cerebrospinal fluid markers of AD pathology, several radioligands have been developed that

bind to AD pathological proteins in the brain (142,143). The first of these markers, Pittsburgh

compound-B (PiB), binds to Aβ plaques, and several similar ligands are now commercially

available (142,144). More recently, radioligands have been developed that bind to tau

neurofibrillary tangles (143). Similar to CSF markers of AD pathology, levels of radioligand

binding to Aβ plaques and tau tangles in CN older adults can be in a similar range as those observed in individuals with AD (145,146).

The development of PET radioligands that bind to AD pathological proteins has allowed for the topography of AD pathology to be assessed *in vivo*. These studies have found that AD pathology shows a predilection for DMN regions during its early stages of accumulation (145,147,148). Specifically, Aβ plaques are found primarily in the PCC/pC, LPC/LOC, and MPFC, while tau tangles are observed in MTL structures, LTC, and vMPFC (145–147). Moreover, concentrations of AD pathological proteins in the CSF are correlated, not only with the level of AD pathology (149), but with the specific topographic distribution of AD pathology (150,151). Therefore, CSF and PET markers of AD pathology provide highly overlapping information. However, CSF markers can detect earlier changes and are easier to treat as continuous variables (152).

Using these AD pathological markers, several studies have explored the relationship between Aβ and DMN TID. In 2009, Sperling et. al. published the first evidence that higher levels of AD pathology were associated with less TID within the PCC/pC (99). Specifically, there was a linear relationship between levels of PiB binding in the PCC/pC and TID in the PCC/pC across CN older adults and individuals with MCI (99). Further, within CN older adults and individuals with MCI, those with high Aβ burden had less DMN TID than those with low Aβ burden (99). Since this initial work, additional studies have found that CN older adults with high Aβ burden show less TID in other portions of the DMN compared to individuals with low Aβ burden (153,154). No study has examined the relationship between radioligand binding to tau and DMN TID nor has any study examined the relationship between CSF markers and TID. It should be noted that several studies have found relationships of lower CSF $A\beta_{42}$ and/or higher tau with reduced DMN rsC (155–157).

Together these studies provide some evidence for the role of increased AD pathology in diminished capacity for DMN TID in older adults. However, reductions in DMN TID may also be associated with mechanisms related to normal aging. Evidence of linear declines in DMN TID are apparent in the 4th and 5th decades prior to the accumulation of AD pathology (96). Further, studies measuring AD pathology in CN older adults have observed declines in TID in older adults without significant AD pathology (99,153,154). The most prominent structural changes in the brain in aging are gray matter (GM) atrophy and decline in WM microstructure (158–161). DMN cortical regions show significant atrophy in aging that occur independently of AD pathology, especially within the PCC/pC, vMPFC, and LTC (162,163). However several studies have failed to find a significant relationship between volume of DMN regions and DMN function after controlling for age (156,164). These results suggest that GM atrophy likely provides minimal contribution to changes in DMN function observed in older adults.

In contrast to GM atrophy, limited work has been done to investigate the role of WM microstructure in contributing to reduced DMN TID in older adults. Only one study to date has investigated this possibility, which found that global reductions in WM microstructure across the brain were non-specifically associated with lower DMN TID in older adults (26). However, several studies have found that lower WM microstructure is associated with reduced rsC between DMN regions (43,45). Further, studies of externally-focused networks have found that lower WM microstructure is associated with altered task-evoked functional responses (26,27,165). Together these studies suggest that WM microstructure may play an important role in the diminished capacity for DMN TID in older adults. Importantly, WM microstructure may be important for the connections between FPCN and DMN regions that may be necessary for inhibition of the DMN, as well as for connections between DMN

regions that are necessary for communication within the DMN. Therefore, it is important to understand how WM microstructure is measured and what it reflects.

1.7. Diffusion tensor imaging and white matter microstructure

DTI is an extension of diffusion weighted imaging that allows for assessment of water in anisotropic diffusion environments (166). Through the use of diffusion gradients (consisting of a de-phase and re-phase pulse pair) in many non-collinear directions, it is possible to estimate both the amplitude and directions of diffusion in a given voxel (166). This diffusion pattern can be represented by the diffusion tensor, which has three orthogonal axes: 1) a primary direction of diffusion is estimated, 2) a secondary direction of diffusion that is orthogonal to the primary direction is estimated, 3) diffusion in a third axis that is orthogonal to the previous two axes is estimated (166). Quantification of diffusion along these three axes allows for the generation of ellipsoids of diffusion, which can be oriented in many directions. This ellipsoid pattern is particularly useful for assessing diffusion in WM, where many possible orientations of fibers are possible (167).

DTI measures diffusion of water molecules on the order of milliseconds. During this time frame, diffusion is primarily confined by microstructural barriers, which, in the brain, consist primarily of membranes (168). Water molecules within the ventricles experience almost no barriers to diffusion, and thus, show high levels of unrestricted diffusion in all directions. Within GM, membranes are relatively randomly ordered resulting in diffusion that is moderately restricted to an equal extent in all directions. However, in WM, axonal and myelin membranes are stacked in parallel to each other. This results in relatively unrestricted diffusion in the direction parallel to axonal orientation and highly restricted diffusion in directions perpendicular to these ordered membranes (167,168). Thus diffusion is highly anisotropic in WM with much greater diffusion parallel to axons than perpendicular to them (166–168).

The degree of anisotropic diffusion can be quantified using a measure called fractional anisotropy (FA) (169). This value is calculated using Equation 1.1. and ranges from 0 (equal diffusion in all directions) to 1 (diffusion in only a single direction). Thus, higher FA values represent greater discrepancies between diffusion along the three axes of the diffusion tensor, independent of the mean diffusion within the voxel. In WM, increased density of axonal and myelin membranes stacked in parallel to each other result in high FA values (168). Decrease in the density or coherence of these membranes results in lower FA values.

$$\text{FA} = \sqrt{\frac{1}{2}} \sqrt{\frac{(\lambda_1 - \lambda_2)^2 + (\lambda_1 - \lambda_3)^2 + (\lambda_2 - \lambda_3)^2}{\left(\lambda_1{}^2 + \lambda_2{}^2 + \lambda_3{}^2\right)}}, \text{ where } \lambda_k \text{ is the eigenvalue of the } k^{\text{th}} \text{ tensor} \qquad \textbf{(1.1)}$$

In human WM, FA values increase throughout childhood and adolescence before peaking in early adulthood (48). This coincides with myelin development and axonal reorganization during brain maturation (170). Following a peak in early adulthood, FA values decrease in many major WM tracts throughout the adult lifespan (48,160,171). As described above, these declines are likely the result of reduced density and/or coherence of axonal and myelin membranes. It should be noted that anisotropic diffusion in WM exists in the absence of myelin, although reducing myelination lowers anisotropic diffusion by around 20% (168,172). In contrast, axonal bundles are necessary and sufficient for anisotropic diffusion, and the loss of axons results in approximately 50-70% declines in anisotropic diffusion (168,173,174). Therefore, declines in FA are a non-specific marker of reduced density of axonal and/or myelin membranes.

The mechanisms underlying declines in WM microstructure in aging are complex (Figure 1.4). Further, these mechanisms may include processes related to normal aging or those related to increased levels of pathology. Post-mortem studies of normal aging have demonstrated loss of axons and myelin within cortical WM, especially in tracts consisting of

small-diameter, lightly-myelinated axons (175,176). In addition, morphological changes in axons and myelin are apparent (177,178). Further, normal aging is associated with a significant decline in synapses, implying the loss or retraction of connecting axons (179). Any or all of these changes could result in lower FA values. Supporting this view, the WM pathways that show the greatest declines in FA in aging are those that consist of small-diameter, thinly-myelinated axons (46).
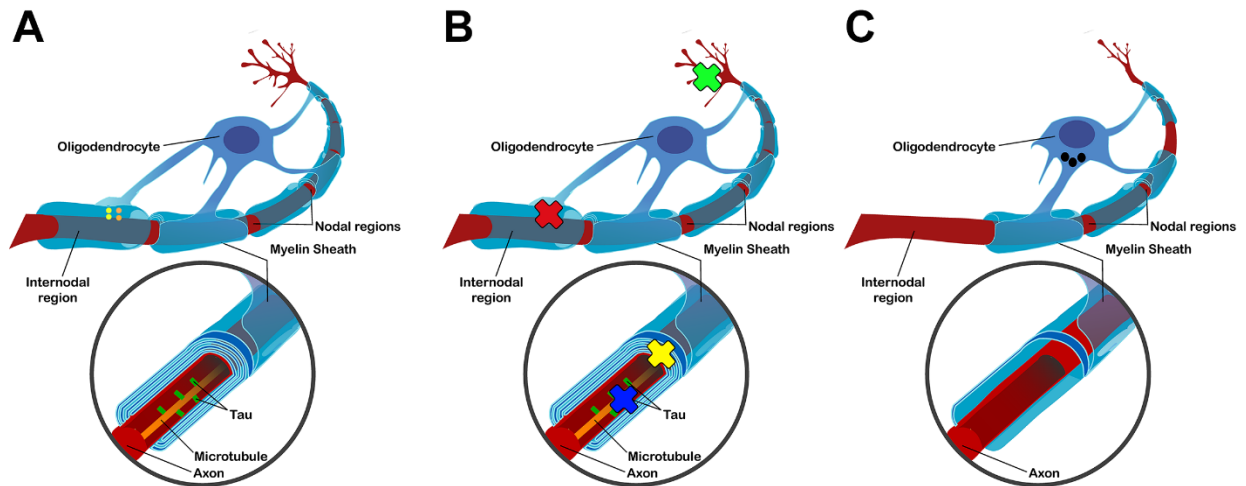
Figure 1.4. Potential microstructural changes in WM. A: Diagram of a healthy axon with high WM microstructural properties. The oligodendrocyte sends out processes, which wrap the axon in tightly-packed, concentric layers of myelin membrane. Within the axon, microtubules provide axonal stability and allow for axonal transport. Note that these stable microtubules contain microtubule-associated tau protein. Between segments of myelin, nodal regions of the axon contain a large number of ion channels that allow for rapid propagation of action potentials along the axon. In contrast, internodal regions of the axon contain few ion channels in order to preserve ionic gradients along these segments. Chemical signaling occurs between the axon and oligodendrocyte (yellow dots) and between the oligodendrocyte and axon (orange dots). These signaling processes are used to promote survival of axons and oligodendrocytes, as well as to trigger myelin repair processes. **B:** Diagram showing various insults that can disrupt WM microstructural properties. Loss of microtubule stability (blue X) due to loss of normal tau functioning may lead to loss of microtubules, which, in turn, disrupts axonal transport. This can contribute to synaptic starvation or failure to transport pro-survival signals back to the neuronal nucleus. Decreased myelin density (yellow X) results from myelin breakdown and repair processes that lay down thinner, less compact myelin sheaths. Further, myelin sheath formation may be inhibited by $A\beta_{42}$, resulting in no new myelin sheaths following breakdown. Loss of axonal/oligodendrocyte communication (red X) may result from damage to the oligodendrocyte due to toxins, ROS, ischemia, and/or AD pathology. In addition, damage to axons due to ischemia and/or inflammation or a lack of action potentials along axons may reduce signaling from axons to oligodendrocytes. Finally, decreased number of synapses (green X) due to synaptic starvation, interference with synaptic signaling processes, and/or damage to the astrocytes that maintain synapses could result in axonal retraction. These changes would also disrupt axonal/oligodendrocyte signaling, myelin repair processes, and microtubule integrity. **C:** Diagram of WM with poor microstructural properties. Myelin is less compact and/or absent from areas. This disrupts axonal signaling due to increased exposure of poorly conducting internodal regions and decreased conduction velocity. Further, loss of microtubules or microtubule integrity, may contribute to axon loss. There are a decreased number of synapses either resulting from or leading to axonal/oligodendrocyte damage. Oligodendrocytes show inclusion bodies (black dots), believed to reflect resorbed myelin and oligodendrocyte processes, and may have reduced ability to repair and produce myelin.

Importantly, WM is also negatively impacted by cerebrovascular disease (CVD) in older adults. CVD pathology can be detected *in vivo* through the use of fluid attenuated inversion recovery (FLAIR) imaging in order to identify areas of WM hyper-intensities (WMH) (180). These WMH lesions are nearly ubiquitous in aging, with over 90% of older adults showing some evidence of WMH (181). Areas of WMH detected *in vivo* correspond with areas showing significant axonal and myelin loss post-mortem (182,183). Further, these areas primarily reflect regions with reduced vascular integrity and increased inflammatory infiltrate (182,184). Importantly, WMHs have been shown to be associated with lower WM microstructure in the tracts they affect (185,186). This may reflect either direct changes associated with axonal loss and inflammatory infiltrate in the specific areas of WMH or effects of WMH on distal portions of these tracts via Wallerian degeneration (186).

CVD pathology is clinically silent for a prolonged period, making preclinical CVD difficult to distinguish from normal aging (181,187) The most prevalent areas of WMH in CN older adults are in periventricular WM (181,188). These areas include lateral aspects of the CC-genu and CC-splenium, which are responsible for connecting DMN regions (44,45). Further, deep WM is also affected, with WMHs in the frontal lobe most common (181,188). The high prevalence of WMH and topography of pathology suggests that DMN WM may be affected by CVD pathology in CN older adults, although no study has specifically addressed this question.

WM microstructure also shows significant declines in AD (189–191). These declines are most apparent in MTL tracts, including the fornix and cingulum, but are also present in other WM association tracts (189,191,192). Of particular interest, WM microstructure in pathways connecting DMN regions is significantly lower in individuals with AD compared to healthy older adults (43,193). Importantly, WM microstructure declines are evident in those at high risk for developing AD years prior to clinical signs or symptoms (194,195). More

recent findings have demonstrated that lower WM microstructure is associated with greater

levels of AD pathology in CN older adults (196–198). Interestingly, many of the associations

between AD pathology and WM microstructure in CN older adults have been found in WM

pathways connecting DMN regions (196,197,199).

There are numerous mechanisms by which increased AD pathology may contribute

to poorer WM microstructure, but the links between these mechanisms and WM changes in

humans have not been established. In animal models and *in vitro* studies, Aβ has been

found to be toxic to oligodendrocytes and inhibit myelin sheet formation, abnormal tau

phosphorylation has been shown to destabilize microtubules, and interaction of Aβ and tau

has been shown to disrupt fast axonal transport (FAT) (200–203). In addition, synaptic loss

and cell death are prevalent in AD (204,205). Any or all of these changes could contribute to

lower WM microstructure associated with increased AD pathology.

1.8. The importance of a multivariate approach

One of the major challenges of aging research is the frequent co-occurrence of processes

related to normal aging and those related to various clinically silent pathologies. Most

studies focus on only one of these processes at a time. However, the frequent overlap

between these different mechanisms makes interpretations of univariate analyses focusing

on any single process particularly challenging. As described in the sections above, DMN TID

has been associated with increasing age and AD pathology, while WM microstructure

declines have been associated with age, AD pathology, and CVD pathology in univariate

analyses. Further, aging is associated with increased prevalence of AD and CVD pathology.

Therefore, without the use of a multivariate approach, it is difficult to assess whether these

various age and pathology-related processes occur via independent or shared mechanisms.

Mediation analysis provides a particularly powerful tool to test how variables are related to each other (206,207). The general model of mediation analysis is shown in Figure 1.5. Within this framework, one can ask whether *X* directly influences *Y* or if *X* indirectly influences *Y* through its influence on *M*. Various coefficients can be calculated by performing first simple and then multiple linear regression analysis. The total effect (*c*) of *X* on *Y* is first calculated by performing a simple regression of *X* on *Y*. Similarly, the relationship between *X* and *M* (*a*) is calculated by performing a simple regression of *X* on *M*. In order to calculate the final two path coefficients, multiple linear regression is performed with both *X* and *M* as simultaneous predictors of *Y*. The β-coefficients of *X* and *M* resulting from this regression analysis are the path coefficients for *b* and *c'*, respectively. The direct relationship between *X* and *Y* is equal to *c'*, while the indirect effect of *X* on *Y* through *M* is the product of *a*b*.
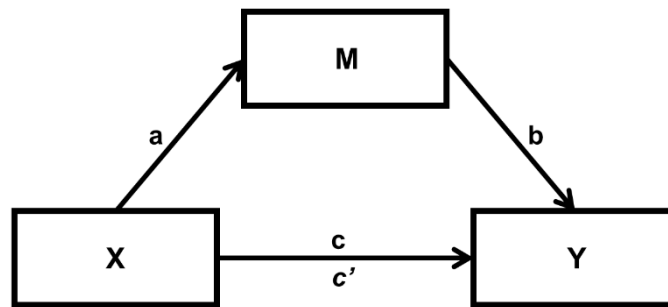
Figure 1.5. Mediation model. Mediation seeks to determine if variable X directly influences Y or indirectly influences Y through M. In this model, the total effect of X on Y is the coefficient c, which is the β-coefficient from a simple linear regression of X predicting Y. The coefficient a is determined by simple linear regression of X on M. The coefficients b and c' are determined by multiple linear regression of X and M on Y. The indirect effect of X on Y through M is equal to the product of a*b, while the direct effect of X on Y is c'.

In the original framework proposed by Baron and Kenny, mediation was said to occur if the relationship between *X* and *Y* decreased in the presence of *M* (*c'* < *c*) (208). However, this definition of mediation has no test for the significance of the mediation effect. Other tests for the significance of mediation were proposed but relied upon the assumption of

normality of mediation effects, which is unlikely to hold true (206). In order to address this problem, Preacher and Hayes developed a new framework in which the significance of mediation could be assessed by examining the indirect effect (209). In the revised model, non-parametric bootstrapping is utilized to develop 95% confidence intervals (CI) for the indirect effect (*ab*). If the 95% CI does not cross 0, then the indirect effect is significant and mediation is said to occur (206,209). This allows for significant mediation effects to occur when the sign of *c* and *c'* differ and/or when a significant direct effect (*c'*) also exists. Importantly, finding a significant indirect effect of *X* on *Y* through *M* does not preclude a significant indirect effect of *M* on *Y* through *X* (210). Therefore, it is important to assess alternative models, especially in cases where the direction of the relationship between *X* and *M* is unknown (210).

1.9. DMN function and WM microstructure in CN older adults

Aim 1: To establish whether less TID is tied to poorer EF.

Extensive research indicates that older adults have a diminished capacity for DMN TID. Decreased DMN TID may have a negative effect on EF due to a disruptive effect of ongoing activity irrelevant to the executive task. The current literature has provided evidence that less TID is associated with poorer performance during high demand tasks, especially those placing high demands on EF. Therefore, the primary hypothesis is that DMN TID contributes to worse performance on tasks placing demands on EF in older adults.

To test this hypothesis, the association between TID and EF will be investigated in low EF demand and high EF demand conditions during fMRI tasks. In Experiment 1, the relationship between TID and task performance will be examined in a task-switching paradigm that manipulates EF demand through the use of non-switch and switch conditions. In Experiment 2, the relationship between TID and task performance will be investigated

using a working memory paradigm placing high demands on EF through the use of multiple target images and repeating, intervening distractors. Finally, Experiment 3 will use neuropsychological tests to assess EF more broadly in order to determine the relationship between DMN TID and these measures in CN older adults.

Aim 2: To identify structural mechanisms contributing to reduced capacity for TID in older adults.

While increasing age and AD pathology have been implicated as potential contributors to reduced DMN TID, current studies have utilized univariate approaches that have made it difficult to determine how these alterations contribute to less DMN TID. One potential mechanism by which age and pathology may contribute to the diminished capacity for DMN TID in older adults is through alterations in WM microstructure. Current literature has demonstrated that WM microstructure influences activity in task-activated networks and is associated with coordinated signaling within the DMN. Further, increasing age and AD pathology are associated with altered microstructure in older adults. In addition, another common age-related pathology, CVD pathology, may also contribute to altered microstructure. Therefore, the hypothesis is that WM microstructure will directly contribute to lower DMN TID associated with aging and clinically silent pathology (Figure 1.6).

To test this hypothesis, mediation analysis will be used to determine whether declines in WM microstructure mediate the relationship between both age and clinically silent pathologies and DMN TID. In Experiment 1, the relationship between DMN WM microstructure and DMN TID will be explored in both low and high demand conditions. In addition, mediation will be used to determine whether WM microstructure significantly mediates age-related declines in DMN TID. In Experiment 2, the relationships of age, AD pathology, and CVD pathology with WM microstructure will be investigated. Further, mediation analysis will be used to test whether WM microstructure is a common pathway for

27

age-related and pathology-related declines in DMN TID. Finally, Experiment 3 will assess the value of these various structural mechanisms in predicting EF decline over a three-year follow-up. Mediation analysis will be used to determine whether WM microstructure is a direct predictor of both non-pathology and pathology-related declines in EF.
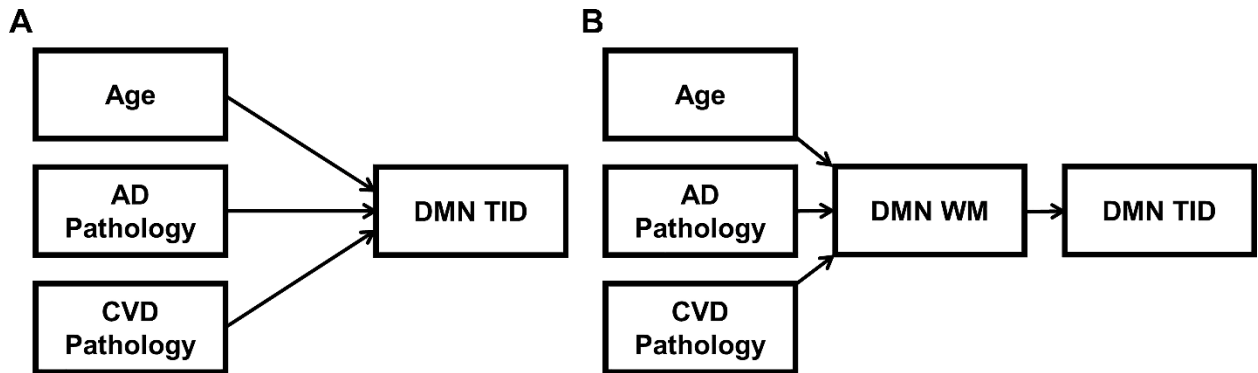
Figure 1.6. Potential relationships between age, AD pathology, and CVD pathology with DMN TID. The effects of age, AD pathology, and CVD pathology may influence DMN TID through direct **(A)** and/or indirect **(B)** mechanisms. One possible indirect mechanism that will be studied here is through altered microstructure in DMN WM pathways. Through the use of mediation analyses, these different possibilities will be tested. Based on current literature, age and AD pathology are associated with less DMN TID, while the relationship between CVD pathology and DMN TID is unclear. To date, no study has directly assessed any of the relationships shown in **panel B**.

Importantly, WM microstructure could affect DMN TID through alterations in the WM pathways within the DMN (i.e. connecting DMN regions to each other) or alteration in WM pathways connecting task-activated networks to the DMN (i.e. connecting FPCN regions within DMN regions). Change in microstructural properties of WM pathways connecting DMN regions could disrupt both excitatory and inhibitory signaling within the network, thus resulting in more poorly regulated signaling within the DMN during tasks. Further, alterations in WM connecting FPCN and DMN regions could disrupt inhibitory signaling to the DMN, resulting in failure to reduce activity during the task. Finally, alterations in both of these WM connections could work in concert to produce the observation of reduced DMN TID in older

28

adults. For example, a decrease in the microstructural properties of WM connecting FPCN and DMN regions could negatively impact both inhibitory signaling to the DMN, while lower WM microstructural properties in WM connecting DMN regions could further diminish the spread of this signal across the DMN. Experiment 1 will test this possibility by investigating whether WM microstructure connecting DMN WM or connecting the TPN to the DMN is more predictive of DMN TID.

2. Experiment 1: White matter microstructure contributes to age-related declines in task-induced deactivation of the default mode network

2.1. Introduction

Functional neuroimaging studies have demonstrated that some brain regions show lower activation during the performance of attention-demanding cognitive tasks compared to simpler baseline conditions (35,37,68). Such TIDs tend to occur within the brain's default mode network (DMN), which includes medial prefrontal cortex, posterior cingulate cortex/precuneus, lateral portions of temporal and parieto-occipital cortices and hippocampus (29,37,68,100). The DMN contributes to a wide variety of internally-generated thought processes (38,68). As such, the capacity to deactivate the DMN is thought to have important functional significance during certain externally-directed cognitive tasks (29,100). It should be noted that externally-directed tasks involving linkage to self-referential processes carried out by DMN regions do not result in deactivation (80)

In the former type of task, younger adults tend to show greater deactivation in the DMN as the task becomes more cognitively demanding (29,100,105,106). Interestingly, several studies have reported that older adults show similar magnitude of DMN TID as younger adults during simple cognitive tasks, but less TID during more difficult active tasks (29,105,106). These findings suggest that older adults may be less able to regulate functional response in DMN cortical regions as cognitive resources are increasingly required by the active task (29,106). Persistent activity in the DMN may degrade executive performance in these circumstances. Reduced deactivation of the DMN during these tasks could thus be a significant contributor to older adult difficulties on attention-demanding tasks.

Despite the broad potential relevance of this issue, little remains known about how TID of the DMN may track with increasing age and its neurobiological sequelae such as reductions in task performance and brain structure. This is in part because previous work has focused solely on comparisons of younger and older adult groups. However, by treating age continuously, it is possible to examine multivariate relationships with other continuous variables, such as neuroimaging measures of potential structural mechanisms contributing to deactivation of the DMN.

We hypothesized that white matter (WM) microstructure may be a potential contributor to deactivation patterns in the DMN for several reasons. First, because WM provides a means for electrochemical signaling across large-scale brain networks, age-related reductions in WM microstructure would be expected to influence the coordinated functioning of brain regions within organized networks such as the DMN (211,212). Second, recent studies have confirmed several underlying WM connections between various portions of the DMN (42,44,45,213). Finally, there is evidence that the WM microstructure measure of fractional anisotropy (FA) is correlated with BOLD magnitude in task-positive networks (TPN) during cognitive task performance (27,165,214–216) and with functional connectivity within portions of the DMN (43,211).

Due to the potential suppression of DMN activity by TPN regions, it is important to investigate the potential role of microstructure both within WM pathways connecting TPN regions with the DMN and within WM connecting the DMN regions themselves. Altered microstructure in WM connecting TPN and DMN regions could diminish inhibitory signaling from TPN regions intended to trigger a decrease in DMN activity, thus resulting in a failure to deactivate the DMN with increasing task demands. Alternatively, poorer microstructural properties in WM connecting DMN regions to each other may disrupt both excitatory and

inhibitory signaling within the DMN, thus resulting in decreased regulation of DMN activity in response to increased task demands.

Here we tested the hypothesis that age-related reductions in WM connectivity could limit the capacity to decrease DMN activity as demands of the active task increase. An fMRI task switching paradigm was used that included two simple perceptual judgment tasks (color and shape judgments) made on stimuli that were identical in each task condition. Difficulty was manipulated by asking participants to either repeat the same task throughout a block or switch (pseudorandomly) between judgment types, placing increased demands on EF processes (18,217). We also investigated the effects of age, DMN WM microstructure, and TID on task performance across the two conditions. Finally, mediation analysis was used to determine whether WM microstructure accounts for the age-related decline in DMN deactivation capacity as cognitive demands increase.

2.2. Materials and Methods

2.2.1. Participants

There were a total of 117 participants in the present study. Participants were community-dwelling adults between the ages of 25 and 83 (mean = 49.7 ± 17.4) with normal or corrected-to-normal vision. Written informed consent was obtained from each participant under an approved University of Kentucky Institutional Review Board protocol. Exclusion criteria were color blindness, a major head injury, stroke, a neurological or psychiatric disorder, high blood pressure, diabetes, use of psychotropic drugs, or presence of metal fragments and/or metallic implants contraindicated for MRI.

Participants completed measures of fluid intelligence and digit span, which are known to correlate with task-switching performance (18). Fluid IQ was measured using the Cattell Culture Fair Intelligence Test (218) because this test assesses non-verbal

intelligence associated with perceiving inductive relationships in shapes and figures, processes relevant to the perceptual task-switching paradigm employed in the present study. Digits forward (DF) and backward (DB) were measured using the Digit Span Subtests of the Wechsler Memory Scale (WMS III) (219). Socioeconomic status was assessed using the Hollingshead 2-Factor Index of Social Position (ISP), which is based on educational and occupational achievement (low scores = higher SES) (220). Demographic information is provided in Table 2.1.

Table 2.1. Demographic and performance scores

	Mean ± SD
N	117
Age	49.7 ± 17.4
M:F	52:65
Education	16.7 ± 2.8
ISP	25.3 ± 13.7
IQ	$124.5 \pm 18.9_{115}$
DF	$10.6 \pm 2.1_{113}$
DB	$10.2 \pm 2.6_{113}$
Single Acc	97.7 ± 2.6
Mixed Acc	95.3 ± 4.6
Single RT	725.3 ± 147.9
Mixed RT	945.3 ± 203.9

ISP, Hollingshead Index of Social Position; IQ, Cattell Culture Fair Intelligence Test; DF, digit span forward; DB, digit span backward; Single and Mixed refer to conditions in the fMRI experiment; Acc: accuracy RT: reaction time. Values listed are mean ± SD. Values for IQ and DB are age-scaled scores. If score values were missing, the number of participants used in the computation is shown as a subscript.

2.2.2 Image Acquisition

Imaging data were collected on a 3T Siemens TIM TRIO scanner at the Magnetic Resonance Imaging and Spectroscopy Center at the University of Kentucky. High resolution anatomic images were acquired using a magnetization-prepared rapid echo gradient-echo (MPRAGE) sequence [repetition time (TR) = 1690ms, echo time (TE) = 2.65ms, flip angle = 12°, 1-mm isotropic voxels]. T2*-weighted functional volumes were collected using a gradient-echo echo-planar imaging (EPI) sequence [33 interleaved slices, TR = 3000ms, TE = 30ms, flip angle = 83°, field of view (FOV) = 224mm^2, matrix = 64 × 64, 3.5mm isotropic voxels]. Diffusion tensor images (DTI) were collected using a double spin-echo EPI sequence [TR = 6900ms, TE = 105ms, flip angle = 90°, FOV = 224mm^2, in-plane resolution = 1.75 × 1.75 mm voxels, 40 contiguous 3-mm-thick axial slices] with 36 non-collinear encoding directions (b = 1000s/mm^2) plus 5 images without diffusion weighting (b = 0 s/mm^2, b0).

2.2.3. fMRI Task Paradigm

Participants completed a task-switching paradigm (Figure 2.1) described in detail elsewhere (27). Briefly, participants performed one of two possible perceptual judgments on every trial. On color task trials, participants decided if a stimulus was red or blue. On shape task trials, participants decided if a stimulus was a circle or square. Participants were asked to respond as quickly and as accurately as possible. During single task blocks the same judgment was made on every trial for the duration of the block (e.g. all color trials), while in mixed task blocks shape and color judgments alternated pseudorandomly with a 50% probability of repeating/switching between judgments on consecutive trials. There were 3 runs, each consisting of four task blocks and five fixation blocks. Task blocks consisted of 20 trials (totaling 60 seconds per block) for each of the single or mixed task conditions. During fixation blocks (lasting 30 seconds), participants were instructed to look at a centrally

presented cross-hair (+). One run consisted of two single blocks of each color and shape

judgments, and the other two runs consisted of one single block for each judgment and two

mixed blocks.
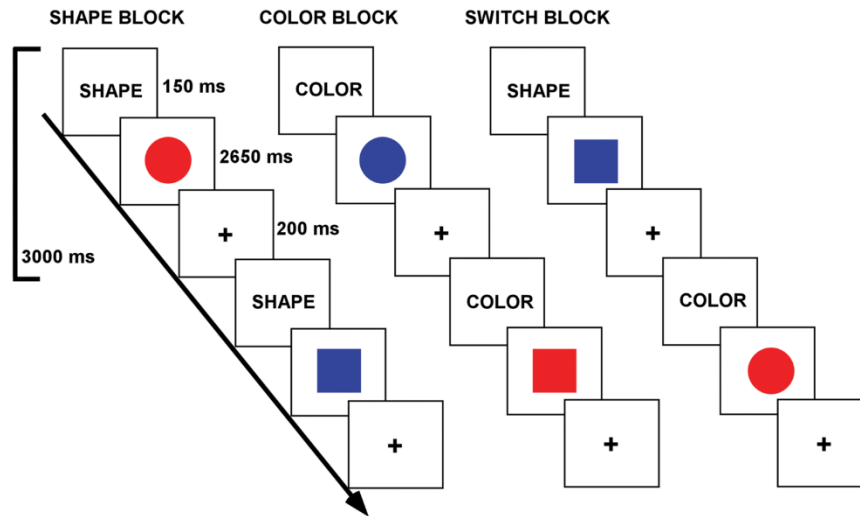
Figure 2.1. Task-switching paradigm. Diagram of single blocks (shape or color block) and mixed block (switch block). Stimuli were identical in all blocks. In single blocks individuals made only one type of judgment (shape or color), while in mixed blocks individuals pseudorandomly switched between shape and color judgments. Participants were cued on which judgment to make for 150ms prior to the presentation of the stimuli for 2650ms. Trials were interleaved by a fixation cross for 200ms. The duration of each task block was 60s and were interleaved by 30s baseline blocks, during which a fixation cross was presented.

2.2.4. fMRI Preprocessing and Analyses

fMRI Expert Analysis Tool (FEAT) v6.0.0, part of the FMRIB Software Library (FSL; 221),

was used for fMRI data preprocessing and statistical analysis. Data were first motion

corrected, smoothed with a 9mm Gaussian kernel and high-pass filtered at 100s. fMRI data

was then co-registered to each individuals high resolution structural scan using boundary-

based registration (222). The high resolution structural image was co-registered to MNI 2 ×

2 × 2 mm space using an initial linear registration followed by nonlinear warping (using

FNIRT; 223). These transformation parameters were then applied to the functional data,

which was re-sliced to 2-mm isotropic voxels during non-linear warping into MNI space.

Single and mixed blocks were modeled separately and convolved with a double-gamma hemodynamic response function. First-level analysis involved contrasts for color and shape (single) blocks compared to fixation and mixed blocks compared to fixation for each participant for each run. Parametric maps from each first-level analysis (Runs 1, 2, and 3) were then carried into a second-level fixed effects model where the results of each first-level model were combined into a single beta-map per condition. Higher-level (group) analyses were performed using FMRIB's Local Analysis of Mixed Effects (FLAME).

2.2.5. Defining a Common DMN Network

A common deactivation network was defined across participants to identify DMN structures of functional relevance to individuals across the age range of our sample. Peak regions of deactivation were identified through a voxelwise contrast of fixation > single task across all participants. Significant clusters of peak deactivation in this contrast were masked at a voxel-wise FWE corrected $p < 0.05$ threshold. The single (i.e. easier) condition was chosen for the contrast given previous evidence of stronger age-differences during more difficult task conditions (29,106). (However, it should be noted that the baseline fixation > mixed task condition contrast produced essentially the same results in our data; peaks within one voxel of those in the fixation > single condition). The overall DMN mask was created by placing 5mm-radius spheres around the peak voxel in each cluster surviving the above criteria in the fixation > single contrast (Figure 2.2). Percent signal change within the overall DMN mask was then extracted for each participant using Featquery.
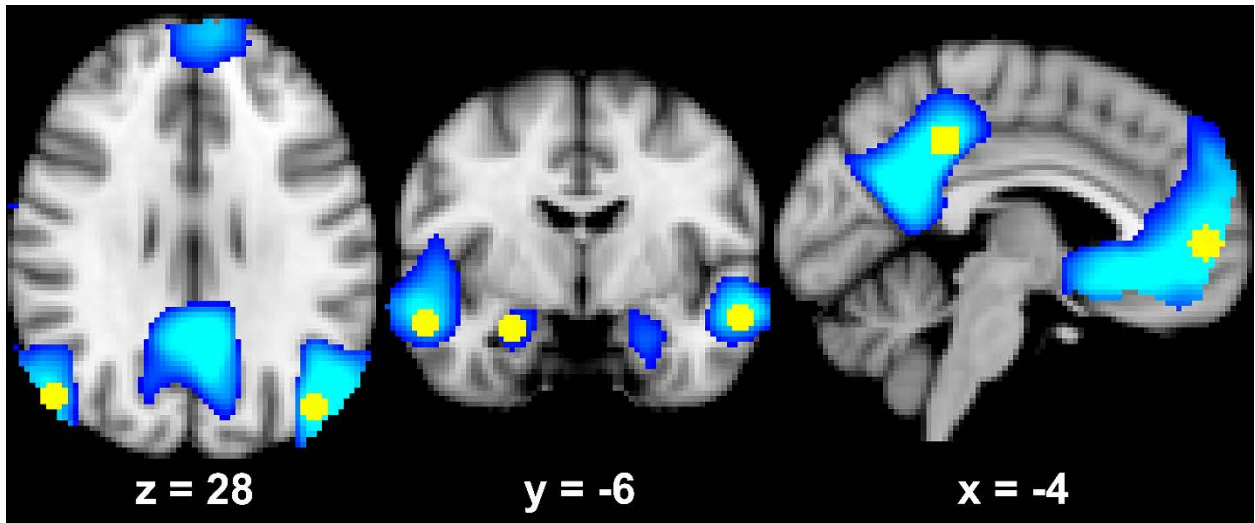
Figure 2.2. DMN ROIs overlaid on MNI152 T1 2mm brain. The 5mm-radius spherical ROIs (yellow) and significant voxels from the fixation > single contrast (blue-light blue gradient) overlaid on the MNI152 T1 2mm^3 brain. All images are in radiological orientation. The MNI coordinate of the slice is below each image. All ROIs except the left hippocampus are shown.

2.2.6. Diffusion Tensor Imaging Preprocessing

FMRIB's Diffusion Toolbox (FDT) v3.0 was used for all DTI preprocessing and analyses. Preprocessing steps performed on raw images involved eddy current correction, brain extraction, and motion correction using a 12-parameter affine transformation to the b0 images. DTIFIT was then used to compute a tensor model and eigenvalues (λ_1, λ_2, λ_3) within each voxel. These eigenvalues were used to calculate fractional anisotropy (FA) images, which were used as input for tract-based spatial statistics (TBSS).

2.2.7. Tract-Based Spatial Statistics

Each participant's FA image was co-registered to the FMRIB58_FA 1mm standard space template using tract-based spatial statistics (TBSS; 224), as shown in Figure 2.3 and described in detail in our previous work (225). Briefly, non-linear voxel-wise registration was used to transform images into MNI space, where FA images from all participants were averaged to generate a mean FA image. The mean FA image was subsequently used to

create a white matter (WM) skeleton with tracts common to all participants. This skeleton

was thresholded at FA > 0.2 in order to minimize partial volume effects after warping across

all participants. Each participants FA image was subsequently projected onto the FA

skeleton in order to account for residual misalignments between participants after initial

registration.
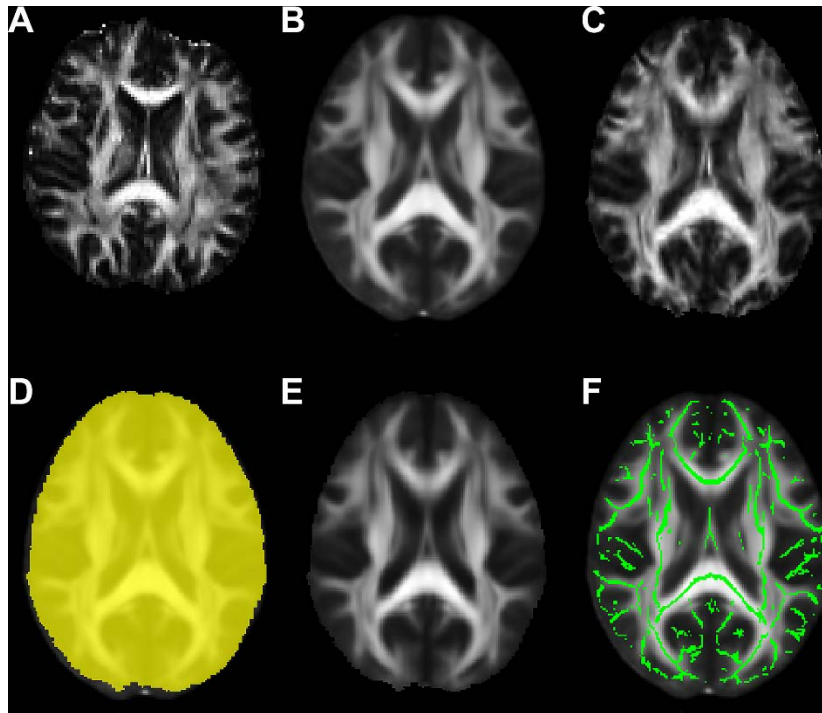
Figure 2.3. Overview of the TBSS pipeline. Each participant's native space FA image **(A)** is non-linearly registered to the FMRIB58 FA 1mm^3 template **(B)** producing each participant's FA image resampled in FMRIB58 FA 1mm^3 space **(C)**. A group mask **(D)** is generated to include only voxels that are present in all participants (yellow). The FA images from all participants are then averaged and masked to produce a group mean FA image **(E)**. This mean FA image is used to create a skeleton **(F)** of WM tracts common to all participants (green). All participant's FA images are projected on to this skeletonized image in order to correct for residual misalignments.

2.2.8. Probabilistic Tractography

Probabilistic tractography was performed to identify the WM pathways connecting the eight

individual fMRI clusters forming the overall 'network-level' DMN-fMRI mask (described in

2.2.5.). Prior to tractography, the fMRI-based cortical seeds were registered to each

participant's native diffusion space. The first step in this process was to transform the cortical seeds from MNI 2 × 2 × 2 mm space to MNI 1mm^3 space using FLIRT. Then the inverse of the non-linear warp from each participant's FA image to MNI 1mm^3 space (described in 2.2.7.) was generated and applied to register all fMRI-based cortical seeds from MNI 1mm^3 space to each participant's diffusion space.

Tractography was performed using FSL's Bayesian Estimation of Diffusion Parameters Obtained using Sampling Techniques (BEDPOSTX) and probabilistic tracking (PROBTRACKX2) tools (226,227). BEDPOSTX (226) was run using a 2-fiber model to determine a probabilistic diffusion model in each voxel, which was used as the input for probabilistic tractography. PROBTRACKX2 (227) was run in network mode using modified Euler streamlining. A total of 5000 samples were generated from each voxel in each seed with a curvature threshold of 0.2 (approximately ± 80°), a step length of 0.5mm with a maximum of 2000 steps, and a fiber volume threshold of 0.01. The Harvard-Oxford Subcortical Atlas brainstem mask was used as an exclusion mask to avoid descending pathways. Successful streamlines were those originating in a voxel within one fMRI-based cortical seed and passing through a voxel in another fMRI-based cortical seed without entering the exclusion mask.

A streamline image (Figure 2.4) was generated showing all successful tracts, which was then registered to MNI 1mm^3 standard space using the non-linear transform described above. Each individual's streamline image was divided by the total number of samples generated (# of samples = # voxels in seed regions * 5000) to create a proportion image. The value of each voxel in the proportion image indicates the proportion of successful streamlines that passed through that voxel. Before creating a group mean image, each participant's proportion image was divided by the total number of successful streamlines generated, or waytotal, as a way to account for differences in "trackability" between each

participant's diffusion data. A group mean image was then calculated from the average of all participants' waytotal-normalized proportion maps. The group proportion image was thresholded at 0.1% of total streamlines passing through a given voxel in order to generate a group mask of successful streamlines. The group mask was restricted to those voxels within the mean FA skeleton to limit the effects of partial voluming. Mean FA values were then extracted from the skeletonized 'DMN-WM' mask for each participant.
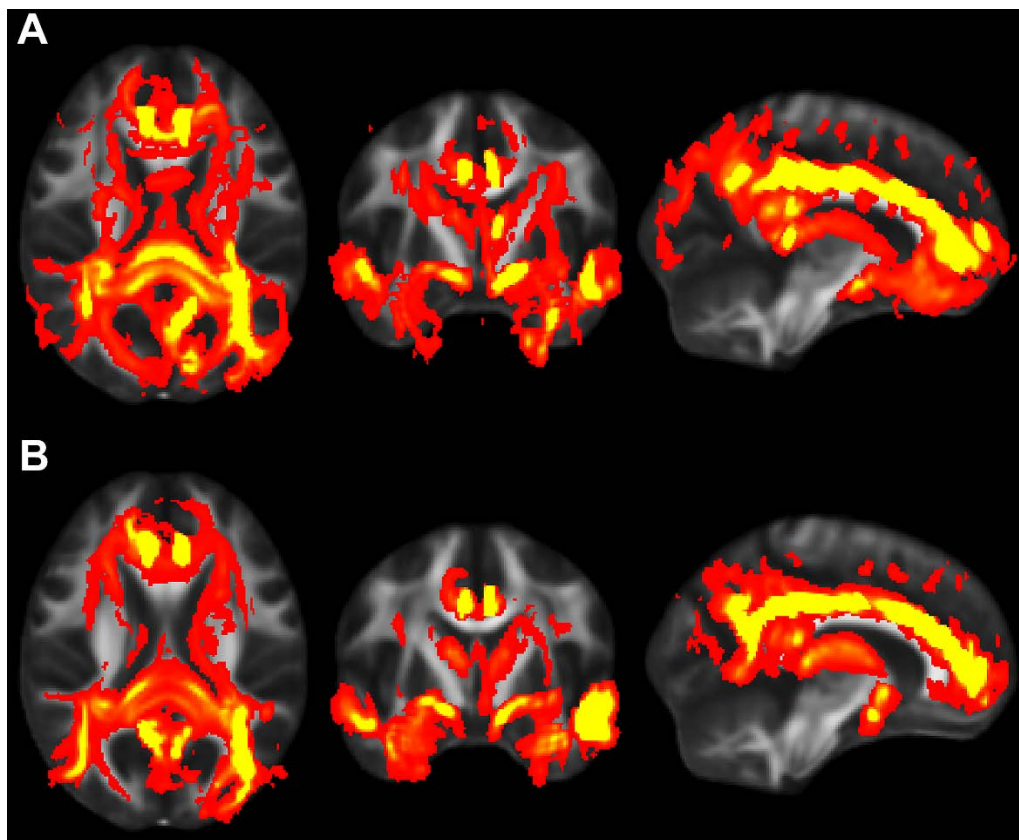
Figure 2.4. Individual tractography results. Tractography results from a younger **(A)** and older **(B)** adult overlaid on the FMRIB58 1mm^3 template. Brighter red and yellow represent voxels with more streamlines passing through them. Note the high overlap across individuals, especially in voxels with more streamlines passing through them (yellow voxels).

2.2.9. Tractography of connections between networks

Due to the potential influence of increased input from the TPN, additional tractography analyses were performed in order to identify WM pathways connecting TPN regions and

DMN regions. Seeds for this analysis were taken from previous work describing functional

response in the TPN during the same task in this cohort (27,228). WM pathways connecting

TPN regions with DMN regions were identified using the same steps described in 2.2.8. Due

to the high overlap between these pathways and those connecting DMN regions in areas

immediately surrounding seed regions, unique portions of WM pathways were identified by

subtracting out any voxels that were identified in both tractography analyses. Therefore, two

unique WM-masks were created: 1) DMN-only WM and 2) TPN-to-DMN-only WM. Each

WM-mask was then restricted to only those voxels belonging to the group skeleton, and FA

was extracted from each participant in each of these skeletonized WM-masks.

2.2.10. Statistical Analyses of Behavioral, fMRI and DTI Data

Statistical analyses were carried out in SPSS 22 (IBM Statistics, Chicago, IL). Three main

analyses were carried out. The first two analyses were intended to assess the contributions

of relevant predictors on (1) DMN TID magnitude and (2) task performance. These analyses

used mixed-effects General Linear Models (GLM), which examined fixed-effects while

accounting for subject-specific variance. The first set of GLMs investigated the between-

subject effect of either age or FA in DMN-WM, the within-subject effect of condition (single

or mixed), and the age/FA × condition interaction on DMN deactivation magnitude.

Standardized beta-values are reported for each effect and *t*-statistics were used as the

inferential statistic to determine significance of each effect in the presence of the others.

Those effects with $p < .05$ were considered significant. Significant interactions were

investigated further by performing linear regression within each condition separately. A sub-

analysis was then carried out to test whether the relationship between FA and DMN

deactivation magnitude was specific to DMN-WM or if it was related to TPN-to-DMN-WM. In

order to test this, the relationship between each of the unique WM masks (DMN-only and

TPN-to-DMN-only) and DMN TID magnitude were explored. A backwards step-wise linear

regression was then performed, entering FA in both sets of WM pathways into the first step, and then performing backward selection with a removal criterion of $p > 0.10$.

The second set of GLMs investigated the between-subject effect of either age, FA, or DMN TID magnitude, the within-subject effect of condition, and the age/FA/TID × condition interaction on task performance (accuracy or reaction time (RT) separately). Again, effects with $p < .05$ were considered significant, and significant interactions were investigated by performing linear regression within each condition separately. The final set of analyses used mediation models to test the hypothesis that DMN WM microstructure accounts for age-related changes in DMN TID magnitude. Mediation analysis based on multiple linear regression was performed using macros (PROCESS; 207) that simultaneously estimate all paths between variables and indirect effects. PROCESS utilizes bootstrapping and generates Monte Carlo confidence intervals to allow for statistical inferences. Indirect effects having 95% confidence intervals not crossing zero were accepted as significant mediation effects.

2.3. Results

2.3.1. Functional deactivations across participants

Results from the voxelwise contrast of the baseline fixation condition compared to the single task condition across participants revealed deactivation in the posterior cingulate cortex (PCC), medial prefrontal cortex (MPFC), and in bilateral portions of lateral occipital cortex (LOC), hippocampus (HC), and lateral temporal cortex (LTC) (Figure 2.5a). Coordinates of peak voxels within each cluster are listed in Table 2.2. A DMN mask was generated surrounding peak coordinates within each cluster (as described in 2.2.5.).
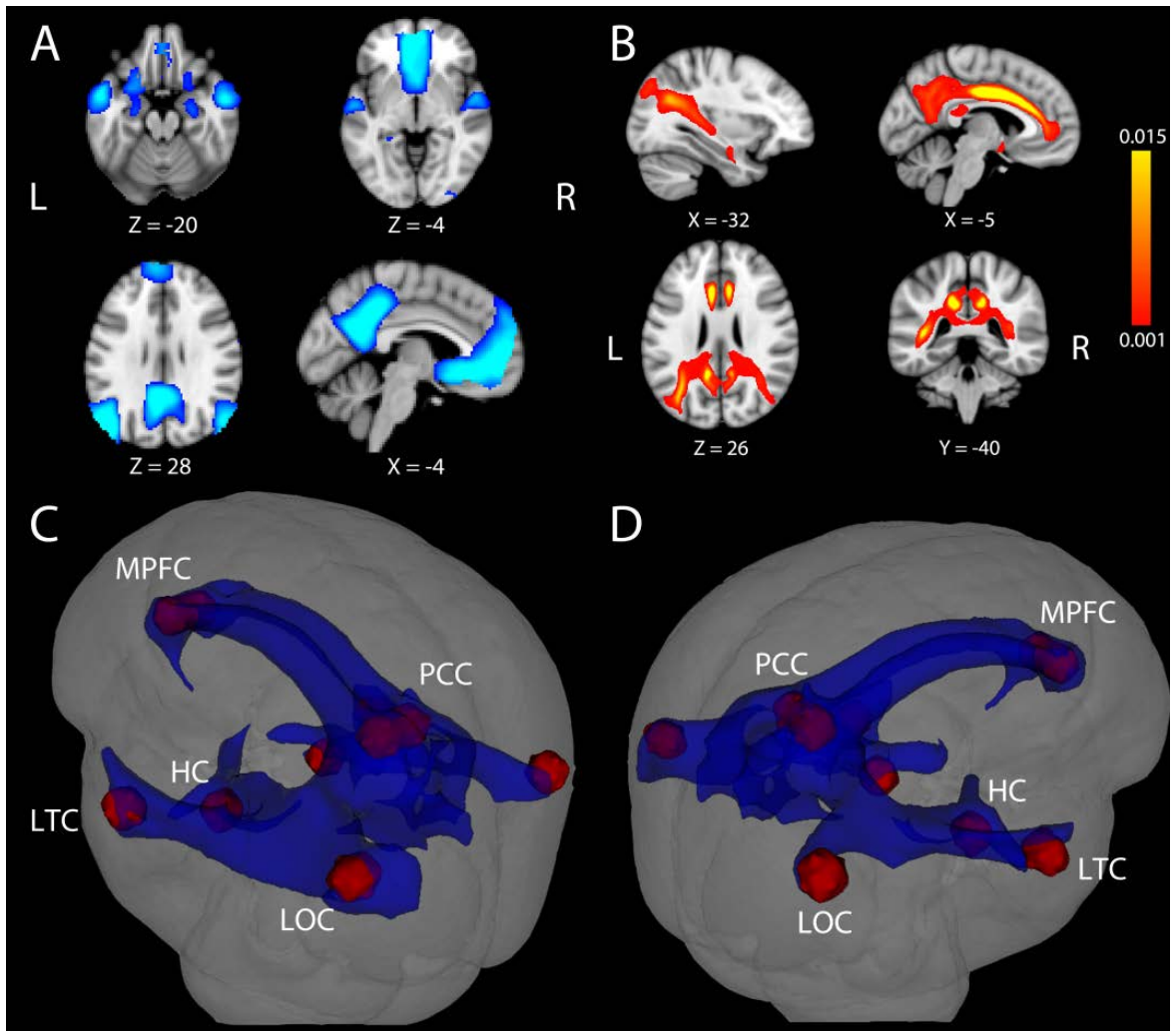
Figure 2.5. Task-induced deactivation in the DMN and DMN WM Pathways. A: Regions showing significant deactivation at FWE-corrected *p* < .05. **B:** Statistical map of probabilistic tractography indicating the proportion of streamlines passing through each voxel. The scale indicates a minimum value of 0.001 (0.1%) of all attempted streamlines passing through a given voxel, while the maximum was set at 0.015 (1.5%) of all attempted streamlines passing through a given voxel. Coordinate below each image is the MNI coordinate for that slice. **C-D:** WM pathways (blue) connecting DMN regions (red) after averaging the entire group and thresholding at 0.1% of all streamlines attempted passing through a voxel. The WM pathways shown in blue were used to extract FA in each participant. LOC, lateral occipital cortex; LTC, lateral temporal cortex; HC, hippocampus; PCC, posterior cingulate cortex; MPFC, medial prefrontal cortex.

Table 2. Peak fMRI Coordinates from Single Condition < Fixation Contrast

Region	Z-max	X	Y	Z
Left Hemisphere				
Hippocampus (HC)	6.00	-26	-14	-20
Lateral Temporal Cortex (LTC)	10.29	-58	-2	-16
Lateral Occipital Cortex (LOC)	12.06	-44	-76	34
Right Hemisphere				
Hippocampus (HC)	6.31	26	-10	-20
Lateral Temporal Cortex (LTC)	9.87	56	-2	-16
Lateral Occipital Cortex (LOC)	9.57	52	-72	30
Midline				
Posterior Cingulate Cortex (PCC)	10.81	-6	-42	40
Medial Prefrontal Cortex (MPFC)	10.81	-6	54	2

Z-max represents the peak Z-value within the cluster. X, Y, and Z are the MNI coordinates of the peak voxel within the cluster.

2.3.2. White Matter Tractography, FA and Age

Results of tractography analysis revealed a set of DMN WM paths containing connections between the fMRI cortical ROIs. This set of DMN WM paths was observed in every participant and group results showed that the paths traveled through several major WM tracts, most prominently through bilateral portions of the cingulum, superior longitudinal fasciculus (SLF), inferior longitudinal fasciculus (ILF), and fornix (Figure 2.5b-d). A 'network-level' DMN-WM mask was generated based on peak effects within these paths (as

described in 2.8.). As expected, regression analysis indicated that age was a significant predictor of FA in the DMN-WM mask (β = -.52, t = -6.49 p < .001).

2.3.3 Effects of Age, Task Condition, and their Interaction, on TID Magnitude within the DMN

There were significant main effects of Age (β = -.48, t = -2.56, p = .01) and Condition (β = .14, t = 3.47, p = .001) such that increasing age and the single condition were associated with less TID. There was also a significant Age × Condition interaction (β = -.13, t = 3.16, p = .002). Examination of this interaction (Figure 2.6a-b) indicated that age did not predict DMN TID in the single condition (β = -.05, t = 0.56, p = .58), but was a significant predictor in the mixed condition (β = -.29, t = -3.24 p = .002).
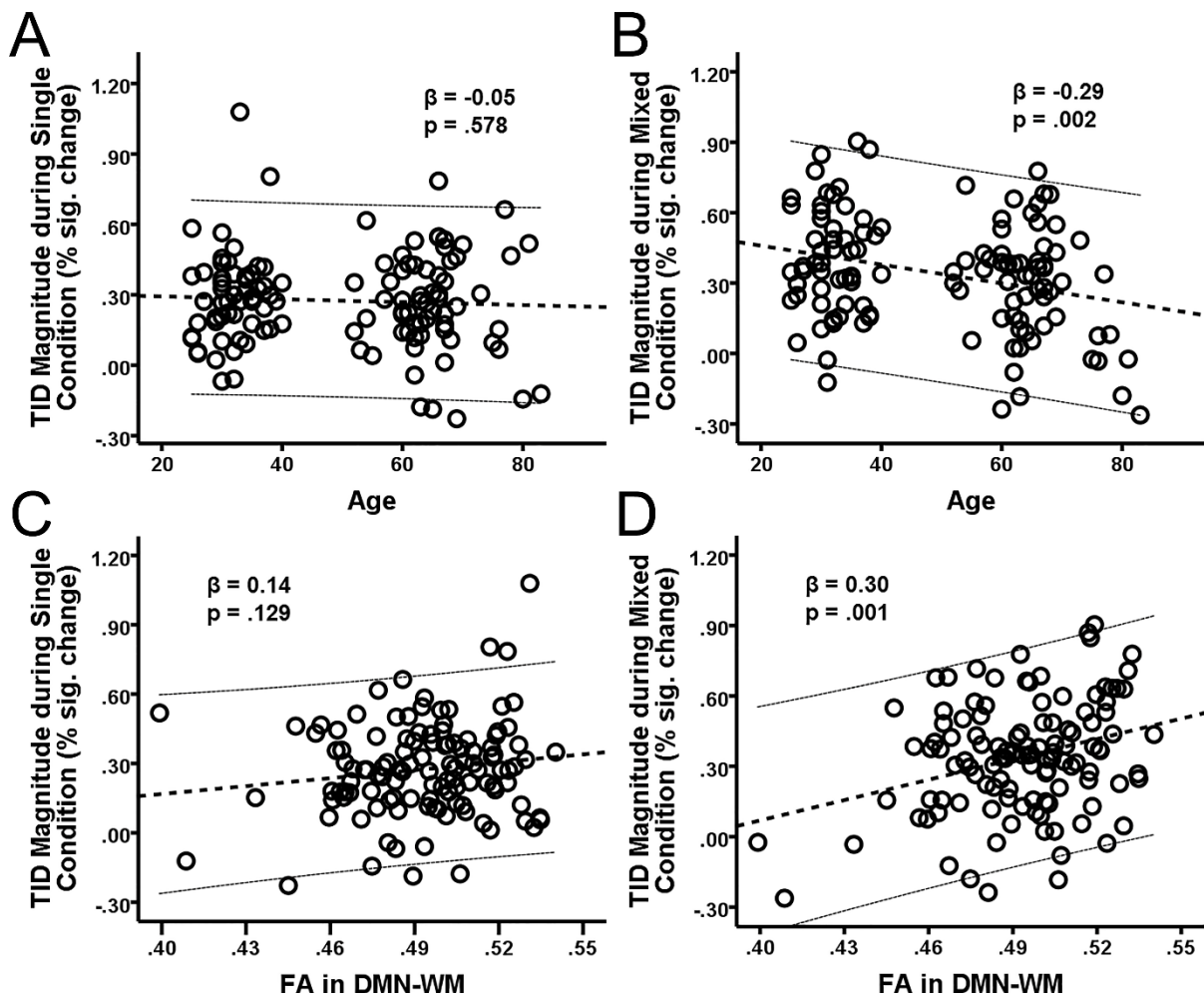
Figure 2.6. Relationship of Age and DMN WM microstructure with TID. The scatter plots show DMN TID magnitude in the single and mixed conditions (greater positive values = greater deactivation) plotted against age **(A-B)** and FA in the DMN-WM mask **(C-D)**. Neither age **(A)** nor FA in the DMN-WM mask **(C)** predicted TID in the single condition. Age **(B)** was a negative predictor and FA in the DMN-WM mask **(D)** was a positive predictor of TID magnitude in the mixed condition. Dashed lines represent the linear best fit of the data.

2.3.4 Effects of FA, Task Condition, and their Interaction, on TID Magnitude within the DMN

Results indicated a main effect of Condition (β = .14, t = 3.41, p = .001) but not of FA (β = .12, t = 1.00, p = .320). There was, however, a significant FA x Condition interaction (β = .10, t = 2.33, p = .02). Examination of this interaction (Figure 2.6c-d) indicated that FA did not predict DMN TID in the single condition (β = .14, t = 1.53, p = .13), but was a significant predictor in the mixed condition (β = .30, t = 3.42 p = .001).

2.3.5. Effects of WM within the DMN and outside the DMN on TID magnitude

WM pathways connecting TPN and DMN regions were identified using probabilistic tractography (Figure 2.7). Due to the high overlap between WM pathways connecting the TPN and DMN and those connecting DMN regions themselves (especially in areas immediately surrounding DMN seed regions), WM unique to either within-network connections (DMN-only) or between network connections (TPN-to-DMN-only) were generated.

46
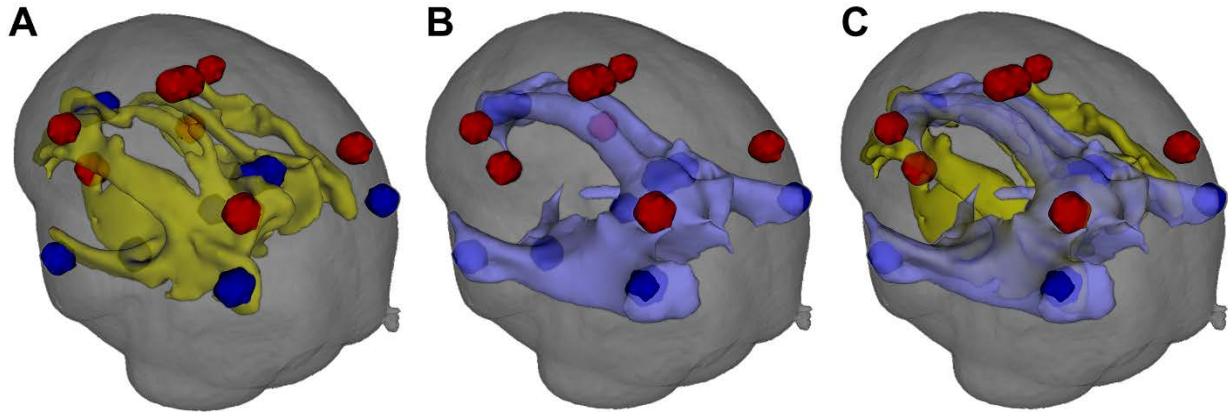
Figure 2.7. WM pathways between the TPN and DMN and within the DMN. A: The WM pathways (yellow) connecting TPN regions (red) with DMN regions (blue). Connections between the TPN and DMN were observed in the SLF, cingulum, corpus callosum, and ILF. **B:** The WM pathways (purple) connecting DMN regions (blue). **C:** The WM pathways connecting the TPN to DMN (yellow) and DMN to itself (purple) are shown together. There was high overlap between WM pathways connecting the TPN to DMN and DMN to itself, especially surrounding seed regions.

Bivariate correlations showed that FA in DMN-only WM ($r = 0.30$, $p = .001$) and TPN-to-DMN-only WM ($r = 0.28$, $p = .002$) were both significantly associated with TID magnitude during the mixed condition. FA in these WM pathways were also highly correlated with each other ($r = 0.88$, $p < .001$). Stepwise linear regression found that that the initial model with FA values from both sets of WM was significant ($F_{2,114} = 5.66$, $MSE = .054$, $p = .005$), but neither set of WM pathways was a significant predictor of TID magnitude. Backward selection led to the removal of FA in between network pathways, resulting in a final model that was significant ($F_{1,115} = 11.29$, $MSE = .054$, $p = .001$) with FA in DMN-only WM significantly predicting TID magnitude ($\beta = 0.30$, $t = 3.36$, $p = .001$). Removal of FA in between-network pathways did not result in a significant loss of variance explained in the reduced (final) model compared to the initial model ($R^2\text{-change} = -.001$, $p = 0.732$).

2.3.6. Effects of Age, FA, and DMN TID Magnitude on Task Performance

Results of the GLMs examining the effects of age, FA, and TID magnitude on task performance are presented in Table 2.3. There were main effects of both age and FA in the

DMN-WM on task performance (accuracy and RT). There was a significant Age × Condition interaction for accuracy. Examination of this interaction indicated that accuracy was only marginally predicted by age during the single condition (β = -.16, t = -1.68, p = .09), but was significantly predicted by age during the mixed condition (β = -.24, t = -2.68, p = .008). There were also marginal Age × Condition and TID magnitude × Condition interactions for RT. Examination of these interactions (Figure 2.8) indicated that age predicted RT in both the single (β = .51, t = 6.38, p < .001) and mixed (β = .46, t = 5.62 p < .001) condition, while TID magnitude predicted RT in the mixed condition (β = -.21, t = -2.32 p = .02) but not the single condition (β = .03, t = 0.31, p = .75).

Table 2.3. GLM Results for Accuracy and Reaction Time

Accuracy			
Variable (*V*)	*V*	Condition	*V* × Condition
Age	β = -.61 *t* = -3.17**	β = -.30 *t* = -7.23***	β = -.09 *t* = -2.19*
TID Magnitude	β = .09 *t* = .96	β = .32 *t* = 7.05***	β = .01 *t* = .21
FA in DMN-WM Mask	β = .43 *t* = 3.40***	β = -.30 *t* = -7.10***	β = .03 *t* = .68

Reaction Time			
Variable (*V*)	*V*	Condition	*V* × Condition
Age	β = .52, *t* = 4.90***	β = .53 *t* = 22.91***	β = .05 *t* = 1.97‡
TID Magnitude	β = .06 *t* = 1.22	β = .52 *t* = 21.41***	β = -.05 *t* = 1.83‡
FA in DMN-WM Mask	β = -.43 *t* = -6.72***	β = .53 *t* = 22.57***	β = -.01 *t* = -.53

V = Main effect of Variable, *V* × Condition = Interaction of variable and condition; ‡*p* < .10, *p* < .05, **p* < .005, ***p* < .001
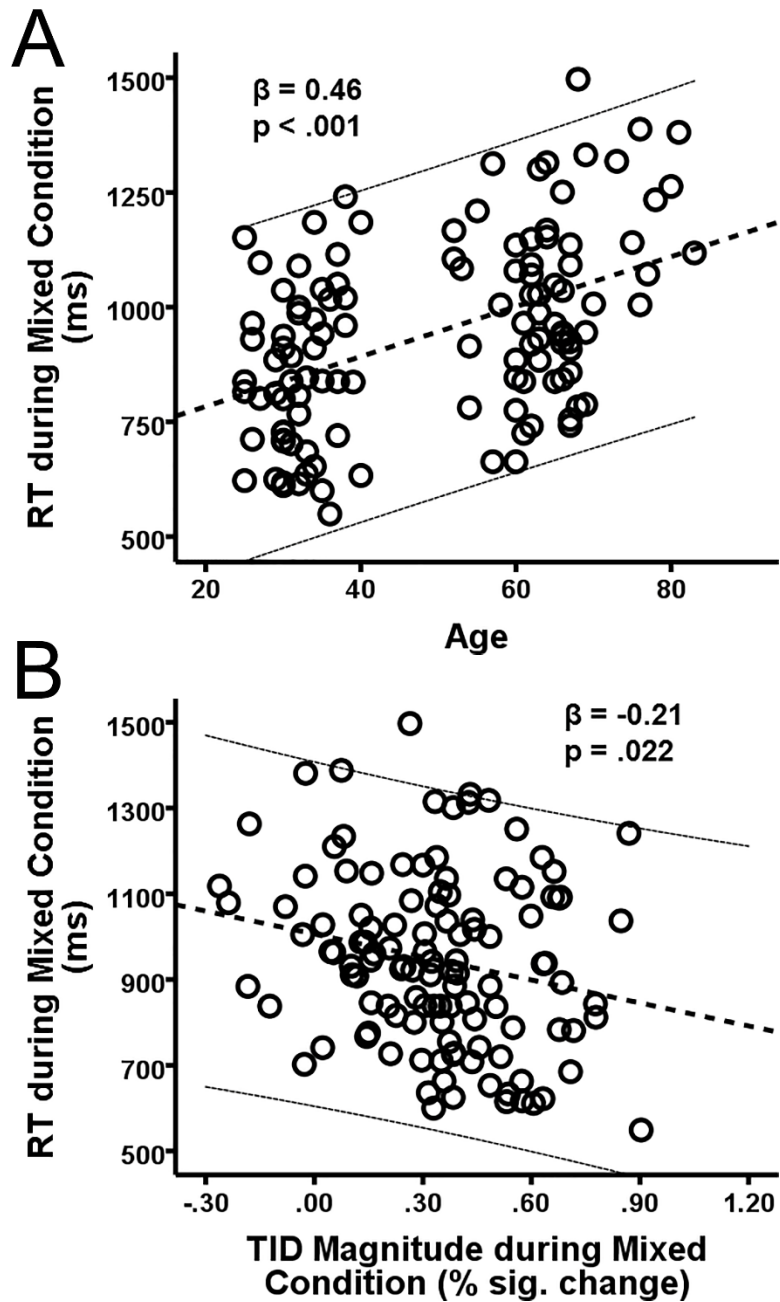
Figure 2.8. Relationship of Age and DMN TID Magnitude with RT in the Mixed Condition. RT in the mixed condition was positively predicted by age (top) and negatively predicted by TID magnitude (bottom). Dashed lines are the linear best-fit line.

2.3.7. Mediation Analyses

Mediation analyses were performed to test the hypothesis that DMN WM microstructure accounts for the relationship between age and DMN TID magnitude in the mixed condition. Two mediation models were tested: Model 1) FA in the DMN-WM mask as the mediator of the relationship between age and DMN TID magnitude and Model 2) an alternative model with age as the mediator between the FA in the DMN-WM mask and DMN TID magnitude. The alternative model (Model 2) was chosen to test whether the FA in the DMN-WM mask and DMN TID were only related because both vary together with age, a condition which requires age to mediate the relationship between the other two variables (210).

Results of Model 1 (Figure 2.9a) indicated that the direct effect of age on magnitude of DMN TID (c' = -0.18, 95% CI [-.38, .02]) was not significant, but instead was accounted for by the significant indirect pathway through FA in the DMN-WM mask (ab = -0.11, 95% CI [-.24, -.004]). Importantly, results of Model 2 (Figure 2.9b) indicated that the direct effect of FA in the DMN-WM mask on DMN TID (c' = .21, 95% CI [.01, .41]) was not significantly mediated by age (ab = .09 [-.002, .21]).
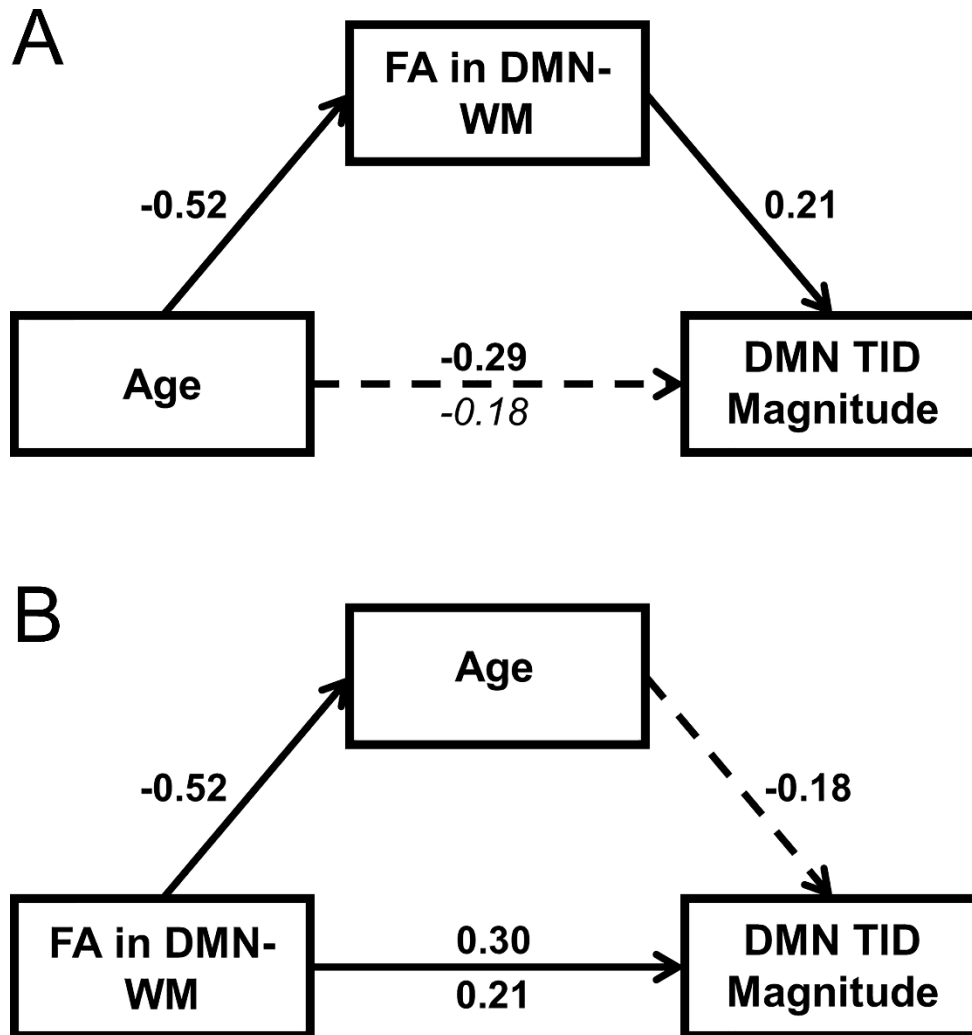
Figure 2.9. Results of Mediation Analyses. A: Age correlated with DMN TID in the mixed condition (dotted arrow), but only the indirect effect through WM microstructure was significant (shown by solid arrows). **B:** Results of Model 2: FA in DMN-WM mask had a direct effect on DMN TID in the mixed condition (solid arrow), and the indirect effect through age was non-significant (shown by dotted arrow). Values are standardized β-coefficients with significant β-values shown in bold. Total effect between the independent and dependent variable in the model is shown above the arrow, and the direct effect is shown beneath the arrow. N = 117.

Due to the small gap between ages 40 and 50 in our sample, we repeated all analyses treating age as a dichotomous variable (< 40 vs >50). The results of these analyses revealed an identical pattern (same significant effects from GLMs and mediation analyses) as those with age as a continuous variable. Additionally, further mediation

analyses were performed using FA in TPN-to-DMN-only WM instead of DMN-WM. Results of these analyses found that FA in TPN-to-DMN WM (ab = -0.10, 95% CI [-.29, .04]) did not mediate the relationship between age and DMN TID magnitude.

2.4 Discussion

We found that individual differences in DMN TID magnitude are influenced by age and task condition, and that these relationships are mediated by WM microstructure. Extending previous findings, our fMRI results indicated interactive effects of age and condition such that increasing age affected TID magnitude during the high EF demand (mixed) condition but not the low EF demand (single) condition. In addition, we found that differences in WM microstructure accounted for a significant portion of the relationship between age and DMN TID magnitude in the high EF demand condition. Our results suggest that age-related declines in WM microstructure contribute to functional regulation of DMN activity in older adults.

We observed functional deactivation in the PCC, MPFC, LOC, LTC, and hippocampus across a participant sample ranging from 25 to 83 years of age. These regions represent a central portion of the DMN in studies of younger and older adult participant groups (37,96,229). Overall TID magnitude across these regions was explored to investigate network-wide changes in DMN function associated with age and task performance. Results indicated relationships between TID magnitude, age and task performance. As expected, less TID was associated with both increasing age and poorer task performance. However, these main effects were qualified by an age by condition interaction, which indicated that increasing age was related to less DMN TID only in the mixed condition and had no effect on TID in the single condition.

In task-switching paradigms such as the present one, mixed conditions differ principally from single conditions in their increased emphasis on EF processes such as switching and inhibitory control (18,217,230). The age by condition interaction in TID that we observed is thus consistent with a view that aging is associated with decline in capacity for DMN TID as cognitive demands increase (29,105,106). Importantly, all participants performed the mixed task with high accuracy (based on a median split, the older half of participants performed the mixed task with 94.6 ± 5.5% accuracy), which indicates that the lack of TID in the mixed condition is unlikely to be due to older adults not being actively engaged in the more difficult mixed task.

We next considered the potential association between DMN TID and WM microstructure. Probabilistic tractography identified a set of WM pathways containing connections between cortical DMN structures commonly deactivated across our participant sample. As can be seen in Figure 2.5, the resulting WM network involved paths traveling through portions of midline tracts containing connections between medial temporal lobe and other limbic structures (bilateral portions of the cingulum and fornix) and long tracts containing connections between widely distributed neocortical structures (i.e. bilateral portions of the SLF and ILF). Results from our tractography analysis are consistent with known anatomical connections between DMN cortical structures and show good correspondence with tracts identified in previous DMN structural connectivity studies conducted in separate groups of younger (42,45,213) and older adults (44,193,231).

As expected, FA within the common network of DMN WM paths was negatively correlated with age. Interestingly, we found a significant FA by condition interaction, such that lower FA was associated with less TID magnitude during the mixed condition, but not associated with TID magnitude in the single condition. Several previous studies have reported correlations between FA and functional connectivity values within portions of the

DMN (44,211,213). However, the present finding of an FA by condition interaction represents the first evidence to our knowledge indicating an increased association between WM microstructure and deactivation of the DMN as task demands increase.

Importantly, we also investigated whether decreased capacity for TID might be the result of breakdown in signaling pathways from outside of the DMN. WM pathways connecting TPN regions and DMN regions were identified using tractography, and FA was extracted from these WM pathways. Results indicated that lower FA in WM pathways connecting the TPN and DMN was associated with less DMN TID. However, in a step-wise linear regression, only FA in DMN-WM was found to be a significant predictor of TID magnitude following a backward selection procedure. Previous studies have found relationships between global FA and DMN TID (26). However, these findings provide the first evidence that, while FA in other WM pathways may be related to TID, microstructure within WM pathways connecting DMN regions are the best predictor of TID magnitude. Further, these findings may suggest that diminished capacity for TID is more closely related to intrinsic properties of the DMN itself, rather than simply reflecting altered input to DMN regions from TPN regions (although this may also contribute).

An alternative possible explanation for the present results could be that DMN structure and function may undergo independent changes in aging, which could reflect either distinct or shared dependence on some other unmeasured biological correlates of aging (210). Our use of continuous variables afforded the opportunity to test between these possibilities using mediation analyses. Results of mediation analyses cannot determine causality. Nevertheless, the overall pattern of results is more consistent with a view that DMN WM microstructure contributed to age-related functional dysregulation of DMN response observed in our study rather than some other (unmeasured) biological correlate of aging.

The finding that FA was related to DMN deactivation in the mixed condition but not the single condition has implications for behavioral results showing that older adults experience more interference from internally generated distraction than younger adults during EF tasks (232). Our results suggest that age-related declines in WM microstructure within the DMN may contribute to such increased internal distraction in older adults during attention-demanding cognitive control processes. For instance, one possibility would be that intact WM connections between DMN regions may enable younger adults to efficiently regulate/reduce functional activity within the DMN in response to increased demands on cognitive processes. In contrast, poorer WM microstructure within the DMN may decrease the capacity of older adults to dampen DMN functional activity when additional resources are required by the active task. The overall outcome would be relatively greater ongoing activity in the DMN during the task, which produces increased internally-generated demands on EF processes and poorer task performance.

Although our results indicated that WM microstructure attenuated a substantial proportion of the variance (38%) in the total relationship between age and TID, they also suggest that more than half of the variance is not accounted for by WM microstructure. There are likely to be many other neurobiological contributors to age-related declines in DMN function not tested here. Amyloid load may be especially relevant as it has been linked with altered DMN activity and functional connectivity (99,155,156,233). Future work will be required to determine the separate and potentially synergistic contributions of WM microstructure and amyloid load to age-related changes in DMN functioning.

The present study has several caveats. First, in order to make stronger conclusions about the process of aging, it will be important to cross-validate these findings using a longitudinal design. Additionally, while DTI provides an indirect measure of WM microstructure, it does not directly measure axons or connections between regions. Rather,

lower WM microstructure could contribute to age-related changes in functional deactivation in a number of ways. For example, alterations in WM connectivity would be expected to affect neurotransmitter signaling and recent evidence suggests that degree of DMN deactivation in younger adults is dependent on the balance between glutamate and GABA concentrations in the pC (234). While challenging, future research should attempt to integrate fMRI, DTI and spectroscopy and/or PET to identify potentially dissociable contributions of WM microstructure and neurotransmitter release on functional dysregulation of the DMN in aging. Finally, neither the roles of gray matter atrophy nor clinically silent pathologies were assessed in the present study. Previous studies have indicated that gray matter volume is not strongly correlated with deactivation magnitudes in older adults without clinical dementia (92,164,235), and therefore likely has minimal effect. Silent pathologies such as AD and CVD cannot be ruled out in the present sample, which could account for some of the age-related changes in deactivation. Future work should look to investigate the independent and synergistic roles of various clinically silent pathologies and WM microstructure in age-related functional changes in the DMN.

In conclusion, our results suggest that reductions in dynamic modulation of DMN activity in response to increases in cognitive demands appear to scale with increasing age. In addition, the present results suggest a contribution of altered WM microstructure to functional dysregulation of the DMN, thus providing evidence for one potential mechanism underlying the failure to modulate DMN deactivation in older adults. Finally, this failure to modulate DMN activity contributes to poorer EF in older adults, which may be due to increased internally-generated distraction from ongoing DMN processes.

3. Experiment 2: White matter microstructure declines mediate diminished default-mode network deactivation and working memory performance associated with age and Alzheimer's disease pathology

3.1. Introduction

The default mode network (DMN) was initially characterized as a set of brain regions showing greater activity during baseline conditions than during attention-demanding, externally-directed cognitive tasks, a phenomena termed task-induced deactivation (TID) (35,37,61). A large body of data has since linked DMN activity with a range of internally-focused thought processes, including autobiographical memory and planning, maintenance of the self, and mind wandering (38,68,80). DMN-related thought processes are thought to be continuously active, as the network maintains low-level activity even during semi-conscious states and minimally-vegetative states (39,85,86).

TID is thought to reflect an active mechanism to prevent interference of continuously active DMN processes from disrupting processes required to address attention-demanding, externally-oriented environmental demands (100). However, capacity for TID is reduced in older adults, which contributes to poorer task performance (29,30,106). Mechanisms contributing to age-related reduction in capacity for DMN TID remain unclear. These mechanisms may be related to processes of normal aging or clinically silent pathology, which become prevalent in older adults (236).

Two pathologies harbored by a significant number of CN older adults are AD pathology and CVD pathology. AD pathology can be measured *in vivo* through either cerebrospinal fluid (CSF) concentrations of or positron-emission tomography (PET) radio-ligand binding to the AD pathological proteins, β-amyloid (Aβ$_{42}$) and tau (135,142,143,237). By utilizing these techniques, AD pathology has been observed in at least 20% of cognitively

normal (CN) older adults over the age of 65 (126,145,146). Similarly, fluid attenuated inversion recovery (FLAIR) imaging can be used to identify areas of WM hyper-intensity (WMH), which are a marker of CVD pathology (180). Studies of CN older adults have found that WMHs are present in up to 93% of these individuals (181).

Clinically-silent AD and/or CVD pathology may contribute to diminished capacity for DMN TID in CN older adults. Several studies have found that increasing AD pathology is associated with less TID in the portions of the DMN (99,153,238). In contrast, CVD pathology has been relatively understudied and results have been equivocal, with one study finding that higher WMHs were associated with less TID in a portion of the DMN (239) and another failing to find a relationship (240).

Alterations in DMN TID may also be the result of subtler changes occurring in normal aging. Through the use of diffusion tensor imaging (DTI), alterations in the density and organizational coherence of axonal and myelin membranes can be assessed through measures of WM microstructure (168,241). Studies utilizing this technique have consistently observed age-related decline in microstructure across the cortical WM pathways (160,161,171). WM is responsible for electrochemical signaling between brain regions, and age-related declines in WM microstructure have been shown to contribute to altered response in several task-positive functional brain networks (26,27,165). Results from Experiment 1 suggest that declines in WM microstructure within pathways connecting DMN regions mediate age-related declines in DMN TID (242).

However, AD and CVD pathology are also correlated with lower WM microstructure. For example, several studies have reported that higher AD pathology was associated with poorer WM microstructure in CN older adults (196,197,199). Of particular relevance to the present work, AD negatively affects microstructural properties of WM tracts connecting the DMN (DMN-WM, 154,205). Similarly, greater WMH volume is associated with lower WM

59

microstructure within the tracts affected in CN older adults (185). Further, WMHs are frequently found in areas of periventricular and frontal WM that may overlap with DMN-WM (188). Therefore, a major question is whether age-related declines in WM microstructure and increases in either AD or CVD pathology represent independent or shared contributors to diminished TID in the DMN.

The present study seeks to test these possibilities by exploring whether age, AD pathology, and CVD pathology influence DMN TID through a common pathway of declining WM microstructure or through independent, direct pathways. Younger and older adults were recruited to perform a visual working memory fMRI experiment. The visual working memory task used is a modified delayed match-to-sample paradigm with multiple targets and repeated intervening distractors, which places greater demands on executive processes (244,245). In addition, individuals underwent diffusion tensor imaging (DTI) in order to identify and measure microstructure within WM pathways connecting DMN regions. Older adults also underwent a lumbar puncture in order to measure cerebrospinal fluid (CSF) markers of AD pathology and FLAIR imaging in order to measure WMHs.

An initial bivariate analysis between DMN TID and working memory performance was used to determine whether less TID contributed to poorer task performance. Further bivariate analyses were then used to compare the relationships between age, DMN function, and DMN WM microstructure across all participants, as well as between these measures and those of AD and CVD pathology within older adults. Finally, Preacher and Hayes mediation analyses were used to test the hypothesis that WM microstructure mediated the relationships of age and AD pathology with DMN TID.

3.2. Methods

3.2.1. Participants

A total of 69 individuals (39 older adults and 30 younger adults) were recruited to participate in the present study. Written informed consent was obtained from each participant under an approved University of Kentucky Institutional Review Board protocol. Older adults were recruited from an existing longitudinal cohort at the Sanders-Brown Center on Aging (SBCoA) who are followed annually for demographic, health, and neuropsychological data (246). Cognitive normality was determined through consensus conference per the procedures outlined in the Uniform Data Set (UDS, 247). Younger adults were recruited from the University of Kentucky and the surrounding area through advertisements.

Exclusionary criteria for all participants were significant head injury (operationally defined as loss of consciousness for greater than five minutes), heart disease, psychiatric or neurological disorder, claustrophobia, pacemakers, or presence of metal fragments and/or metallic implants contraindicated for MRI. Quality control measures (described below) led to the exclusion of 4 older adults (one due to excessive motion and three due to task performance or response rate > 3 standard deviations between the group mean) and one younger adult (due to an artefact on MR images). Characteristics of the final cohort of 35 older adults and 29 younger adults are shown in Table 3.1.

3.2.2. Cerebrospinal fluid sampling (CSF) and analysis

Older adults underwent a lumbar sampling of CSF in the morning following overnight fast, as previously described (196). Samples were shipped on dry ice to the Biomarker Research Laboratory at the University of Pennsylvania Medical Center. The multiplex xMAP Luminex Platform (Luminex Corp, Austin TX) with Innogenetics (INNO-BIA, AlzBio3; Ghent, Belgium) immunoassay kit was used for analysis as previously described (127). CSF concentrations

of $A\beta_{42}$ and total tau (t-tau) were measured, and $A\beta_{42}$ and the tau/$A\beta_{42}$ ratio were used as statistical predictors due to their relative sensitivity and specificity for AD (127). These CSF values were log-transformed before statistical analyses due to their skewed distribution.

3.2.3. fMRI paradigm and behavioral analysis

Participants performed a visual working memory paradigm during fMRI scanning. The paradigm was a modified delayed-match-to-sample task (Figure 3.1) with multiple targets and repeating intervening distractors, which increases demands on executive processes (244,245). The task stimuli were two-dimensional pictures of common objects selected from Snodgrass and Vanderwart (248). During task blocks, participants were asked to 'hold in mind' the two target images and indicate (via button press) whether or not each of 12 serially presented single samples represented a match with either target image. Sample images were either one of the two target (match) images presented at the beginning of the task block or distractor (non-match) images, which were repeated between 2-4 times in a block. The ratio of targets to distractors in each block ranged from 5:7 to 7:5. During baseline blocks, participants viewed scrambled versions of sample images (created by Fast Fourier transform algorithms). Participants completed a brief practice session prior fMRI scanning.

The experiment was divided into two fMRI runs. Each run consisted of 8 task blocks (28 sec/per) and 8 visuomotor baseline blocks (10 sec/per). Responses were made using MRI compatible hand-held response button boxes, with button press response mappings counterbalanced across participants. Stimuli were presented using E-prime software (Psychology Software Tools, Inc., Pittsburgh, PA) and projected to a screen using an MRI compatible projector. Participants viewed the screen via a mirror mounted on the MRI head coil. The stimulus presentation program was used to log response time and accuracy for each working memory trial. Task accuracy was analyzed using corrected recognition (CR),

which is the hit rate (number of targets correctly identified as targets) minus the false alarm rate (number of distractors incorrectly identified as targets). Mean response time (RT) was also calculated for each individual by averaging RT on all trials.
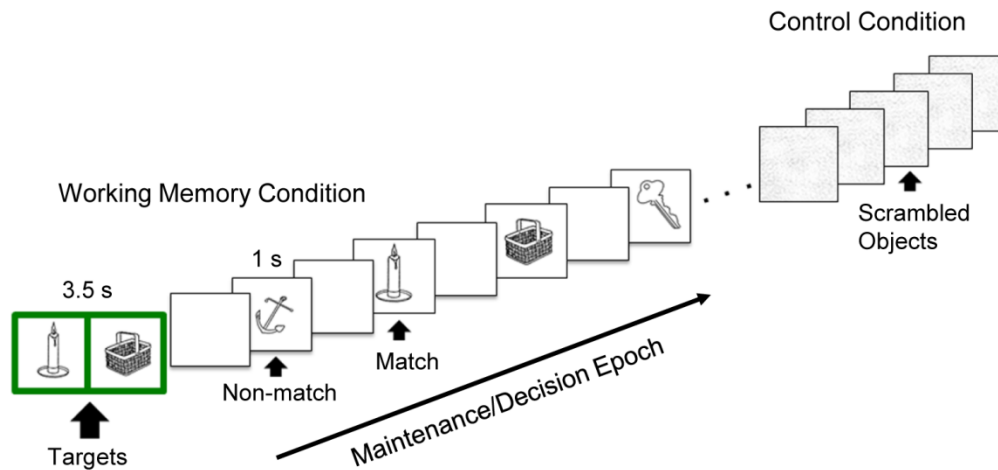
Figure 3.1. Working memory paradigm. A schematic of the working memory paradigm. Task blocks involved presentation of two target images surrounded by a green border followed by 12 single 'test' images (match or non-match). Participants were asked to hold 'in mind' the target images and decide whether each single test image represented a match, or a non-match, with either of the target images. Blank screens between images represent temporal jittering. The control condition (baseline blocks) involved viewing 5 sequentially-presented scrambled images. Analyses compared BOLD signal during a portion of the maintenance/decision epoch with BOLD signal during a portion of the control condition.

3.2.4. Imaging protocol

All participants underwent the same core imaging protocol using a Siemens Trio TIM 3 Tesla scanner with a 32-channel head coil at the University of Kentucky Magnetic Resonance Imaging and Spectroscopy Center (MRISC). The core protocol consisted of: 1) High resolution T1-weighted anatomical image, 2) Two task-based (tb)-fMRI blood-oxygen-level dependent (BOLD) T2*-weighted functional imaging runs, 3) one rs-fMRI BOLD T2*-weighted functional imaging run, and 4) diffusion tensor imaging (DTI). In addition to the

core protocol, older adults also underwent fluid-attenuated inversion recovery (FLAIR) imaging.

The high resolution T1-weighted image was acquired using a magnetization-prepared rapid echo gradient-echo (MPRAGE) sequence [Repetition time (TR) = 2530ms, Echo time (TE) = 2.26ms, inversion time (TI) = 1100ms, Flip angle (FA) = 7°, acquisition matrix = 256 × 256 × 176, field of view (FOV) = 256mm^2, 1mm isotropic voxels]. Tb- and rs-fMRI were acquired using gradient-echo echo-planar imaging (EPI) [TR = 2000ms, TE = 27ms, FA = 83°, acquisition matrix = 64 × 64, FOV = 224mm^2, 3.8mm isotropic voxels, 36 interleaved slices]. DTI was acquired using a double-refocused spin-echo EPI sequence [TR = 8000ms, TE = 96ms, FA = 90°, FOV = 224mm^2, 2mm isotropic voxels, 52 contiguous slices] with 60 non-collinear encoding directions (b = 1000s/mm^2) plus 8 images without diffusion weighting (b0). FLAIR images were collected using a fat saturated, turbo-spin echo (TSE) sequence [TR = 9000ms, TE = 89ms, TI = 2500ms, FA = 130°, acquisition matrix = 256 × 174 × 34, 1 × 1 × 4mm voxels].

3.2.5. Image pre-processing and quality control

The FMRIB Software Library [FSL, (221,249) v.5.0.9] was used for all image processing and analysis unless otherwise stated. The T1-weighted structural image was bias-field corrected using FAST and brain extracted using BET(250,251) . Each participant's structural image was registered to the MNI152 T1 2mm template using FLIRT to generate an initial linear affine transformation (252), followed by non-linear warping using FNIRT with 20mm warp resolution (223).

fMRI data were motion corrected using MCFLIRT, smoothed with an 8mm Gaussian filter, and high-pass filtered at 90s using FEAT v.6.0.0 (221). Participants with > 1.5mm root mean square relative motion were excluded (one older adult). Frame-wise displacement

(FD) was calculated using the FSL motion outlier utility, and volumes with FD > 0.5mm were considered motion outliers (253). A threshold of no more than 20% of volumes being identified as outliers was applied but did not lead to the exclusion of any functional runs. Each functional run was registered to the individual's high-resolution T1-weighted structural image using boundary-based registration (222), and then transformed into MNI152 T1 2mm space by applying the non-linear warp for the structural image (described above).

6mm Gaussian spheres were created in the lateral ventricles and frontal, temporal, parietal, and occipital WM to generate a CSF region-of-interest (ROI) and WM ROI. Time-series were extracted from both the CSF and WM ROIs for each of the functional runs. Regression was performed on each functional run using the fsl_glm utility with the following parameters: 1) Six motion parameters generated from MCLFIRT, 2) parameter for each volume classified as a motion outlier, 3) Time-series from the CSF ROI, and 4) Time-series from the WM ROI. The residuals of the regression analysis were saved as the cleaned functional data for further analyses.

3.2.6. Independent component analysis (ICA)

ICA was performed with FSL MELODIC using the concatenation approach with dimensionality set to 20 components (254). Group-level analysis was performed using the cleaned functional data for each functional run separately. In each run, a component including the canonical DMN regions was visually identified. The FSL independent component cross-correlation utility was then used to confirm high correlation between the time series of the selected DMN components from the two tb-fMRI runs. The components from the two tb-fMRI runs were then averaged together and thresholded at $p < .005$ (which met an FDR-corrected threshold of $p < .05$ using FSL's fdr utility). In order to confine analyses to DMN regions showing both TID during the task and connectivity at rest, the tb-ICA results were then masked by the DMN component identified from rs-fMRI (which was

also thresholded at $p < .005$). Clusters were then identified using a threshold of Z > 0 (as all voxels remaining had already been determined to reach significance) in order to locate peak voxels (Table 3.2). The resulting clusters were used as ROIs for time-series analyses (see Figure 3.4).

3.2.7. DMN TID analysis

Time-series were extracted across all ROIs for each participant/run/block. BOLD signal during baseline was computed by averaging the middle 6s of all baseline blocks (in order to avoid the upshoot and downshoot associated with the onset/offset of blocks). BOLD signal during the task was computed by averaging the middle 6s of all working memory blocks (to parallel sampling of the baseline blocks). TID was then computed as percent signal change by subtracting the BOLD signal during the task from the BOLD signal during baseline, dividing by the BOLD signal during baseline and multiplying by 100. The sign of percent signal change was then inverted to indicate the magnitude of TID for ease of interpretation of findings (i.e. more positive TID magnitude = more negative % signal change during the task).

3.2.8. DTI analysis

FMRIB's Diffusion Toolbox (FDT) v.3.0 was used for pre-processing and analyses. FSL's EDDY tool v. 5.0.8 was used for motion and eddy-current correction with automatic replacement of outlier volumes (255,256). The b0 images were averaged to form a single b0 image, which was then brain extracted using BET in order to form a brain mask for DTI data. DTIFIT was used to fit a voxel-wise tensor model, and each participant's FA image was registered to the FMRIB58 1mm template using the tract-based spatial statistics (TBSS) pipeline (224). Data were projected onto a group skeleton with a threshold of FA > 0.2mm to minimize partial volume effects and correct for residual misalignments.

In order to identify WM pathways connecting DMN cortical regions, probabilistic tractography was performed. BEDPOSTX was used to fit a probabilistic diffusion model with 3 fibers in each voxel (226,227). PROBTRACKX2 was run in network mode using modified Euler streamlining with parameters described previously (242). Before use as seeds for tractography, the functionally-defined DMN ROIs were transformed to the FMRIB FA 1mm template using the resultant parameters from registering the MNI152 T1 2mm template to the FMRIB FA 1mm template using FLIRT. The DMN ROIs were then transformed to each participant's native diffusion space using the inverse of the non-linear warp generated in TBSS (described above). Additionally, a mask of the brain stem from the Harvard-Oxford Structural Atlas, which was used as an exclusion mask to avoid descending tracts, was transformed from FMRIB FA 1mm space to each participant's native diffusion space.

Successful streamlines were those originating in one DMN cortical seed and passing through another DMN cortical seed without passing through the brainstem exclusion mask or violating any of the other tractography parameters. A group template of DMN WM pathways was formed in FMRIB FA 1mm space using a series of steps described in our previous work (199). The resulting DMN-WM group template was then masked by the mean FA skeleton generated in TBSS to minimize partial volume effects, resulting in a skeletonized DMN-WM group template. Mean FA was then extracted from the skeletonized DMN-WM group template in all participants.

3.2.9. FLAIR analysis

A semi-automated process (Figure 3.2) was used to identify white matter hyperintensities (WMH) on older adult FLAIR images using a framework similar to one previously described (257). Briefly, FreeSurfer (258,259) segmentation was performed on each participants' T1-image to create a WM template. Following registration to the 3D-FLAIR brain using FLIRT, the T1-WM template was dilated using MIPAV and a 1mm Gaussian blur was applied using

FSL's SUSAN. This WM template was then used to mask the 3D-FLAIR image. A two-Gaussian model was used to fit a voxel intensity histogram, from which the mean and standard deviation of the dominant (normal appearing WM) Gaussian fit were identified. These values were then used to threshold the FLAIR-WM image to include only voxels > 2.33 SD above the mean in order to form a WMH mask. The WMH mask was manually edited to remove artefactual voxels in regions between the lateral ventricles and in inferior slices (257). WMH volumes were then computed for each older adult. In addition, FLAIR images were used to compute estimates of WMHs related to WM within the DMN of older adults (described below).
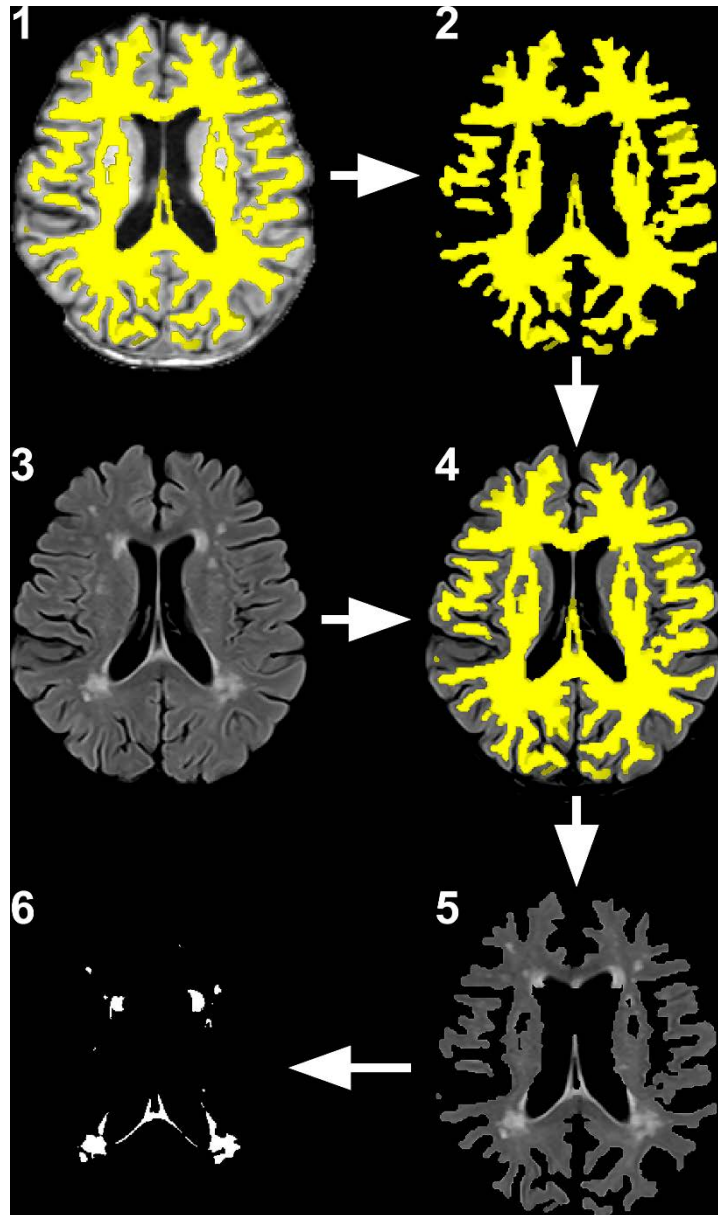
Figure 3.2. Overview of the WMH pipeline. 1: Inhomogeneity-corrected high-resolution T1-weighted images were segmented using FreeSurfer in order to identify WM (yellow). **2:** Results of segmentation were smoothed and dilated to create a final WM mask (yellow). **3:** The FLAIR image was inhomogeneity corrected using the N3 algorithm in MIPAV. **4:** The WM mask was registered the inhomogeneity-corrected FLAIR image using a linear transformation matrix generated from registration of the T1 image to the FLAIR image. **5:** The WM mask was used to form a FLAIR WM image. The voxel intensity distribution of this image was plotted and the mean and standard deviation of the dominant appearing curve was used to calculate the threshold of 2.33 SDs above the mean. **6:** Thresholding the image at 2.33 SDs above the normal appearing WM mean identified areas of WMH, which were then manually edited to exclude artefactual areas between the lateral ventricles and in inferior slices.

3.2.10. Computing FA in Normal Appearing WM in Older Adults

This analysis sought to estimate FA in the DMN-WM of older adults within regions free from WMH, that is, areas of normal appearing WM (naWM; all WM was considered naWM in younger adults, in whom WMHs are rare). The first step was to generate a DMN naWM mask by registering older adult's WMH masks to their DTI space using the following steps: The FLAIR image of each older adult was registered to their b0 image using FLIRT, and the resultant parameters were used to transform each participant's WMH mask to native DTI space. The TBSS non-FA pipeline was then used to register each participant's WMH mask to the mean group skeleton in FMRIB FA 1mm space. A DMN naWM mask was then generated for each older adult by subtracting their WMH-mask from the group skeletonized DMN mask. FA was then extracted from the DMN-naWM skeletonized mask in each older adult.

3.2.11. Computing WMH volume in the DMN-WM of Older Adults

This analysis sought to estimate the percentage of voxels within the DMN-WM of older adults affected by WMHs (Figure 3.3). DMN-WMH volume was calculated for older adults by masking each individual's WMH image by the unskeletonized DMN-WM mask. The volumes of non-zero voxels were computed using fslstats and divided by the volume of the DMN-WM mask in order to calculate the % of DMN WM identified as WMH.
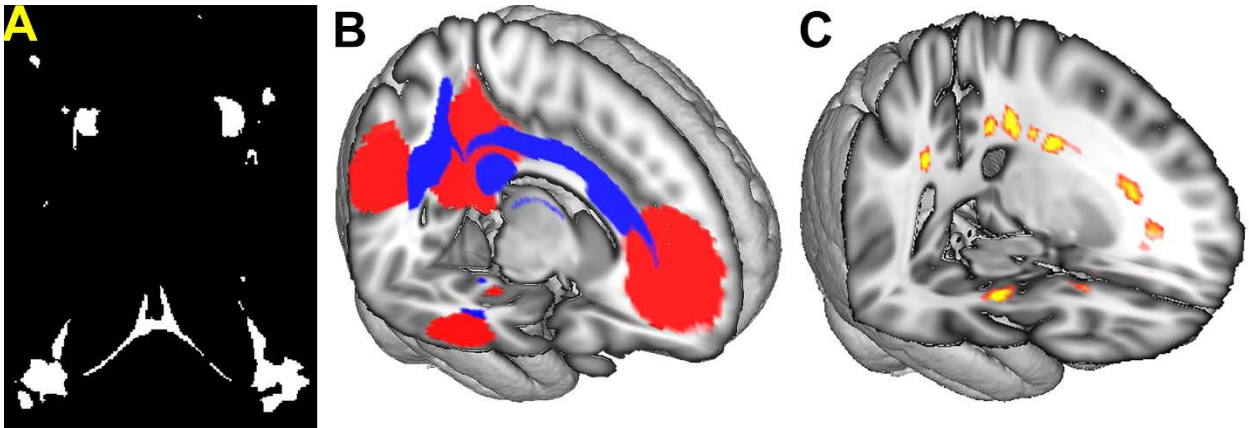
Figure 3.3. Identification of DMN WMH. A: Example of WMHs identified using the pipeline described in 3.2.9 (same as panel 6 in Figure 3.2). **B:** DMN WM pathways identified using methods described in 3.2.8 (see 3.3.3 and Figure 3.7 for more detailed description of results). **C:** WMHs located within DMN WM pathways were identified by masking WMHs **(A)** with the DMN-WM mask **(B)**.

3.2.12. Statistical analysis

SPSS 23 (IBM, Chicago, IL) was used for all statistical analyses. Paired t-tests were performed to determine the difference between FA in DMN-WM and DMN-naWM within older adults. FA in DMN-naWM was used in all further analyses. Bivariate relationships were explored using partial correlations controlling for sex and education when testing age effects across all participants and controlling for age, sex, and education when testing effects of pathology within older adults. As bivariate relationships were primarily used to determine variables to use for mediation analyses, a liberal significance threshold of $p < .05$ was used.

Multivariate relationships were explored using Preacher and Hayes mediation analyses using the PROCESS macro for SPSS (207). Preacher and Hayes mediation uses multiple linear regression methods to simultaneously test direct and indirect effects and uses Monte-Carlo confidence intervals (CI) to assess significance. Effects that had 95% CIs that did not cross 0 were considered significant. In order to test whether the effects of age and pathology on DMN TID were mediated by DMN-naWM, separate mediation analyses were performed to test whether DMN-naWM mediated the effects of age and pathology on DMN

TID. Alternative models were also tested in order to determine if DMN-naWM had a direct effect on DMN TID or if it was mediated by either age or pathology.

3.3. Results

Younger and older adults did not differ in male:female ratio ($\chi^2 = 0.03$, $p = 0.87$) or years of education ($t = 0.26$, $df = 62$, $p = 0.80$). Demographic and mean outcome measures are shown in Table 3.1. Older adults had significantly lower corrected recognition (CR; $t = -4.29$, $df = 62$, $p < .001$) and higher reaction time (RT; $t = 9.59$, $df = 62$, $p < .001$) compared to younger adults (Figure 3.4). Further, CR was inversely correlated with RT after controlling for age, sex, and education ($r = -0.31$, $df = 59$, $p = .017$).
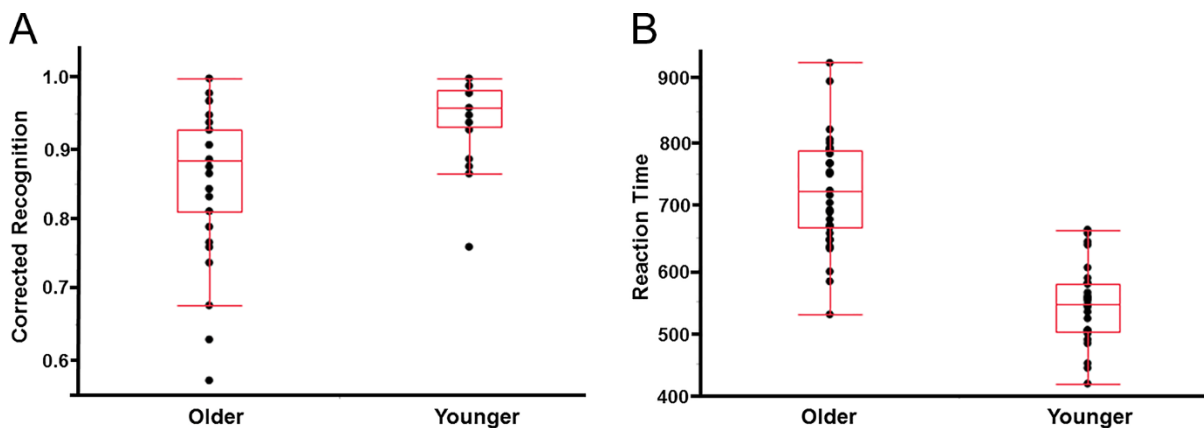
Figure 3.4. Working memory performance. A: Corrected recognition was lower in older adults compared to younger adults. There was also greater variability in older adult performance compared to younger adult performance, mostly due to a ceiling effect in performance. **B:** Reaction time was slower in older adults compared to younger adults.

Table 3.1. Group demographics and mean outcome measures

	Younger adults (n = 29)	Older adults (n = 35)
Age (Years)	24.14 ± 3.88	76.69 ± 7.15
M:F	12:17	15:20
Education (Years)	16.59 ± 2.10	16.64 ± 2.41
Corrected Recognition	0.947 ± 0.052	0.861 ± 0.098
Reaction Time (ms)	543.1 ± 61.9	725.1 ± 85.3
DMN TID (% signal change)	-0.15 ± 0.09	-0.09 ± 0.12
FA in all DMN-WM	0.62 ± 0.01	0.57 ± 0.030
FA in DMN naWM	0.62 ± 0.01	0.58 ± 0.027
Total WMH Volume (%ICV)	--	0.44 ± 0.24
DMN WMH Volume (% DMN WM)	--	3.63 ± 3.15
CSF $A\beta_{42}$ (pg/mL)	--	271.1 ± 80.6
CSF t-tau/$A\beta_{42}$ ratio	--	0.23 ± 0.14

Values are mean ± standard deviation.

3.3.1. ICA results

The ICA analyses for each tb-fMRI run produced a component that included DMN regions and other non-DMN (task-specific) regions. Cross-correlation between the component from each run was high (r = 0.95). After averaging, thresholding at an FDR-corrected level of $p <$ .005 (Figure 3.5a), and masking by the rs-fMRI DMN component (Figure 3.5b), the final set of DMN regions (Figure 3.5c) consisted of: the midline posterior cingulate cortex/precuneus (PCC/pC) and ventromedial prefrontal cortex (vMPFC), as well as bilateral dorsal medial prefrontal cortex (dMPFC), lateral occipital/parietal cortices (LOC/LPC), and lateral temporal cortices (LTC). In addition, the DMN included the right hippocampus (HC) and left parahippocampal gyrus (PHG). Peak coordinates for each of these regions are shown in

Table 3.2. One-way t-tests found that both younger and older adults showed significant TID

(t = 8.93, 4.41; df = 28, 34; p < .001) during the working memory task across the DMN.
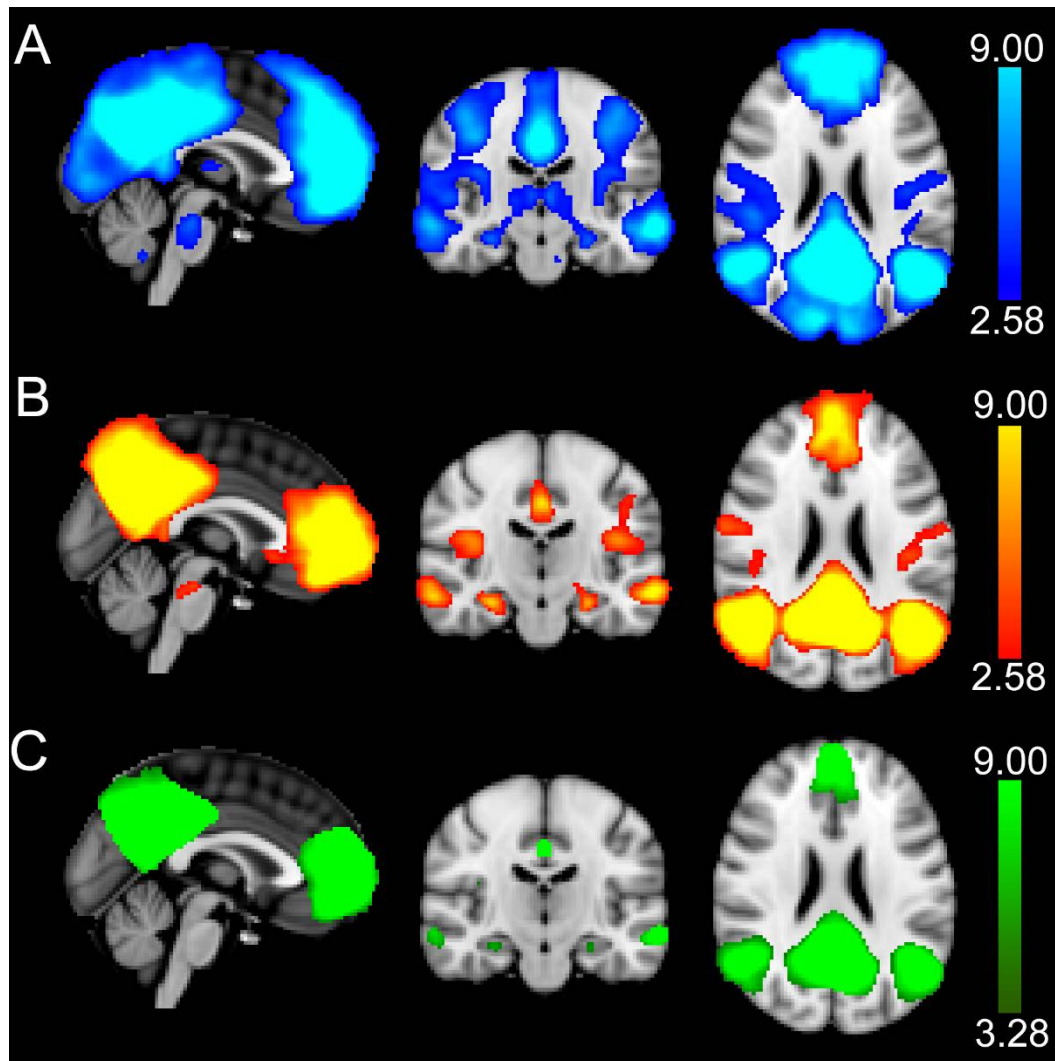
Figure 3.5. Identification of DMN. ICA was performed separately for each task-based run and then averaged together **(A)**. The task-based DMN was then masked by the DMN component identified in rs-fMRI data **(B)** to form a final mask of DMN regions **(C)**. The clusters in this final mask were sued for all functional analyses and as seeds for probabilistic tractography. **A-C**: The DMN regions overlaid on top of the MNI151 T1 2mm^3 standard brain. Color scale is shown to the right, with values representing the minimum and maximum Z-values shown.

Table 3.2. Peak coordinates of ROIs

Region	Peak Z	# Voxels	MNI X	MNI Y	MNI Z
Midline					
Posterior cingulate cortex	33.7	9050	-6	-52	26
Ventral medial prefrontal cortex	24.8	5481	-2	56	-2
Left Hemisphere					
Lateral occipital/parietal cortex	24.2	2965	-44	-68	36
Dorsal medial prefrontal cortex	20.4	1042	-18	34	44
Lateral temporal cortex	14.4	557	-60	-10	-14
Parahippocampal gyrus	7.12	218	-24	-36	-10
Right Hemisphere					
Lateral occipital/parietal cortex	17.1	2322	52	-60	34
Dorsal medial prefrontal cortex	14.4	790	22	36	42
Lateral temporal cortex	12.4	696	60	-6	-16
Hippocampus	5.16	78	30	-20	-16

Peak coordinates for ROIs are the peak Z-value from the average tb-DMN after masking with the rs-DMN. The number of voxels is the total number of voxel belonging to the cluster (size of each ROI)

3.3.2. Association between DMN TID and Working Memory Performance

Partial correlations were performed between DMN TID and working memory performance across all participants and within older adults. There was no association between DMN TID and CR on the working memory task across all participants or within older adults ($r = 0.16$, $df = 60$, $p > .21$). However, significant relationships (Figure 3.6) were observed between less DMN TID and slower RT on the working memory task across all participants ($r = -0.41$, $df =$

60, *p* = .001) and within older adults (*r* = -0.59, *df* = 30, *p* < .001), but not in younger adults (*r* = 0.16, *df* = 24, *p* = .434).
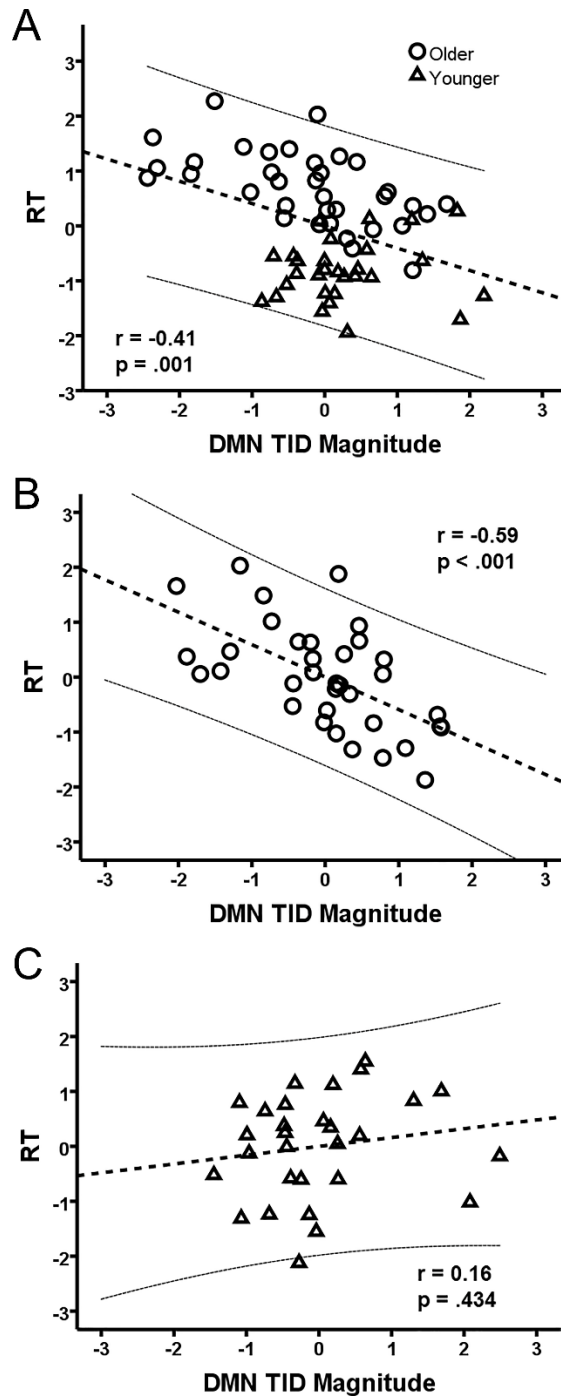
Figure 3.6. Relationship between DMN TID and working memory performance. Scatter plots of RT against DMN TID across all participants **(A)** and within older adults **(B)** show a significant inverse relationship, while there was no significant relationship within younger

adults **(C)**. Values are standardized residuals after regressing out the effects of sex and education **(A)** or age, sex, and education **(B-C)**. The r- and p-values are for the linear best fit (thick dashed line). Thin dashed lines indicate the 95% confidence interval for the predicted response.

3.3.3. Probabilistic tractography results

A common set of DMN WM pathways (tracts connecting DMN cortical regions) was

identified across younger and older adults (Figure 3.7a-c). The common DMN WM pathways

included midline association tracts (cingulum and fornix), lateral association tracts (inferior

fronto-occipital fasciculus, superior longitudinal fasciculus, and inferior longitudinal

fasciculus) and commissural tracts (genu and splenium of the corpus callosum).
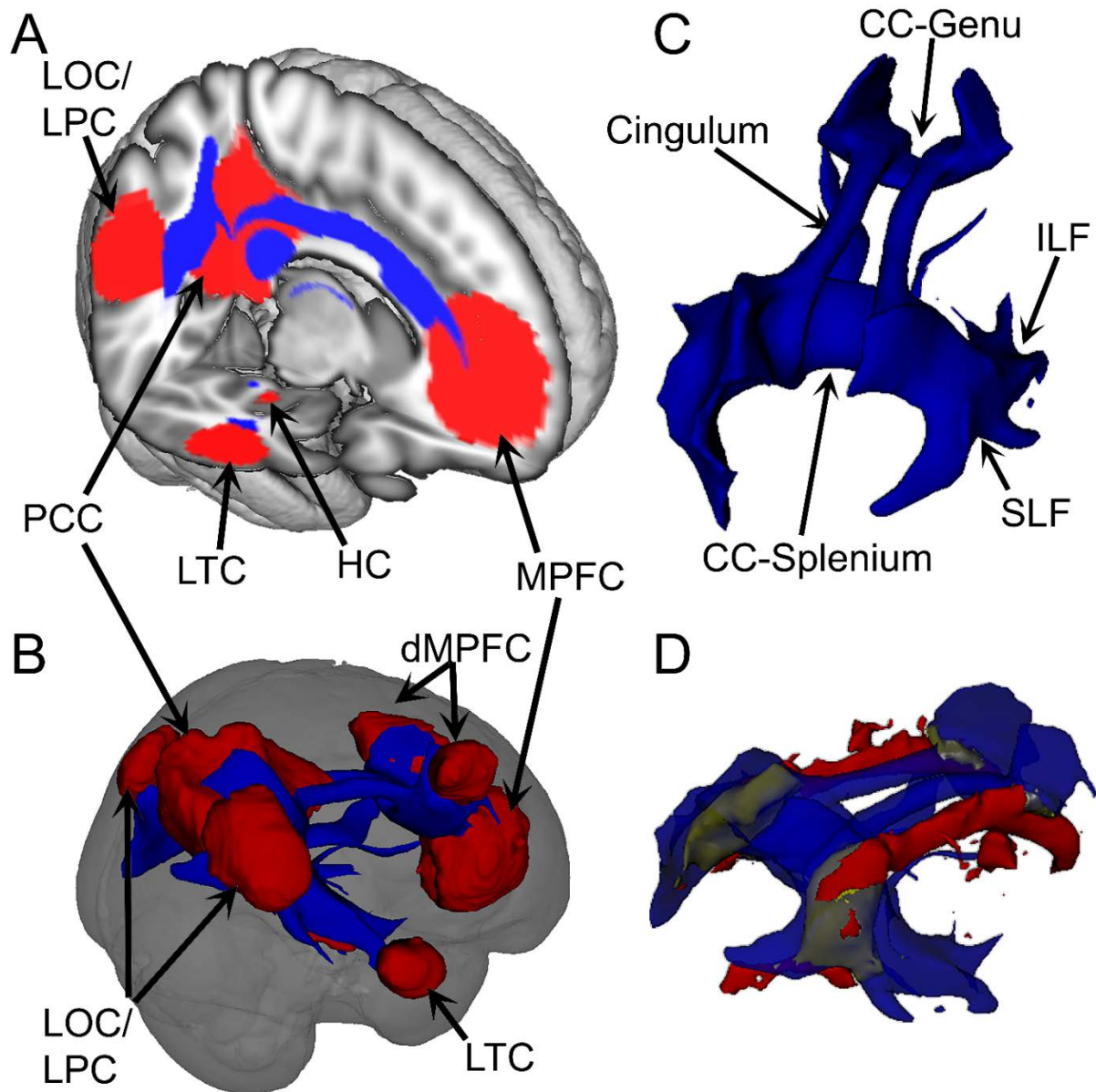
Figure 3.7. Results of probabilistic tractography and WMH analyses. The group template formed from combining individual tractography results is shown. **A-B:** Seeds used for tractography (red) and WM pathways connecting these seeds (blue). **C:** DMN WM pathways include portions of the cingulum, fornix, corpus callosum splenium and genu, superior and inferior longitudinal fasciculi, and other unnamed association tracts. **D:** Voxels classified as WMH in at least 2 participants that overlapped (green) or did not overlap (red) with DMN WM show that DMN WM pathways are relatively spared from WMH. PCC: posterior cingulate cortex, MPFC: medial prefrontal cortex, dMPFC: dorsal medial prefrontal cortex, LTC: lateral temporal cortex, LOC/LPC: lateral occipital/parietal cortex, HC: hippocampus, CC: corpus callosum, SLF: superior longitudinal fasciculus, ILF: inferior longitudinal fasciculus.

3.3.4. WMHs in the DMN-WM of Older Adults

On average, 3.6 ± 3.1% of all DMN WM voxels (median = 2.4%, range = 0.4-13%) were affected by WMHs. For visualization purposes, a mean WMH mask thresholded to show voxels in which at least 2 participants had a WMH was created and overlaid on the DMN WM template (Figure 3.7d). Within older adults, FA in all DMN-WM was significantly lower that FA in DMN-naWM (t = -5.29, df = 34, p < .001). Further, DMN-WMH volume was correlated with FA in all DMN-WM (r = -0.48, df = 30, p = .005) but not with FA in DMN-naWM (r = -0.29, df = 30, p = .11) after controlling for age, sex, and education within older adults. Repeating the analyses without age as a covariate resulted in similar results, although DMN-WMH volume was marginally correlated with FA in DMN-naWM (r = -0.32, df = 31, p = .06).

3.3.5. Age-related alterations in DMN function and WM microstructure

Increasing age was associated with less DMN TID (r = -0.26, df = 60, p = .043) and lower FA in DMN-naWM (r = -0.76, df = 60, p < .001). Further, lower FA in DMN-naWM was associated with less DMN TID (r = 0.38, df = 60, p = .002). Results of Preacher and Hayes mediation analyses (Figure 3.8a), revealed that FA in DMN-naWM mediated the effect of age on DMN TID magnitude (ab = -0.32 [-0.62, -0.07], c' = 0.06 [-0.30, 0.43]). In contrast, the alternative model (Figure 3.8b), revealed that DMN-naWM had a direct effect on DMN TID that was not mediated by age (c' = 0.44 [0.06, 0.82], ab = -0.05 [-0.32, 0.24].
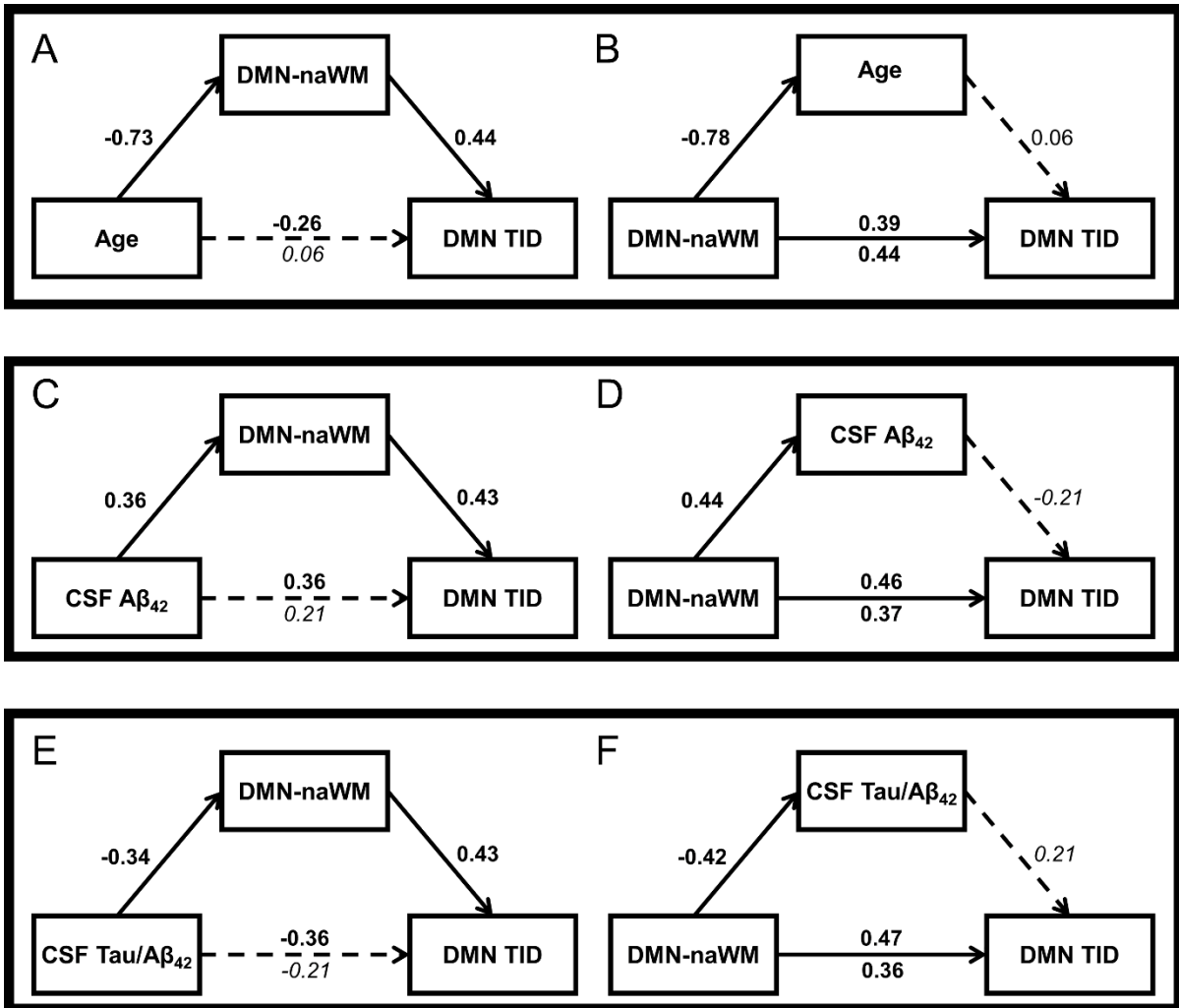
Figure 3.8. Results of age mediation analyses. A-B: Results of mediation analyses show that FA in DMN-naWM mediates the relationship between age and DMN TID magnitude across all participants, but age does not mediate the relationship between FA in DMN-naWM and DMN TID magnitude. **C-F:** Results of mediation analyses show that the FA in DMN-naWM mediates the relationship between CSF Aβ₄₂ and DMN TID **(B)** and between CSF tau/Aβ₄₂ and DMN TID **(D)**. The alternative models found that neither CSF Aβ₄₂ **(D)** or CSF tau/Aβ₄₂ **(F)** mediated the relationship between FA in DMN-naWM and DMN TID. Instead, there was a direct effect of DMN-naWM on DMN TID and AD pathology, but AD pathology was not related to DMN TID in the presence of DMN-naWM. **A-F:** Values are standardized β-coefficients, with significant paths shown as solid lines with bold β-values, while non-significant paths are shown as dashed lines with β-values in italics. Values above the horizontal arrow are the total effect (c) and values below the arrow are the direct effect (c').

3.3.6. AD pathology related alterations in DMN function and WM microstructure

Results of bivariate relationships are shown in Table 3.3. Significant relationships were observed between AD markers (CSF $A\beta_{42}$ and tau/$A\beta_{42}$), DMN TID, and FA in DMN-naWM. DMN WMH volume was not correlated with AD pathology or DMN TID. Results of mediation analyses (Figure 3.8c-f) found that the relationship between $A\beta_{42}$ and DMN TID magnitude was mediated by FA in DMN-naWM (ab = 0.15 [0.02, 0.47], c' = 0.21 [-0.16, 0.59]). Similarly, the relationship between the tau/$A\beta_{42}$ ratio and DMN TID magnitude was also mediated by FA in DMN-naWM (ab = -0.15 [-0.49, -0.003], c' = -0.21 [-0.58, 0.15]). In contrast, neither $A\beta_{42}$ (ab = 0.11 [-0.06, 0.35]) nor tau/$A\beta_{42}$ ratio (ab = 0.11 [-0.03, 0.41]) mediated the relationship between FA in DMN-naWM and DMN TID magnitude.

Table 3.3. Bivariate relationships within older adults

	Lg($A\beta_{42}$)	Lg(Tau/$A\beta_{42}$)	DMN WMH Volume	FA in DMN-naWM	DMN TID
Lg($A\beta_{42}$)	--	**-0.77**	*-0.18*	**0.43**	**0.36**
		(<.001)	*(.333)*	**(.014)**	**(.043)**
Lg(Tau/$A\beta_{42}$)		--	*-0.11*	**-0.41**	**-0.36**
			(.566)	**(.020)**	**(.045)**
DMN WMH Volume			--	*-0.29*	*-0.09*
				(.105)	*(.611)*
FA in DMN-naWM				--	**0.44**
					(.012)

Values are partial correlation coefficients while controlling for age, sex, and education. P-values are shown in parentheses, with significant relationships in BOLD and non-significant relationships italicized. All tests had *df* = 30.

3.4. Discussion

These results provide novel evidence that age-related declines in WM microstructural properties contribute to diminished DMN TID associated with age and AD pathology. Consistent with previous findings, age-related reduction in TID was associated with poorer task performance in CN older adults. In addition, TID was negatively affected by both age and AD pathology. However, the effects of age and AD pathology on DMN TID were driven by a shared pathway through disruption of WM microstructure. Together these findings suggest that disruptive effects of age and AD pathology on DMN function may operate in part via a "double-hit" on WM microstructure.

3.4.1. TID magnitude is positively associated with working memory performance

The DMN is defined by high levels of connectivity at rest and deactivation during some externally-directed cognitive tasks (35,37,65). However, portions of the DMN may not deactivate during certain tasks that place demands on the cognitive processes carried out by those regions (38,80). Further, many regions that do not belong to the DMN show TID in a task-dependent manner (33,34). Therefore, we focused on the DMN response relevant to EF by masking regions showing TID during a working memory task by a resting-state DMN identified in the same participants in order to identify regions showing both TID and rsC. This approach identified a set of DMN regions including the midline PCC and vMPFC, bilateral LOC/LPC, LTC, and dMPFC, as well as right HC and left PHG (24,25,37).

As expected, TID in the DMN was reduced in older compared to younger adults. Further, within older adults, lower TID was associated with slower working memory performance, which is consistent with the view that DMN TID is of functional relevance to executive task performance (29,30,242). It is noteworthy that slower performance reflected poorer performance on our working memory task, rather than a speed-accuracy trade-off, as

there was a negative relationship between working memory RT and accuracy. The reason for the lack of correlation between DMN TID and CR is unclear but may be due to near ceiling performance on the task. Nevertheless, the relationship between less TID and poorer task performance is thought to reflect that greater ongoing activity in the DMN during the task (less TID) increases interference with task-relevant executive control processes(29,242).

3.4.2. TID is associated with microstructural declines in WM connecting DMN regions

We sought to understand the extent to which diminished TID in the DMN is associated with reduced anatomical connectivity between DMN cortical regions. Probabilistic tractography used functionally-defined seed regions to identify WM pathways connecting DMN regions in each individual. A group template was generated using a previously established method in order to identify the average paths connecting DMN regions across younger and older adults, which has been shown to minimize bias towards one age group (199). This approach identified a core set of tracts prominently involving paths connecting limbic structures (cingulum and fornix), cross-hemispheric pathways (CC-genu and CC-splenium), and long cortico-cortical association pathways (SLF, ILF, IFOF).

Consistent with previous work, our results indicated that altered microstructure within WM pathways regions connecting DMN regions (DMN WM) was associated with DMN TID during executive task performance (26,242). Decline in WM microstructure through decreased axonal, myelin, and/or synaptic density is thought to contribute to a noisier signaling environment (165,260,261). Our results suggest that capacity for DMN TID is disrupted by a noisy WM signaling environment. One possibility would be that a noisier signaling environment may negatively impact the efficiency of synaptic communication by disrupting temporal and spatial summative processes. This disruption of synaptic communication may reduce the capacity of older adults to dampen DMN activity during a

demanding executive tasks (242). Thus, greater ongoing activity in the DMN results in increased interference from internally-generated thought processes and poorer task performance (29,242).

3.4.3. DMN WMHs play a minor role in altered DMN structure and function in older adults

WMH distribution was heterogeneous across individuals. However, periventricular WMHs were common (continuous anterior-posterior band in Figure 3.7d). Interestingly, WMHs showed minimal overlap with DMN WM, affecting ~3.5% of all DMN WM. The main areas of overlap were in periventricular regions, especially at the posterior horn of the lateral ventricles. While there was a significant inverse relationship between WMH volume and microstructure in all DMN WM, there was no relationship with microstructure in DMN naWM (which represented nearly 97% of all DMN-WM). Finally, DMN TID was not correlated with DMN WMH volume. Together, these findings suggest that early-stage CVD pathology in CN older adults, due to its relatively circumscribed periventricular distribution, does not appear to significantly affect DMN function. Future research should explore the effects of WMH on DMN function in later disease stages as pathology becomes more advanced and widespread (188,262).

3.4.4. DMN WM microstructure is negatively associated with increasing age and AD pathology

Increasing age and increasing levels of AD pathology were associated with altered in microstructure within naWM of DMN pathways. Age-related reductions in WM microstructure are well-established (160,161,171). More recently, several studies have reported negative associations between WM microstructure and AD pathology (196–198). The present results show that AD pathology is associated with lower FA in a distributed set of tracts inter-connecting the DMN. In contrast to WMHs, microstructural alterations within naWM are

thought to reflect subtler alterations in the quality of WM (263). These alterations may include decreases in the density of axonal and/or myelin membranes (168). The relationships between age and AD pathology with microstructure in naWM along with the lack of relationship of DMN WMH volume with age or AD pathology suggest that age and AD pathology are associated with these subtle alterations in axonal/myelin integrity in a manner that is independent of CVD pathology.

3.4.5. WM microstructure mediates relationships between age/AD pathology and DMN function

The most important finding of the present study is that both age and AD pathology are associated with less DMN TID through a common pathway of lower FA in DMN WM (Figure 3.9). These results may suggest that a potential "double hit" of increasing age and AD pathology on WM microstructure contributes to diminished DMN TID in older adults. However, it remains unclear if the relationships we observed generalize to clinical populations. Future studies should seek to understand these effects in individuals with more diminished DMN TID, such as those with mild cognitive impairment or AD (95,98). Nevertheless, the current results underline the importance of elucidating the mechanisms underlying WM microstructure declines in aging and AD.
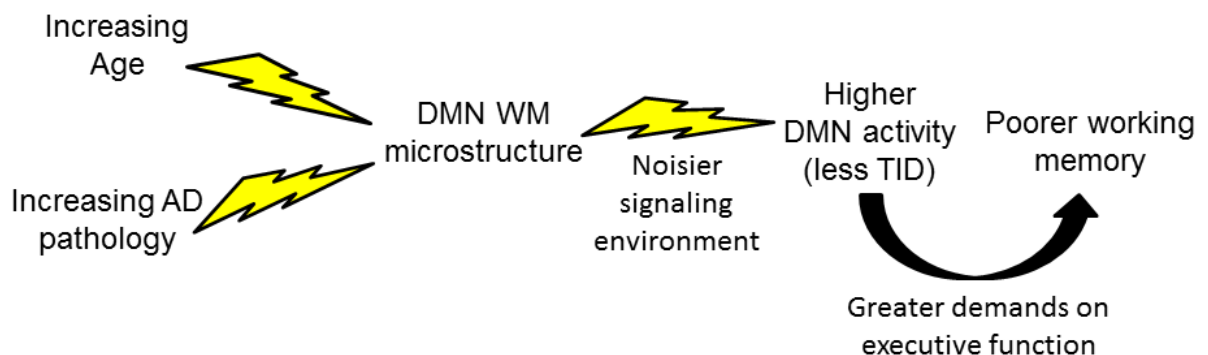
Figure 3.9. DMN WM microstructure as common pathway contributing to diminished DMN TID. Diagram depicting the proposed role of DMN WM microstructure as a common

pathway by which age and AD pathology contribute to DMN function. Decline in WM microstructure creates a noisier signaling environment, which leads to the increased DMN activity (and default-mode processes) during the working memory task, which impairs performance. This dysfunctional response in the DMN may only become apparent once WM microstructure is significantly impacted by both age and AD pathology.

Aging is associated with a loss of axons and myelin content (264). Further, it appears that small-diameter, lightly-myelinated axons, such as those seen in DMN-WM, are particularly vulnerable (47,175,176). Age-related myelin loss is met with increasing myelin repair processes (260,265,266). However, myelin laid down during repair is typically thinner and less compact, which may result in decreased measures of WM microstructure (265). In addition, both axons and oligodendrocytes are vulnerable to a variety of toxins, ROS, and hypo-perfusion (267–270). Finally, synaptic loss is well-characterized in normal aging, which may be indirectly reflected due to the loss of underlying axons or synaptic dysfunction leading to axonal retraction (179,271). It is likely that each of these cellular alterations contribute to age-related reduction in WM signaling within the DMN.

Increasing AD pathology may also negatively affect WM microstructure through various mechanisms. We observed relations with both $A\beta_{42}$ alone and the tau/$A\beta_{42}$. This suggests that $A\beta_{42}$ may be associated with declining WM microstructural properties independently of tau, as well as in a synergistic manner with increasing tau pathology. Studies performed *in vitro* have demonstrated that increasing concentrations of $A\beta_{42}$ are toxic to oligodendrocytes and to formation of new myelin sheaths (200,201,272). Further, post-mortem studies have found that increasing concentrations of soluble $A\beta$ species are found in the WM of individuals with AD and are associated with significant loss of axons and myelin (273,274). Finally, tau and $A\beta_{42}$ may act via a synergistic pathway in order to disrupt FAT (203,275). Disruption of FAT interferes with myelin repair processes, axonal integrity, and synaptic viability (260).

It should be noted that results of the alternative models (Figure 3.8d,f) indicate that we cannot rule out the possibility that AD pathology and reduced TID both occur independently following decline in WM microstructure (note the solid arrows representing significant pathways between WM and both AD pathology and TID). Consistent with this view, the myelin model of AD suggests that increased $A\beta_{42}$ and tau are by-products of increased myelin repair processes that occur in aging (260). Further, these interpretations are not mutually exclusive, as initial deposition of AD pathology via processes described by the myelin model may in turn negatively influence WM microstructure through the mechanisms described above. Alternatively, initial age-related declines in WM microstructural properties may lead to increased synaptic activity, which itself contributes to greater AD deposition (276,277). Considerable future multimodal, longitudinal studies will be necessary to distinguish between these different possibilities.

3.4.6. Limitations

As noted, this study is cross-sectional, and future longitudinal work should look to better understand the temporal order of alterations in diminished DMN TID, WM microstructure, AD pathology, and CVD pathology. Nevertheless, our findings indicate that age and AD pathology are only associated with DMN function to the extent that they are associated with WM microstructure. Second, this study recruited groups of younger and older adults but not middle-aged adults. Future studies should look to recruit middle-aged adults in order to test these findings across the lifespan. In addition, while relationships were observed between DMN TID and RT, no relationships were observed between TID and task accuracy. This is likely due to the near ceiling performance on the task. Future studies should seek to use tasks that are capable of producing greater variability in task performance such that relationships between brain function and task accuracy can be adequately assessed. Finally, AD and CVD pathology were treated as a continuous variable in the present study. It

87

is unclear whether the effects of pathology are better assessed through group comparisons or by treating pathology as a continuous variable. In addition, only CN older adults were included in the present study, which might underestimate the association between pathology and DMN function because only early changes were studied. Future work should recruit large samples across disease spectrums, in order to assess pathology through group comparisons and through treatment as a continuous variable across and within both pathological and clinical groups.

3.4.7. Conclusions

The present study provides further evidence that altered WM microstructure is a key contributor to diminished DMN TID in older adults. Moreover, subtle WM microstructural alterations are sufficient to disrupt DMN function in older adults in the absence of more advanced cerebrovascular pathology. Finally, microstructural declines in WM represent a shared pathway by which increasing age and AD pathology are associated with this dysfunctional response in the DMN. At the broadest level, DMN WM microstructure may serve as a valuable biomarker that captures the combined effects of both age and AD pathology.

4. Experiment 3: Breakdown in default mode network circuitry predicts baseline and longitudinal change in executive function in cognitively normal older adults

4.1 Introduction

Executive function (EF) underlies the human capacity for flexible and adaptive thought processes, such as working memory, task switching, and inhibitory control (10). Older adults are known to show significant declines in EF compared to younger adults (1). Much of the research seeking to understand the basis for these declines in the brain have focused on frontal and parietal regions belonging to the executive-control network (19–21). However, recent evidence suggests that alterations in the default mode network (DMN) significantly contribute to EF in older adults (29,30,106). While the DMN is responsible for internally-focused thought processes, failure to deactivate these processes during externally-directed tasks appears to interfere with EF processes involved in the task-at-hand (29,242).

The DMN is negatively impacted by aging, with declines in DMN function occurring linearly across the adult lifespan (92,96,211). However, alterations in the DMN contributing to EF in older adults may also be associated with preclinical Alzheimer's disease (AD). AD pathology is the most prevalent neurodegenerative pathology in older adults, and preclinical pathology is present in over 20% of cognitively normal (CN) older adults over the age of 65 (124–126). Of particular interest, AD pathology shows a predilection for the DMN with both abnormal accumulations of β-amyloid (Aβ$_{42}$) and tau occurring during the preclinical disease stage (38,145,146). Further, increased AD pathology in CN older adults is negatively associated with DMN function (Chapter 3, 99,156).

Interestingly, declines in DMN function associated with aging and AD pathology may occur through a common pathway of declining white matter (WM) microstructure (Chapter 3). WM is responsible for electrochemical signaling between the distant brain regions

making up large-scale brain networks, such as the DMN. WM microstructure reflects alterations in the density and coherence of axonal and myelin membranes as measured by diffusion tensor imaging (DTI) (168). These declines are apparent in normal aging (160,161,171) and have recently been associated with greater AD pathology in CN older adults (196–198). Our recent results demonstrated that declining WM microstructure in the pathways connecting DMN regions mediated both age- and AD pathology-related declines in DMN task-induced deactivation (TID) in CN older adults (Chapter 3). This lower level of TID was in turn associated with poorer performance on a working memory task.

These previous findings suggest that the DMN may contribute to EF declines in older adults associated with both normal aging and AD pathology. However, it is unclear whether these findings extend to more broadly used, clinical measures of EF. Finally, it is unknown if these measures of DMN structure and function may predict longitudinal change in EF. In order to assess these questions, we used baseline measures of DMN TID, WM microstructure, and AD pathology from our previous study to predict neuropsychological test scores of EF both at baseline and over a three-year follow-up period. In addition to testing bivariate relationship, mediation analyses were used to determine if baseline DMN WM microstructure mediated longitudinal change in EF predicted by baseline levels of AD pathology.

4.2. Methods

4.2.1. Participants

Thirty-two CN older adults (age at baseline: 66-93 years old) were selected from our previous neuroimaging study (Chapter 3) of 39 CN older adults (ages 65-93) based on availability of longitudinal neuropsychological testing and quality neuroimaging data. The original cohort was recruited from a larger cohort of CN older adults followed by the

University of Kentucky Sanders-Brown Center on Aging (SBCoA), which has been

described previously (246). Seven participants from the original cohort were excluded from

the current study due to: poor neuroimaging data quality ($n = 4$, see Chapter 3 for details),

decision not to enroll in neuropsychological testing portion of the study ($n = 2$) or loss to

follow-up after baseline visit ($n = 1$). Inclusion and exclusion criteria were the same as

previously reported (Chapter 3). Demographic characteristics of the final cohort of 32 CN

older adults are shown in Table 4.1.

4.2.2. Evaluation of EF

All participants underwent the standard battery of neuropsychological tests included in the

UDS-2 at baseline (16). Individuals returned annually to undergo the UDS battery. Three

tests from the UDS were used in the present study: Trailmaking Test Part A (TMT-A),

Trailmaking Test Part B (TMT-B), and the Digit Symbol test from the Weschler Adult

Intelligence Scale-IV (WAIS-DS). Raw scores were first standardized based on age, sex,

and education using scores generated from the larger SBCoA cohort, as previously

described (278). Age, sex, and education-standardized scores for TMT-A were then

regressed out of TMT-B and WAIS-DS standardized scores in order to exclude components

of raw processing and motor speed common to all tests (14). The resulting residuals were

then combined to form a composite EF score by subtracting the TMT-B residuals (higher

scores = worse performance) from the WAIS-DS residuals (higher scores = better

performance) and dividing by 2 (Figure 4.1). Therefore, higher EF composite scores

reflected better performance.
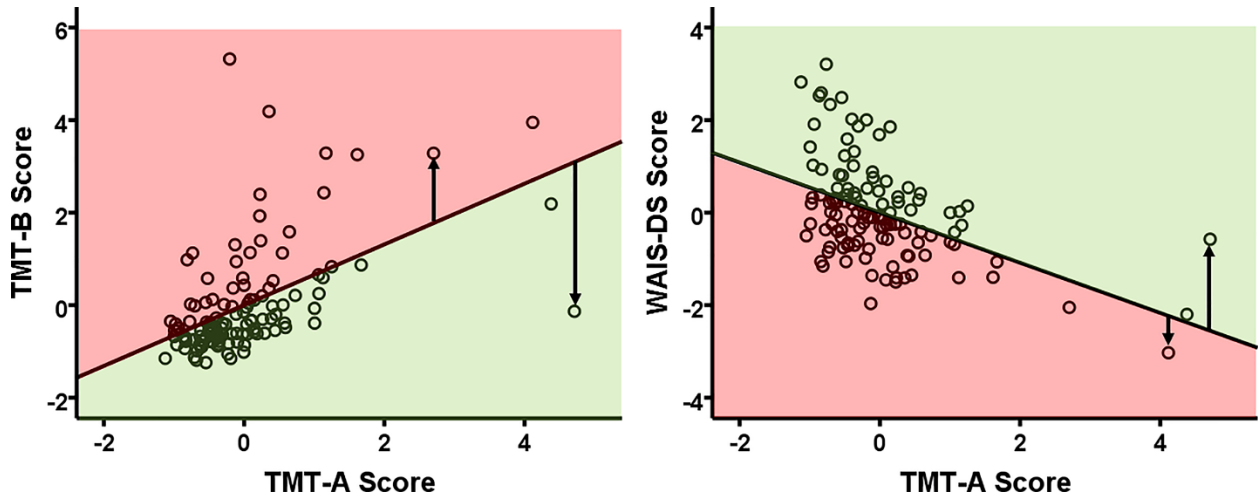
Figure 4.1. Formation of EF composite score. The EF composite score consisted of combining the standardized residuals of the TMT-B score (left) and WAIS-DS score (right) after regressing out TMT-A scores in order to control for processing and perceptual-motor speed. Areas shaded in green represent better EF (performed better than predicted based on speed alone), while areas shaded in red represent worse EF (performed worse than predicted based on speed alone). The arrows represent the residuals, with longer arrows representing larger residuals and shorter arrows representing smaller residuals. Larger, positive residuals for WAIS-DS represented better EF, while larger, negative residuals for TMT-B represented better EF. Therefore, the EF composite was calculated by subtracting the TMT-B standardized residual from the WAIS-DS standardized residual, such that higher, positive composite EF scores reflected better EF.

The EF composite was calculated for each participant at each visit. One-year change between each visit was calculated by subtracting the EF score of the current visit from the previous visit (i.e. EF composite at Year 1 visit – EF composite at baseline visit). Each participant's average annual change in EF was then calculated by averaging all of that individual's available one-year change scores (average the change from year 0 to year 1, year 1 to year 2, and year 2 to year 3).

4.2.3. Data from previous study

Neuroimaging data (DMN TID and WM microstructure) and cerebrospinal fluid (CSF) concentrations of $A\beta_{42}$ and tau/$A\beta_{42}$ from our previous study were used. The methods for obtaining these measures are described in detail in our previous study (Chapter 3) and outlined briefly below.

All participants underwent a standard neuroimaging protocol and lumbar puncture at baseline (year 0) within 8 months of their initial neuropsychological testing (mean = 6.43 ± 110.92 days, max = 243 days). Lumbar puncture was performed following an overnight fast, and CSF was shipped to the University of Pennsylvania on dry ice. CSF was analyzed using the xMAP-Luminex platform with Innogenetics Ino-BIA (Alz3Bio, Ghent, Belgium) immunoassay kit as previously described (127). The neuroimaging protocol included, T1-weighted high-resolution structural images, T2*-weighted functional runs, diffusion tensor imaging, and fluid-attenuated inversion recovery (FLAIR) imaging. Individuals performed a modified delayed match-to-sample paradigm during fMRI (245). The FMRIB software library (FSL) version 5.0.9 (221,249) was used for pre-processing and analysis of neuroimaging data. T1-weighted images were brain extracted (251), bias-field corrected (250), and non-linearly warped to the MNI152 T1 2mm^3 template using a 20mm warp resolution (223). Functional runs were motion-corrected, registered to high resolution image using boundary-based registration (222), and then registered to the MNI152 T1 2mm^3 template using the warp fields for the T1-weighted image.

fMRI data were scrubbed for motion with both regression of motion parameters and removal of motion outliers using a frame-wise displacement threshold of > 0.5mm (253). Further nuisance regression removed signal of white matter and CSF (Chapter 3). The residuals from these pre-processing steps were then used as inputs for independent component analysis (ICA) using MELODIC's concatenation approach (279). A network of DMN regions was identified during the task and masked by a resting-state DMN to form a final region-of-interest (ROI). The time-series were extracted from the DMN ROI and mean TID was calculated by subtracting BOLD signal during the middle 6s of the task-blocks from the middle 6s of baseline blocks (Chapter 3).

DTI data were brain extracted, corrected for eddy currents and motion (255,256), and registered to the FMRIB58 FA 1mm^3 template using TBSS after initially fitting a voxel-wise tensor model using FDT (224). Probabilistic tractography utilized BEDPOSTX and PROBTRACKX to generate a set of WM pathways connecting DMN regions (DMN-WM) after initially fitting a voxel-wise diffusion model with 3 fibers (226,227). FLAIR images were used to identify WM hyper-intensities (WMH) using a semi-automated protocol. A mask of normal-appearing DMN-WM (DMN-naWM) was then created for each participant by masking out areas of WMH in each participant from the group DMN-WM template. FA was then extracted from each participants DMN-naWM.

4.2.4. Statistical Analyses

SPSS 24 (IBM, Chicago, IL) was used for all statistical analyses. Baseline relationships were first explored using bivariate correlations between all baseline variables: EF composite, DMN TID, FA in DMN-naWM, CSF Aβ_{42}, and CSF tau/Aβ_{42} ratio. Separate linear regression models were then used to test whether any baseline variables could predict average annual change in EF (ΔEF) after controlling for baseline EF. Due to the presence of multivariate relationships, Preacher and Hayes mediation analyses (207) were used to determine if any variables mediated the relationships between another variable and ΔEF. Indirect effects with bootstrapped 95% confidence intervals not crossing 0 were considered significant.

4.3. Results

Neuropsychological data was available for 31 participants at one-year follow-up, for 29 participants at two-year follow-up, and 28 participants at three-year follow-up. The average number of annual visits (including baseline) available per participant was 3.75 ± 0.51 (range = 2 – 4, median = 4). Average annual changes scores were calculated based on an average

of 2.59 ± 0.71 annual change scores (range = 1 – 3, median = 3). Three individuals were identified as outliers in ΔEF and were not included in the regression analyses. Demographics and mean outcome measures are reported for the initial group of 32 participants and the group of 29 participants used in longitudinal analyses in Table 4.1.

Table 4.1. Demographic and Outcome Measures

	Baseline (n = 32)	Longitudinal (n = 29)
Age	77.7 (6.57)	77.8 (6.82)
Sex (M:F)	14:18	13:16
Education	16.5 (2.41)	16.7 (2.44)
DMN FA	0.58 (0.026)	0.58 (0.027)
DMN TID Magnitude (% signal change)	0.10 (0.119)	0.11 (0.109)
CSF Aβ$_{42}$ (pg/mL)	271.4 (79.21)	270.2 (79.11)
CSF Tau (pg/mL)	56.9 (16.29)	57.2 (16.75)
CSF Tau/Aβ$_{42}$	0.24 (0.140)	0.24 (0.142)
Baseline EF Composite	-0.12 (0.907)	0.08 (0.621)
Average Annual ΔEF	--	-0.04 (0.228)

Mean (S.D.) for individuals included in baseline analyses (left) and longitudinal analyses (right)

4.3.1. Baseline relationships

At baseline, only DMN TID magnitude was correlated with EF (r = 0.47, p = .006), which survived Bonferroni correction (Figure 4.2). FA in DMN-naWM had a trend-level relationship with EF (r = 0.31, p = .086), while no other variables were related to baseline EF (p > .23). Baseline DMN TID, FA in DMN-naWM, and AD pathology were all correlated (Table 4.2).
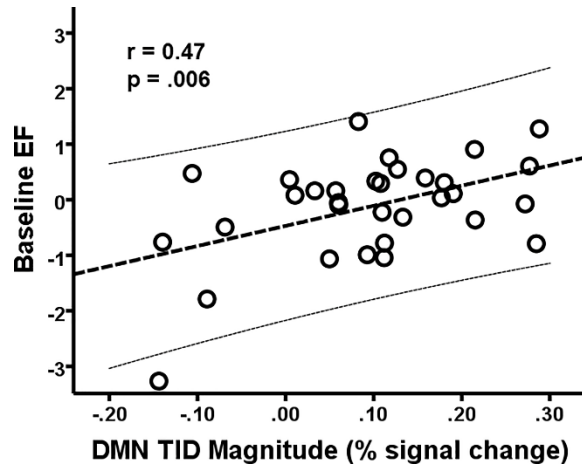
Figure 4.2. Relationship between DMN TID magnitude and EF at baseline. Scatter plot of EF composite at baseline against DMN TID magnitude (higher values = more deactivation) at baseline shows a significant positive relationship. The thick dashed line represents the linear best-fit and thin dashed lines are the 95% confidence interval for the predicted response.

Table 4.2. Baseline relationships between imaging and CSF measures

	DMN TID magnitude	FA in DMN-naWM	CSF $A\beta_{42}$	CSF tau/$A\beta_{42}$
DMN TID magnitude	--	**0.40** (**.025**)	0.34 (.054)	**-0.39** (**.029**)
FA in DMN-naWM		--	**0.37** (**.040**)	**-0.35** (**.047**)
CSF $A\beta_{42}$			--	**-0.78** (**.000**)
CSF tau/$A\beta_{42}$				--

Values are Pearson-r with p-values in parentheses. Significant ($p < .05$) relationships are shown in bold. All analyses had $n = 32$.

4.3.2. Predicting Longitudinal Change in EF

EF declined -0.04 ± 0.228 units annually over the 3-year follow-up period. Baseline EF was

negatively associated with ΔEF ($r = -0.46$, $p = .011$). Separate linear regression analyses

were performed to determine whether DMN TID magnitude, FA in DMN-naWM, CSF $A\beta_{42}$,

or CSF tau/$A\beta_{42}$ ratio could predict ΔEF. All models were significant ($F_{2,26} > 6.63$, $p \leq .005$),

and the addition of a baseline imaging or AD measure provided a significant increase in

variance explained over and above baseline EF ($F\text{-}change_{1,26} > 4.80$, $p \leq .038$). Results of

these separate analyses (Figure 4.3) showed that DMN TID magnitude ($\beta = 0.36$, $p = .038$),

FA in DMN-naWM ($\beta = 0.46$, $p = .001$), CSF $A\beta_{42}$ ($\beta = 0.37$, $p = .032$), and CSF tau/$A\beta_{42}$ (β

$= -0.45$, $p = .005$) predicted ΔEF. Only FA in DMN-naWM and CSF tau/$A\beta_{42}$ would be

considered significant after Bonferroni correction for multiple comparisons.
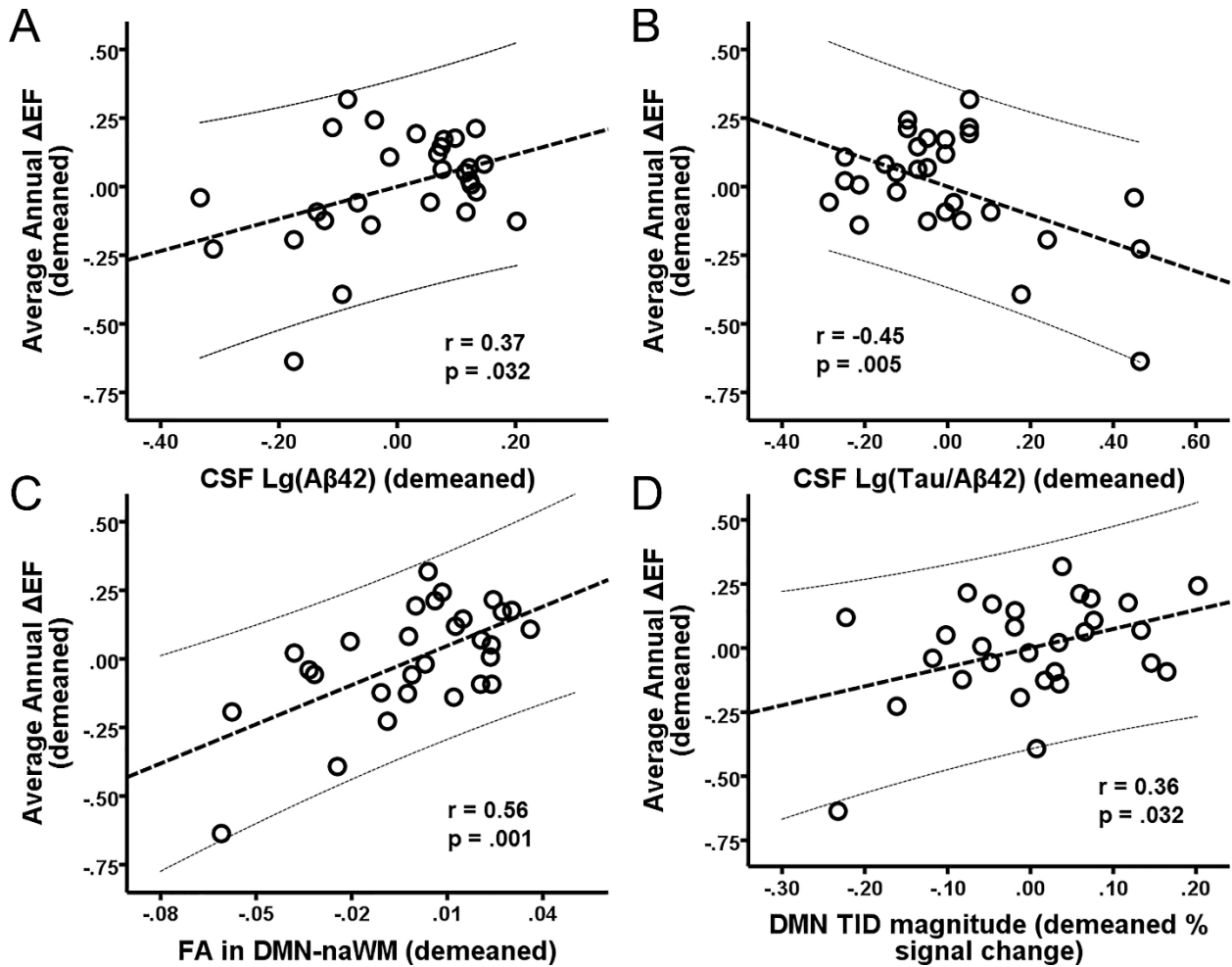
Figure 4.3. Prediction of longitudinal ΔEF by baseline measures. Partial regression plots of average annual ΔEF against CSF Aβ$_{42}$ **(A)**, CSF Tau/Aβ$_{42}$ ratio **(B)**, FA in DMN-naWM **(C)**, and DMN TID magnitude **(D)** after controlling for baseline EF. All values are demeaned. The thick dashed lines represent the linear best-fit and thin dashed lines are the 95% confidence intervals for the predicted response.

4.3.3. Mediation Analyses

FA in DMN-naWM and CSF tau/Aβ$_{42}$ were correlated at baseline and both predicted ΔEF after correction for multiple comparison. Therefore, mediation analyses were performed to determine whether: 1) FA in DMN-naWM mediates the relationship between CSF tau/Aβ$_{42}$ and ΔEF, or 2) CSF tau/Aβ$_{42}$ mediates the relationship between FA in DMN-naWM and ΔEF. Results of these mediation analyses (Figure 4.4) found that FA in DMN-naWM

98

mediated the relationship between CSF tau/Aβ_{42} and ΔEF (ab = -0.19 [-0.561, -0.009], c' = -0.26 [-0.574, 0.047]), but CSF tau/Aβ_{42} did not mediate the relationship between DMN-naWM and ΔEF (ab = 0.11 [-0.003, 0.384], c' = 0.43 [0.113, 0.745]).
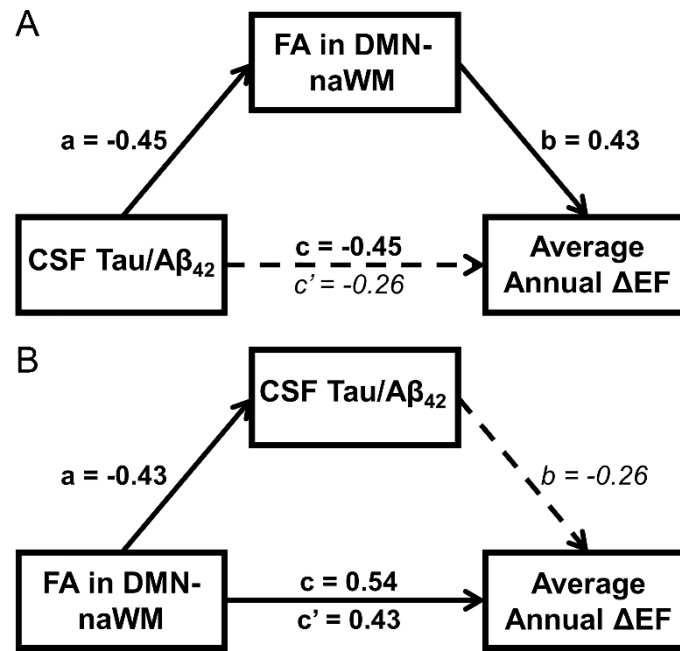
Figure 4.4. Results of primary mediation analyses. Preacher and Hayes mediation analyses revealed that the relationship between CSF Tau/Aβ_{42} ratio and average annual ΔEF was mediated by FA in DMN-naWM **(A)**, but the relationship between FA in DMN-naWM and average annual ΔEF was not mediated by CSF Tau/Aβ_{42} **(B)**. Values are standardized β-estimates. Significant paths are shown as solid arrows with β-estimates in bold, while non-significant paths are shown as dashed arrows with β-estimates in italics.

Supplementary mediation analyses (Figure 4.5) were performed to determine if either FA in DMN-naWM or CSF tau/Aβ_{42} mediated the relationship between DMN TID and ΔEF, and to determine if FA in DMN-naWM mediated the relationship between CSF Aβ_{42} and ΔEF. Results showed that both FA in DMN-naWM and CSF tau/Aβ_{42} mediated the relationship between DMN TID and ΔEF. A model testing these mediation effects simultaneously found that the mediation effect of FA in DMN-naWM remained significant (ab = 0.17 [0.039, 0.478]) but the tau/Aβ_{42} ratio did not (ab = 0.10 [-0.017, 0.333]). Further,

DMN-naWM mediated the relationship between CSF $A\beta_{42}$ and ΔEF ($ab = 0.22$ [0.046,

0.581], $c' = 0.17$ [-0.145, 0.491]). None of the alternative models found significant mediation

effects of DMN TID or CSF $A\beta_{42}$.
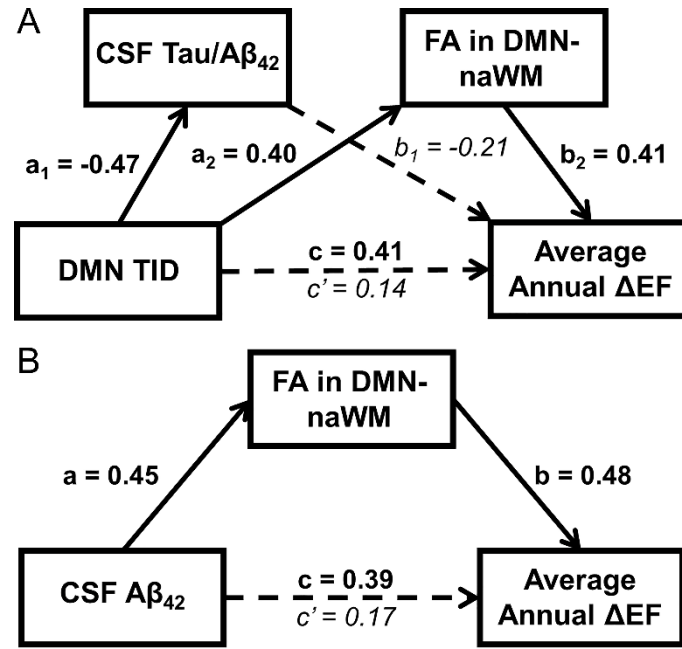
Figure 4.5. Supplementary mediation analyses. Preacher and Hayes mediation analyses found that FA in DMN-naWM mediated the relationships of both DMN TID **(A)** and CSF $A\beta_{42}$ **(B)** with average annual ΔEF. **A:** A single model including both CSF Tau/$A\beta_{42}$ and FA in DMN-naWM was tested after initial models showed that both mediated the DMN TID-EF relationship. Results of this model show FA in DMN-naWM, but not CSF Tau/$A\beta_{42}$ mediates this relationship. **A-B:** Values are standardized β-estimates. Significant paths are shown as solid arrows with β-estimates in bold, while non-significant paths are shown as dashed arrows with β-estimates in italics.

4.4. Discussion

The present study provides evidence for the role of the DMN in predicting both cross-

sectional and longitudinal measures of EF. Baseline EF was predicted exclusively by DMN

TID magnitude, while ΔEF was predicted by a variety of baseline neuroimaging and AD

pathological markers. Importantly, DMN WM microstructure mediated the relationship

between all other predictors and ΔEF, while neither measures of DMN function or AD

pathology mediated the relationship between DMN WM microstructure and ΔEF. Together, these findings suggest that measures of DMN TID and EF are strongly overlapping at baseline, but that measures of DMN WM microstructure may represent a valuable marker for predicting both AD pathology-related and non-AD pathology-related change in EF over a three-year period.

4.4.1. Baseline EF is predicted by DMN TID

In the present study, DMN TID magnitude was the only predictor of EF at baseline. These findings are consistent with a growing body of research showing that less DMN TID is associated with poorer performance during tasks placing high demands on EF in older adults (29,30,242). However, this is the first study to extend these findings to more broadly used clinical measures of EF. Together, with previous studies, these results indicate that DMN TID is an important contributor to EF performance in older adults. This may be due to higher levels of DMN activity ongoing during the task placing greater demands on executive control processes (29,242). Therefore, conceptually, individuals must devote greater EF resources to suppress interference from ongoing DMN processes, thus leaving fewer EF resources to devote to the task-at-hand.

4.4.2. Longitudinal change in EF is predicted by baseline DMN WM microstructure

Several baseline measures were predictive of longitudinal change in EF over the three-year follow-up period. However, mediation analyses found that DMN WM microstructure mediated the relationship between all other baseline measures and ΔEF, while no other baseline measure mediated the relationship between DMN WM microstructure and ΔEF. Together these findings indicate that DMN WM microstructure is the most direct predictor of change in EF over three-year follow-up. These results are consistent with previous studies

showing that baseline WM microstructure predicts longitudinal change in working memory (280) and fluid intelligence (281) over a period of years.

Our mediation results provide the first evidence that AD pathology is associated with change in EF over time only through its relationship with DMN WM microstructure. We found that both $A\beta_{42}$ and the tau/$A\beta_{42}$ ratio had an indirect effect on longitudinal change in EF through DMN WM microstructure. $A\beta_{42}$ has been shown to disrupt myelin sheath formation and is toxic to oligodendrocytes responsible for maintenance and repair of myelin (200,201,272). Further, abnormal aggregation of tau contributes to microtubule destabilization due to the loss of normal tau function (202). Finally, tau and $A\beta_{42}$ interact to disrupt fast axonal transport (FAT), which in turn contributes to decline in axonal, myelin, and synaptic integrity (203,260,275). Our results found the strongest relationship between the tau/$A\beta_{42}$ ratio and change in EF, which may suggest that the combined effects of tau and $A\beta_{42}$ on DMN WM microstructure result in the greatest declines in EF. It may also be the case that WM microstructure is a surrogate marker for alterations due to tau and $A\beta_{42}$ pathology occurring elsewhere in the neuron (e.g. at synapses). However, it will only be possible to assess this possibility once a marker of synaptic structure/integrity matching the level of sensitivity provided by DTI is developed.

The direct effect of DMN WM microstructure on change in EF suggests that additional, non-AD pathology-related changes in EF are also predicted by WM microstructure. Importantly, we used FLAIR imaging to identify and mask out region areas of WMH in order to study normal appearing WM (Chapter 3). WMHs are ubiquitous in aging (181) and are thought to primarily reflect areas of severe cerebrovascular pathology resulting from a breakdown in vascular integrity (182). In contrast, declines in naWM are thought to reflect subtler declines in the microstructural organization of WM (263). These change may be the result of age-related declines in synapses (albeit indirectly via axonal

retraction), axonal loss, or myelin breakdown, all of which would reduce WM microstructure through loss of membrane density and organizational coherence (46,175,176,271). In addition, these changes may also reflect distal effects in tracts negatively impacted by cerebrovascular pathology (263). Therefore, WM microstructure likely provides the best predictor of ΔEF because it reflects a combination of age-related, AD pathology-related, and cerebrovascular pathology-related processes that each contribute to poorer EF outcomes over time.

Alternatively, our mediation results could be interpreted as evidence for independent effects of DMN WM microstructure on increasing AD pathology and change in EF. Alternative models (Figure 4.4b) found that DMN WM microstructure had a direct effect on AD pathology and change in EF, but that AD pathology did not have an effect on change in EF when accounting for WM microstructure. This interpretation is consistent with the myelin model of AD (260). According to this model, age-related breakdown in myelin is a triggering event in the AD pathology cascade. DMN WM primarily consists of late-myelinating tracts, which are most susceptible to age-related breakdown (46,47). Following myelin breakdown, repair processes are initiated, a by-product of which are high levels of $A\beta_{42}$ and tau. However, repaired myelin is thinner and less compact than the myelin it is replacing (260,264,265). These poorly myelinated axons result in disruption of signaling processes, which contribute to poorer cognition (260). Therefore, the final result of this process is lower WM microstructure, increased AD pathology, and reduced cognition.

4.4.3. Different measures of DMN integrity predict baseline EF and longitudinal change in EF

The DMN was found to be an important predictor both of baseline EF and ΔEF. However, baseline EF was exclusively predicted by DMN TID, while DMN WM microstructure was the most direct predictor of ΔEF. This shift may represent a shift from mechanisms of cognitive

reserve to those of brain reserve (28). Cognitive reserve refers to altered cognition and/or functional patterns resulting from life experience that protect against functional impairment/decline but are not necessarily manifested through measurable structural alterations in the brain (28,282). These experiences may include education, intellectually stimulating career and/or leisure activities, and other environmental and personal factors (e.g. bilingualism). In contrast, brain reserve refers to altered cognition and/or functional patterns resulting from measurable structural differences in the brain that protect against functional impairment/decline (282).

DMN TID is partially explained by DMN WM microstructure, however large variability still exists in levels of TID after accounting for WM microstructure, age, and/or AD pathology (Chapter 3). This suggests that DMN TID is impacted by variables outside of brain structure, which may include aspects of cognitive reserve (28). Therefore, DMN TID may incorporate aspects of brain structure, pathology, and unmeasured reserve variables, thus making it the best predictor of EF at baseline. In contrast, baseline DMN TID was only marginally predictive of ΔEF, and this relationship was mediated by DMN WM microstructure. This suggests that only the elements of DMN TID associated with WM microstructure were associated with ΔEF. This may indicate that brain reserve variables become more important compared to cognitive reserve variables in predicting longitudinal trajectory. One possible explanation for this finding is that cognitive reserve becomes depleted over time, so aspects of brain reserve become more important (282). Future studies should seek to measures reserve variables in order to directly assess their influence on DMN TID and EF.

4.4.4. Limitations

The current study has several limitations that must be considered. First, while baseline measures predicted ΔEF, causality cannot be directly inferred from the present results. While not yet feasible, future studies should look to assess both EF and measures of DMN

104

structure/function and AD pathology longitudinally while performing experimental manipulations aimed at affecting DMN structure/function and/or AD pathology in order to better understand causal relationships. Further, as individuals age, the likelihood of mixed pathologies (Lewy body, vascular, and other) increases. As these pathologies were not directly assessed in the present study, the potential effects of these pathologies might have been attributed to AD or aging processes. In addition, the present study had a limited sample size, and, therefore, may have been underpowered to detect smaller effects on EF cross-sectionally and longitudinally. Future work should use larger cohorts in order to better detect subtler effects. In addition, we examine only CN older adults. It is unclear whether these relationships are maintained in states of mild cognitive impairment and clinical dementia. Future studies should seek to investigate the role of DMN WM and TID predicting EF in these later clinical stages. Finally, we treated AD pathology as a continuous variable, but it is unclear whether the relationship between AD pathology and other measures may be different above and below certain thresholds. Future studies should be performed with larger samples and longer durations in order to assess the effects of AD pathology on brain structure/function and EF both within sub- and supra-threshold groups and across all participants with adequate follow-up.

4.4.5. Conclusions

The current study provides novel evidence that EF is influenced by DMN structure and function both cross-sectionally and longitudinally. While more dynamic measures of DMN TID predicted EF at baseline, DMN WM microstructure was the most direct predictor of ΔEF, suggesting a potential shift from cognitive reserve to brain reserve. Further, measures of DMN WM microstructure predicted both AD pathology-related and non-AD pathology-related changes in EF over a three-year follow-up period. Therefore, DMN WM microstructure may be a valuable marker of multiple age- and pathology-related changes that influence

longitudinal EF trajectory. Finally, DMN WM microstructure might serve as a potential

therapeutic target for interventions aimed at preventing longitudinal EF declines resulting

from multiple age and disease processes.

5. General Discussion

These three studies investigated the role of WM microstructure in diminished DMN TID associated with aging and presence of AD pathological proteins in cerebrospinal fluid. The results provide novel evidence of a relationship between lower WM microstructure and less DMN TID in CN older adults. Further declines in WM microstructure mediated the relationships of both age and AD pathology with DMN TID. Finally, these results demonstrate that breakdown in DMN circuitry is negatively associated with cross-sectional levels of EF and are predictive of longitudinal change in EF in these older adults.

5.1. Less DMN TID is associated with poorer EF: A dysfunctional response

All three experiments provide strong evidence for a relationship between less DMN TID and worse performance on tests of EF in older adults. In Experiment 1, DMN TID was associated with task performance specifically during the switching condition of a task-switching paradigm. Experiment 2 extended these findings to a working memory paradigm, while Experiment 3 extended these findings to common clinical assessments of EF. These findings are consistent with previous studies in which DMN TID was associated with poorer performance on a cognitive control task (29) and a working memory n-back task (30,106). Together these results provide compelling evidence that lower levels of DMN TID contribute to poorer performance on tests of EF in older adults, which reflects a dysfunctional response in the aging brain.

Interestingly, the link between DMN TID and task performance appears to be unique to tasks of EF in CN older adults. In Experiment 1, DMN TID was not associated with task performance during the non-switching condition, which was a simple perceptual judgment task. This is consistent with a previous study which found no relationship between DMN TID and performance on a perceptual judgment task during either low difficulty or high difficulty

conditions (105). Further, this lack of relationship occurred despite parametric increases in

DMN TID with increasing difficulty in younger adults that were absent in older adults.

Therefore, greater ongoing activity in the DMN (less TID) places greater demands on EF,

which only results in performance detriments when the externally-directed task also places

significant demands on EF, such that the total demands exceed EF capacity (Figure 5.1). If

the task does not place high demand on EF, failure to deactivate the DMN does not affect

task performance, as EF is able to successfully inhibit these interfering DMN processes.
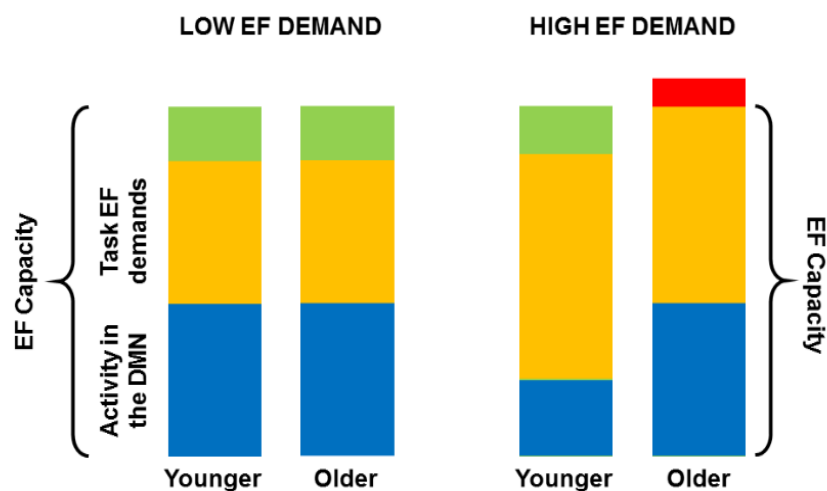
Figure 5.1. Level of DMN activity and EF demands in younger and older adults. DMN activity (blue bars), task EF demands (orange bars), and reserve EF resources (green) during low demand (left) and high demand (right) conditions. **Left:** Younger and older adults show similar DMN activity during the low demand condition, which, along with task EF demands, do not exceed EF capacity. Thus, both exhibit successful DMN function. **Right:** During conditions with high EF demand, younger adults show greater TID, and DMN activity, along with task EF demands, does not exceed EF capacity. In contrast, older adults fail to further deactivate the DMN. Therefore, total EF demands (DMN + task) are in excess (red bar) of EF capacity, resulting in poorer task performance. This represents a dysfunctional response.

Of particular interest, two previous studies have found that reduced DMN TID co-

occurs with increased recruitment of regions associated with executive control (29,30). One

potential implication of these co-occurring phenomena is that age-related over-recruitment

of executive regions in the brains of older adults may represent a compensatory response to

greater ongoing activity in DMN regions (29). Interestingly, older adults frequently show recruitment of the dorsolateral prefrontal cortex (DLPFC) during tasks with minimal demands on EF, while younger adults show no such recruitment (96,283,284). This has been labeled as a compensatory response in studies with minimal demands on EF (19,285,286). However, studies placing demands on EF have demonstrated that increased activity in DLPFC is either unrelated to behavior or associated with poorer performance (27,28,287).

If these increases in DLPFC activity are in response to greater DMN activity, then increased activity during tasks placing low or no demands EF would reflect successful inhibition of interfering DMN processes. However, during tasks placing high demands on EF, the limited EF resources in older adults are split between inhibiting interfering DMN processes and the task-at-hand. Thus, greater activity may be associated with poorer performance. Over-recruitment of these EF regions may also be further exacerbated by structural and/or pathological alterations within the FPCN (27,165,288).

5.2. White matter microstructure is a limiting factor of capacity for DMN TID

Experiments 1 and 2 provide substantial evidence that poorer microstructure in WM pathways connecting DMN regions are negatively associated with DMN TID. Further, results of Experiment 1 demonstrated that WM microstructure is associated with capacity for TID in aging. Specifically, lower FA was not associated with DMN TID during a low demand condition but was associated with less DMN TID during a high demand condition, during which older adults showed reduced capacity for TID compared to younger adults (Figure 5.1). In addition, microstructure within WM pathways connecting DMN regions was a better predictor of capacity for TID than microstructure in WM pathways connecting TPN regions to DMN regions. Similarly, lower FA was associated with less TID during a working memory task specifically designed to place high demands on EF through the use of multiple target images and repeated intervening distractors (244,245).

These findings are consistent with previous studies in task-positive networks, which have demonstrated that lower WM microstructure is associated with higher BOLD signal in these regions during the task (27,165,228). Further, longitudinal declines in WM microstructure are associated with longitudinal increases in BOLD signal in task-positive regions (216). Along with the present results, these studies suggest that increased BOLD signal correlated with lower WM microstructure reflects a noisier signaling environment. Specifically, loss of axons, synapses, and/or myelin might disrupt the coordination of signaling within networks. This in turn would result in diminished temporal (loss of myelin) and spatial (loss of axons/synapses) summative processes that aid efficient synaptic communication. Therefore, greater input is necessary in order to achieve the desired output (Figure 5.2), which results in higher BOLD signal.
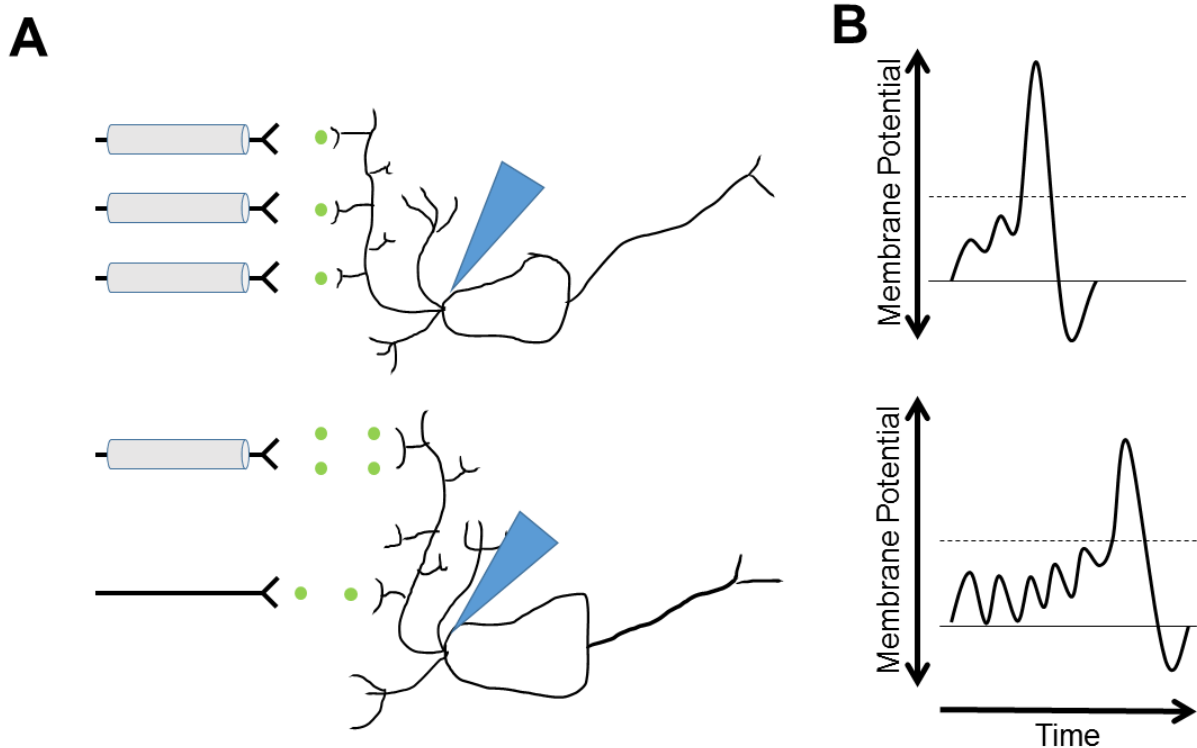
Figure 5.2. Schematic figure of the impact of WM microstructure on synaptic activity. **A:** Diagram of WM with high microstructure **(top)** and low microstructure **(bottom)**. Gray cylinders represent myelin, ⊰ represent axon terminals, ● represent neurotransmitters, and ⊢ represent post-synaptic dendritic spines. In the setting of low WM microstructure **(bottom)** decreases in axons and myelin are depicted. The large blue arrows represent the hypothetical electrode positioning for the recordings shown in panel B. **B:** Hypothetical recordings of the post-synaptic neuron in a setting of high microstructure **(top)** and low microstructure **(bottom)**. The solid line represents resting potential of the neuron, while the dashed line represents the threshold for generation of an action potential. Membrane potential is on the y-axis and time is on the x-axis. In the setting of high WM microstructure **(top)**, highly coordinated release of neurotransmitters allows for spatial and temporal summation to efficiently produce the desired response in the post-synaptic neuron. However, in a setting of low WM microstructure **(bottom)**, axonal and myelin loss disrupt this system. Decreased myelination results in less coordinated neurotransmitter release and decreased temporal summation, while loss of axons leads to decreased spatial summation. As a result, much greater synaptic activity is necessary to achieve the desired response.

While these findings are intuitive in relation to task-related activations, interpretation is less intuitive in the context of TID. However, TID simply reflects the degree to which communication between regions can be maintained at a level that does not interfere with the task-at-hand. Therefore, the same loss of temporal and spatial summative processes would

require greater input in order to achieve the desired output (whether inhibitory or excitatory). Within this context, WM microstructure is most closely associated with the minimal level of synaptic activity at which DMN communication can be carried out (although DMN activity and WM microstructure may be mildly correlated prior to reaching TID capacity) because WM microstructure imposes a physical limit, or floor, for DMN activity. Viewed through this lens, relationships between WM microstructure and BOLD signal in task-activated and task-deactivated regions likely reflect the same phenomenon and may further explain why these changes co-exist in aging.

5.3. DMN WM microstructure provides a marker of alterations associated with age and AD pathology that negatively affect DMN TID and EF

Experiments 2 and 3 provide evidence that DMN WM microstructure is a useful marker that captures the effects of age and AD pathology on DMN TID and EF. In Experiment 2, DMN WM microstructure mediated the relationships of age and AD pathology with reductions in DMN TID that were negatively associated with task performance. Further, results of Experiment 3 demonstrated that WM microstructure predicts longitudinal declines in EF associated with AD pathology as well as further declines in EF not predicted by AD pathology. Together these results suggest that WM microstructure is a valuable marker of the integrity of DMN circuitry important to EF in older adults.

These findings suggest that age and AD pathology may exert a "double-hit" on DMN WM microstructure, such that declines in DMN function and EF are influenced both by age-related and AD pathology-related mechanisms. Determining the specific mechanisms by which age and AD pathology are negatively associated with DMN WM microstructure is outside of the scope of this work. However, previous literature offers several potential mechanisms that may give rise to this association. Age-related changes in DMN WM microstructure may result from increased breakdown of myelin in aging (175,260). The late-

myelinating tracts that make up a majority of those connecting the DMN are the most

susceptible to myelin breakdown in aging (46,175,176). While myelin repair processes are

maintained throughout life, the new myelin laid down through repair is less compact and

thinner than the myelin it is replacing (265,266). In addition, aging is associated with

disruption of FAT and increased iron levels, toxins, and ROS, all of which contribute to either

axonal breakdown and oligodendrocyte toxicity (260,268–270). Finally, cerebral perfusion

declines in aging, which may result in subtle ischemic injury in WM (267,268). While

significant ischemic events result in WMHs (which had minimal overlap with DMN WM),

subtler, transient periods of hypoperfusion may disrupt microstructure in naWM (263).

In addition to age-related mechanisms, increased AD pathology may also contribute

to declines in WM microstructure. Specifically, increased levels of soluble Aβ species are

found in WM and are associated with significant losses of axons and decreased myelin

content (273,274). Further, Aβ$_{42}$ is toxic to oligodendrocytes and formation of new myelin

sheaths *in vitro* (200,272,289). In addition, increased tau may result in microtubule

destabilization (202), while interactions between tau and Aβ$_{42}$ disrupt FAT (203,275).

Disruption of FAT interferes with myelin repair processes and may lead to synaptic

starvation (260).

As causation cannot be determined by cross-sectional studies, alternative

possibilities must be considered. These results may also be consistent with two alternative

models. First, the myelin model of AD suggests that AD pathology arises as a byproduct of

myelin repair processes (260). As discussed above, DMN WM is particularly susceptible to

myelin breakdown, and, thus, is a site of high levels of myelin repair. According to the myelin

hypothesis, Aβ$_{42}$ aggregates at the site of myelin repair due to the role of β- and γ-

secretases in cleaving important myelin repair proteins, which inadvertently leads to the

cleavage of amyloid precursor protein into Aβ$_{42}$ (260). Further, auto-phosphorylation of

GSK-3β results in the phosphorylation of myelin basic protein and tau in order to temporarily disrupt FAT, so as to allow for the accumulation of myelin repair proteins at the site of injury. Following successful myelin repair, the aggregates of Aβ$_{42}$ and tau are transported to the synapse where they are released (260).

Another possibility is that increased Aβ$_{42}$ results from consistently higher levels of synaptic metabolism within the DMN. Both *in vitro* neurophysiology studies and *in vivo* studies in rodents have demonstrated that increased synaptic metabolism is associated with greater release of Aβ$_{42}$ (276,277,290). Further, the resulting increases in interstitial Aβ$_{42}$ concentrations promotes plaque formation (277). The DMN is already among the most metabolically active sites in the human brain during its baseline state (37,291). Failure to deactivate the DMN, results in consistently higher levels of synaptic metabolism within the DMN at all times. Further, it is possible that failure to deactivate the DMN during externally-directed cognitive tasks may also apply to other situations during which DMN activity should be reduced, such as sleep. Therefore, if higher levels of DMN synaptic metabolism persist during these states that are normally less active, Aβ$_{42}$ accumulation may accelerate and result in formation of abnormal plaques.

The mediation results of Experiment 2 indicated that the relationship between Aβ$_{42}$ and DMN TID are mediated by WM microstructure. Therefore, the aberrant activity specifically associated with declining WM microstructure could be responsible for the increased formation of plaques in this framework. This seems plausible as Aβ$_{42}$ secretion associated with normal levels of DMN activity may be able to be cleared from the brain, while excess activity results in a level Aβ$_{42}$ secretion that could serve to overwhelm these clearance processes.

It should be noted that AD is associated with hypo-metabolism in DMN regions (147). However, discrepancies exist between studies investigating the relationship between AD

114

and glucose metabolism in DMN regions. Initial studies demonstrated that glucose metabolism is reduced in individuals at high genetic risk of developing AD due to the presence of the ApoE ε4 allele (292,293). More recently, some studies have provided evidence that a hyper-metabolic phase may precede this hypo-metabolic phase (294–297). The exact timing of this transition is unclear, but one study found that individuals with subjective memory complaints (believed to be a late, preclinical stage) show hypometabolism in the DMN compared to those without memory complaints, suggesting a transition occurs during the preclinical stages (298). Further, it is also likely that measures of resting glucose metabolism include both aberrant metabolic activity for synaptic processes associated with lower WM, which was found to be associated with AD pathology in these studies, and potential decreases in beneficial metabolic activity associated with crucial biosynthetic and neuroprotective pathways.

While the specific mechanisms leading to the association between WM microstructure and DMN TID must be addressed in future studies, the present studies provide evidence that WM microstructure can serve as a useful biomarker for assessing the alterations in DMN function and EF associated with both age and AD pathology. Regardless of the specific mechanisms, the present results indicate that age and AD pathology are only associated with DMN function and EF due to their shared variance with WM microstructure. Thus, WM microstructure may be a valuable biomarker of the breakdown in DMN circuitry that is predictive of future decline in EF associated with the combined effects of aging and pathological processes. These findings also suggest that WM microstructure may serve as a therapeutic target for pharmaceutical or behavioral interventions, as preserving or improving WM may help to ameliorate the negative consequences of both aging and pathological processes on cognition.

5.4. Limitations

The present work has several limitations, however. First, the cross-sectional nature of Experiments 1 and 2 prevents the determination of casual relationships. Future studies can address causality through experimental manipulation of the various measures investigated in the present study. However, the current state of technology and scientific knowledge limits these studies to those assessing the causal effects of DMN TID. The use of transcranial magnetic stimulation (TMS) may allow for investigation of the influence of reducing DMN activity on EF. However, TMS is limited in spatial extent, and likely could only be used to reduce activity in DMN hubs, such as the PCC. Levels of Aβ may also be able to be manipulated. Several Phase II trials have demonstrated that Aβ_{42} immunotherapies are able to clear plaques from the brain (299,300). However, Phase III trials have had more limited success in clearance of plaques and failed to produce improvements in cognition (301). If the efficacy of these drugs at clearing Aβ_{42} can be improved and adverse effects decreased, then they may provide a research tool for investigating the effects of lowering Aβ_{42} on DMN WM, TID, and cognition in CN older adults.

Further, the current studies included groups of younger (<40 years old) and older adults (primarily >60 years old). While comparing age groups is beneficial for assessing group differences, the lack of middle-aged adults prevents strong conclusions related to linearity of declines through the adult lifespan. Previous studies have suggested that DMN TID and WM microstructure occur linearly across the adult lifespan (48,96), but it is unclear if these measures are linearly related to each other throughout the adult lifespan. Future studies should seek to include middle-aged adults in order to better assess the trajectory of this relationship across adulthood. These studies would also be aided by considering dementia risk factors, including those associated with AD (i.e. ApoE ε4) and CVD (i.e. diabetes).

In addition to middle-aged adults, the present studies did not include those with either MCI or dementia. Therefore, the effects of the age and AD pathology on WM microstructure or those of WM microstructure on DMN function in these later disease stages cannot be determined from these studies. Previous studies have demonstrated that DMN WM microstructure and TID continue to decline across the disease spectrum (94,98,193,231). In contrast, $A\beta_{42}$ pathology plateaus during early disease stages, while tau continues to accumulate until more advanced stages (302). Therefore, it is likely that the relationships between these variables may differ in MCI and dementia. Further, it is possible that CVD pathology may play a more important role in these later stages. As over 50% of individuals with MCI have significant levels of both AD pathology and other pathologies (primarily CVD) on autopsy (303), vascular processes may be contributing to TID changes as well. Future work should investigate how these relationships might change from states of normal cognition to MCI to dementia, as well as assess the potential role of CVD pathology in these later disease stages.

5.5. A Testable Framework for Future Studies of the DMN in Aging

Despite these limitations, the present study, along with the current literature, allow for the development of a testable model of how WM microstructure may play a pivotal role in the increasingly dysfunctional response within the DMN in aging and AD (and potentially other pathologies). Many of the mechanisms discussed in this model have been described in the sections above (see 5.3) and will only be briefly re-stated. This model, depicted in Figures 5.3 and 5.4, will be described in the following paragraphs:

1) Age-related decline in WM microstructure (see 5.3):

Declines in WM microstructure begin shortly after maturation of the brain's WM in the 3rd-4th decades of life (48). The combined effects of myelin breakdown, hypo-perfusion,

increased inflammation, iron accumulation, exposure to toxins, and disruption of FAT contribute to decreased density of axons, myelin, and/or synapses. These age-related changes likely represent the earliest alterations in WM microstructure in the DMN.

2) Higher floor for minimal DMN activity (see 5.2):

Lower WM microstructure serves as a limiting factor for TID capacity within the DMN. Decreased spatial and temporal summative processes result in higher levels of input in order to maintain the desired level of output (and thus communication within the DMN). This results in an overall greater level of activity ongoing in the DMN during tasks. The consequences of decreased TID are:

2a) Increased demand on EF processes (see 5.1):

Increased levels of DMN processes interfere with processes needed to respond to the external environment. EF allows for these processes to be inhibited, but limits the amount of EF resources that can be utilized to address external demands. This may also contribute to over-recruitment of executive control networks in older adults.

2b) Increased demands on oxidative phosphorylation (see 1.5):

Higher levels of ongoing DMN activity place consistently greater demands on synaptic mitochondria to facilitate neurotransmitter release through oxidative metabolism of glucose. Excessive demands on oxidative respiration can lead to increased development of free radicals, which could damage mitochondria and/or surrounding structures (115).

2c) Greater demands on aerobic glycolysis (AG) for synaptic processes (see 1.5):

Similarly, higher levels of DMN activity place greater demands on glial AG in order to facilitate neurotransmitter recycling. This higher level of AG, along with greater neuronal oxidative phosphorylation, contribute to the lack of decrease in BOLD signal observed in older adults.

2d) Increased $A\beta_{42}$ plaque formation (see 5.3):

The increase in DMN synaptic activity associated with lower WM microstructure may lead to increased $A\beta_{42}$ release at synapses. Based on mediation results, aberrant increases in DMN activity associated with lower WM microstructure, rather than DMN activity as a whole, contribute to accumulation of $A\beta_{42}$ plaques.

3) AD pathology-related decline in WM microstructure (see 5.3):

$A\beta_{42}$ may accumulate as a result of increased DMN activity as described above, as a result of myelin breakdown and repair, or other unknown mechanisms. Further, tau pathology may result from the breakdown of microtubules, myelin repair processes, neurodegeneration, or other unknown mechanisms. Once pathology accumulates, it may exert a negative effect on WM microstructure (even in the case of the myelin model, in which AD pathology is a by-product of reduced WM microstructure). This may occur through oligodendrocyte toxicity, inhibition of myelin sheath formation, impairment of synaptic communication, and/or disruption of FAT.

4) Increased oxidative stress and neurodegeneration

Increased demands on mitochondrial activity may create a pro-inflammatory environment in the DMN, especially in older adults where mitochondrial function may already be impaired (113,114). Further, increased levels of AG dedicated to synaptic metabolism may diminish the neuroprotective AG pathways that produce important molecules for ROS-scavenging , NADPH (119,123). Greater levels of ROS could in turn lead

to mitochondrial damage and synaptic loss (116). In addition, consistently higher demands on mitochondrial activity could also alter the neuronal redox environment resulting in the opening of non-specific Ca^{++} mitochondrial pores and mitochondrial swelling and bursting (115,117). Mitochondrial bursting results in the release of cytochrome c in the cytosol leading to increased activation of apoptotic pathways (115,117).

5) Cascade of breakdown in DMN WM, loss of TID, increased AD pathology, and neurodegeneration:

These changes result in a positive feedback loop, in which initial declines in WM microstructure contribute to reduced TID and increased AD pathology, which in turn results in further declines in WM microstructure (and so on). Further, increases in inflammatory and apoptotic pathways could result in significant synaptic and neuronal loss, which is commonly observed in the DMN during later disease stages (147).

Figure 5.3. Model of the increasingly dysfunctional response in the DMN in aging and AD. This potential model is based on the results of the present studies and current literature. For a detailed description of the model, see the section 5.5. Briefly, age-related declines in WM microstructure contribute to a higher floor in DMN activity. This results in increased demands on mitochondrial activity, increased AG dedicated to synaptic processes, less TID, and increased deposition of $A\beta_{42}$ plaques. Decreases in DMN TID result in declines in EF and potentially to increased recruitment of the executive control network. Increases in mitochondrial demands contribute to greater oxidative stress, which in turn increases neurodegeneration. Increased $A\beta_{42}$ deposition further damages WM microstructure, as does neurodegeneration. This cycle continues over time as a positive feedback loop. Two-way arrows represent the possible contribution of WM microstructure declines to increased $A\beta_{42}$ and tau pathology.

6) Disconnection of the DMN

The end consequence of this feedback loop is disconnection of the DMN. Individuals

with AD have significantly reduced structural connectivity compared to healthy older adults

(193). This structural disconnection could underlie the significant reductions in DMN rsC and

loss of TID observed in AD (94,304,305). Disconnection would also result in significant

neurodegeneration, which, along with lack of DMN functional integrity, may contribute to

DMN hypometabolism observed in AD (147,306). Finally, DMN processes such as autobiographical memory and concept of self may be diminished or lost during dementia.
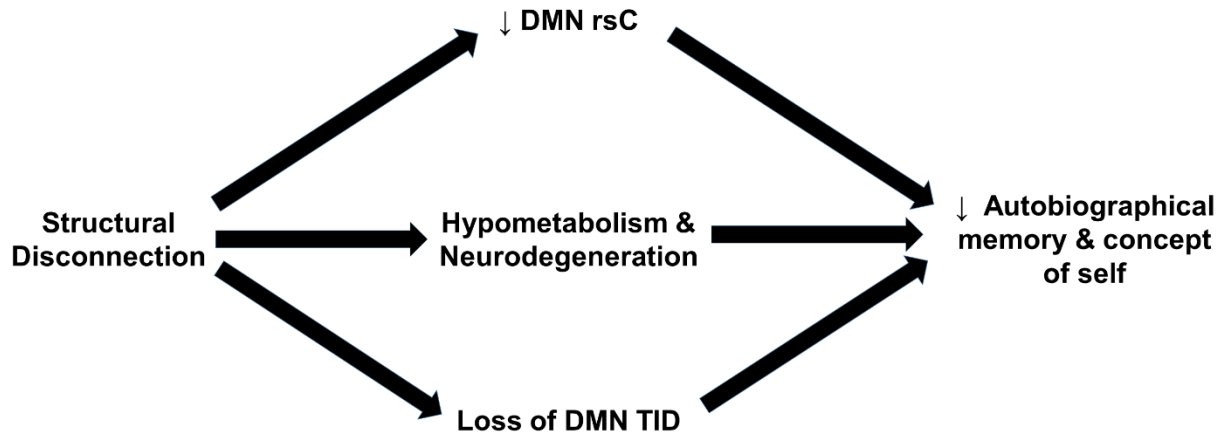
Figure 5.4. Model of later-stage DMN structural disconnection. Over time, the positive feedback loop shown in Figure 5.3 gives rise to structural disconnection of the DMN. Loss of structural connectivity may be responsible for decreased rsC, loss of TID, hypometabolism, and neurodegeneration. As the DMN becomes extensively damaged, DMN processes, such as autobiographical memory and self-maintenance, may be diminished or lost.

5.6. Testing the model

In order to test this preliminary model, future studies must utilize large populations with longitudinal designs. Large sample sizes provide greater power for simultaneously assessing the effects of multiple age-related and pathology-related variables on DMN WM, TID, and EF using multivariate methods. Further, longitudinal designs would aid in determining the temporal ordering of these changes. Importantly, the study population would need to span a significant age-range in order to allow for the inclusion of individuals who are just beginning to develop age-related declines in DMN WM as well as those in clinical stages of MCI and dementia. In addition, tasks that both activate and deactivate the DMN should be used in order to determine whether the same mechanisms underlie increased activity in the DMN during activation and deactivation. The collection of additional

neuroimaging measures, such as glucose metabolism, CBF, and oxygen utilization, would be beneficial in order to better understand the metabolic changes occurring within the DMN in older adults. In addition, post-mortem analysis of brain pathology and microscopic alterations in axonal, myelin, and synaptic morphology should be compared with *in vivo* measures of pathology and WM microstructure in order to better understand the specific changes captured by these *in vivo* markers. Finally, neuroimaging studies assess brain structure and function at a high level, and collaborations with those performing cellular and molecular studies will be necessary in order to better understand the mechanisms underlying changes observed through neuroimaging.

5.7. Conclusions

Diminished capacity for DMN TID contributes to poorer EF in older adults, which reflects a dysfunction response in the aging brain. Both aging and AD pathology contribute to diminished DMN TID in CN older adults. Despite representing independent processes, aging and AD pathology influence DMN function through a common pathway of declining WM microstructure. As a result, WM microstructure provides a valuable marker of both the age-related and AD pathology-related processes contributing to an important breakdown in DMN circuitry that predicts poorer EF in both cross-sectional and longitudinal analyses. These findings indicate that WM microstructure is both a useful biomarker for future research and a potential therapeutic target for future interventions aimed at preventing the negative effects of both age and AD pathology on EF.

In addition, the present results, along with the current literature, allow for the generation of a testable model of the dysfunctional response in the DMN in aging and AD. Future studies will be necessary to test the validity of this model, as many casual pathways and specific mechanisms are yet to be determined. Testing this model will require large samples and longitudinal designs, as well as a multidisciplinary approach that spans clinical

123

and basic researchers examining changes ranging from the network to molecular level. Finally, these studies demonstrate the importance of a wide-angled lens when seeking to understand the aging brain. Focusing solely on a single disease process or "normal aging" almost certainly misses important contributions from other processes. Therefore, a more holistic view of brain aging and disease processes and implementation of multivariate models will help to better elucidate the mechanisms contributing to cognitive decline in older adults.

The following plots included in the appendix are additional data from Experiment 2. All

methods and statistics used for these plots are described in Chapter 3 (3.1-3.4).
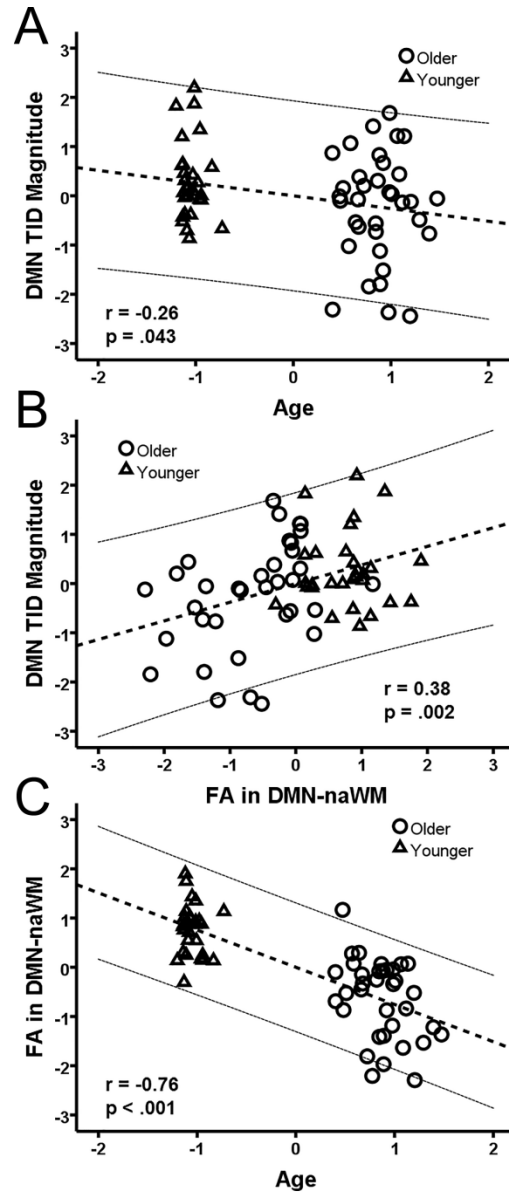
Relationships between Age, FA in DMN-naWM, and DMN TID. A-B: DMN TID magnitude
plotted against age **(A)** and FA in DMN-naWM **(B)** across all participants. **C:** FA in DMN-
naWM plotted against age. **A-C:** All values are standardized residuals after controlling for
age, sex, and education. The thick dashed line is the linear best-fit, and thin dashed lines
are the 95% confidence interval for the predicted response. R- and p-values are for the line
of best-fit.
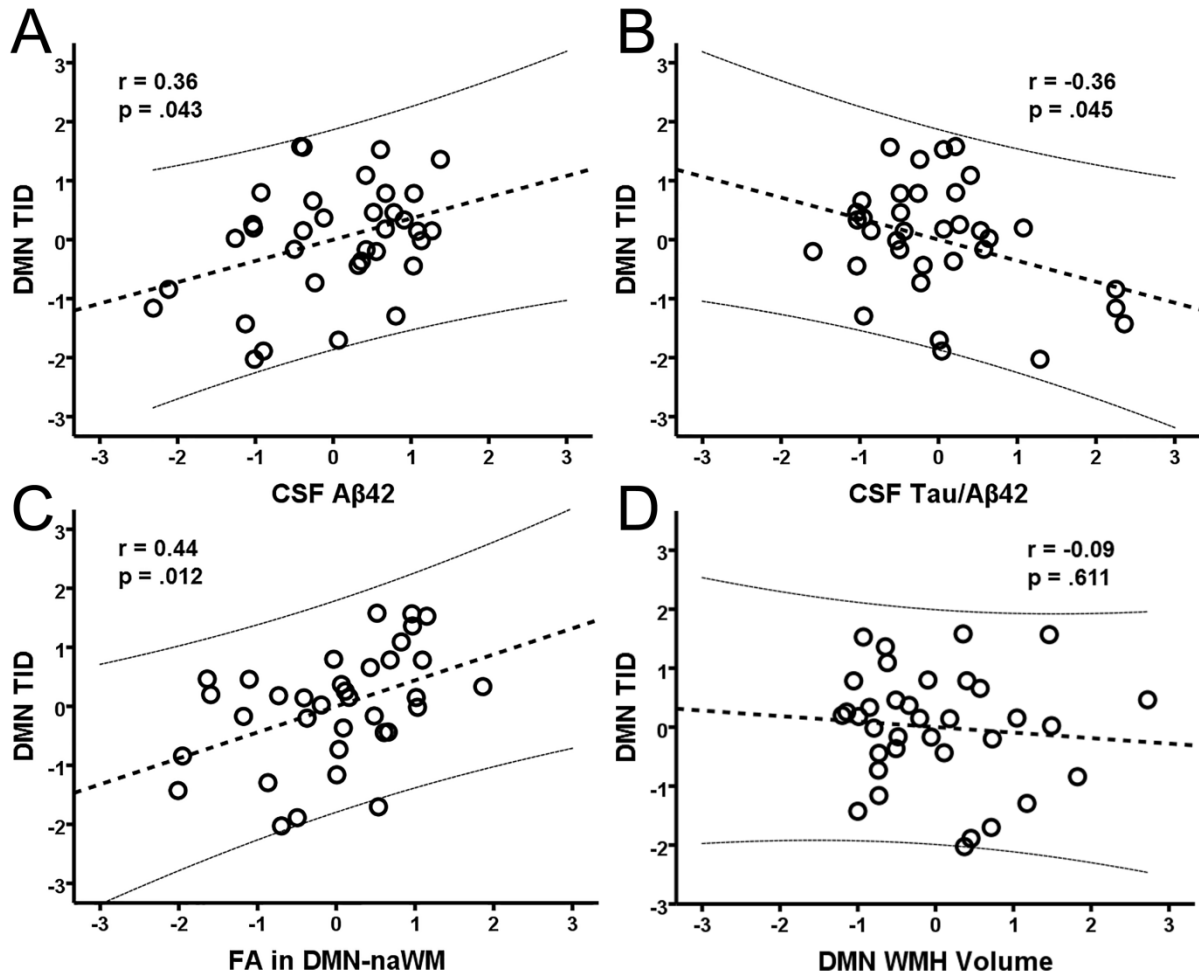
Relationships of AD pathology, CVD pathology, and FA in DMN-naWM with DMN TID.
DMN TID magnitude is plotted against CSF $A\beta_{42}$ **(A)**, CSF Tau/$A\beta_{42}$ ratio **(B)**, FA in DMN-naWM **(C)**, and DMN WMH volume **(D)**. CSF values and WMH volumes were log-transformed prior to analysis. All values are standardized residuals after controlling for age, sex, and education. Thick dashed lines are the linear best-fit, and thin dashed lines are the 95% confidence interval for the predicted response. R- and p-values are for the line of best-fit.
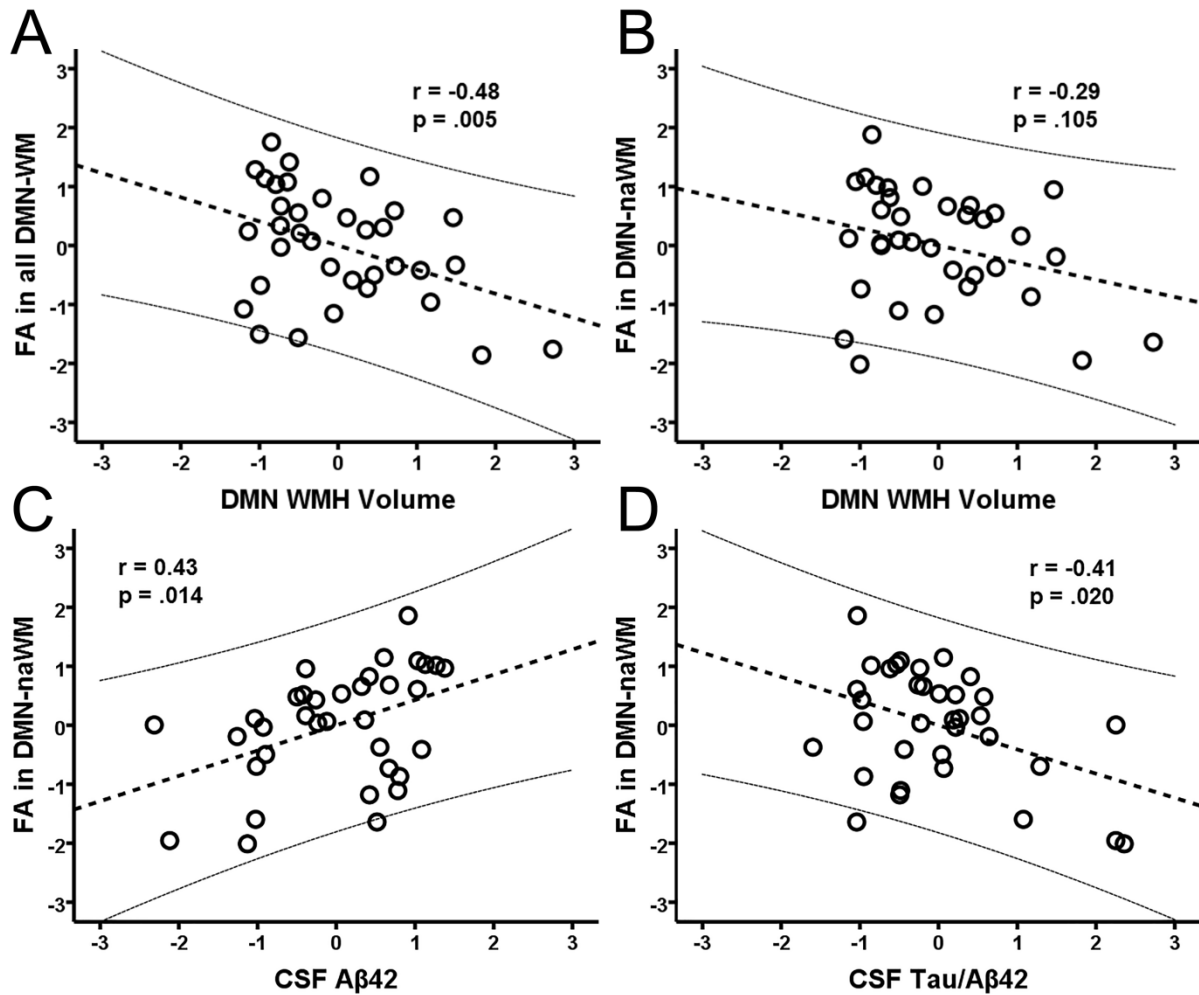
Relationship of CVD pathology and AD pathology with FA in DMN WM. A-B: FA in all DMN-WM **(A)** and FA in DMN-naWM **(B)** plotted against DMN WMH volume. There was a significant relationship between WMH volume and all WM but not with naWM. **C-D:** FA in DMN-naWM plotted against CSF $A\beta_{42}$ **(C)** and CSF $Tau/A\beta_{42}$ ratio **(D)**. **A-D:** WMH volumes and CSF concentrations were log-transformed prior to analyses. All values are standardized residuals after controlling for age, sex, and education. Thick dashed lines are the linear best-fit, and thin dashed lines are the 95% confidence interval for the predicted response. R- and p-values are for the linear best-fit.
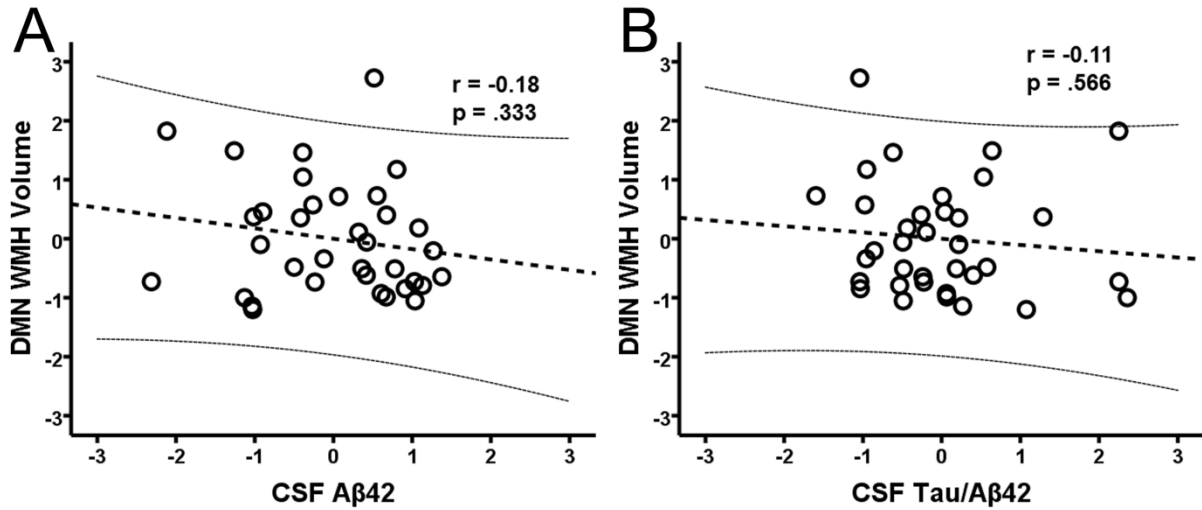
Relationship between AD and CVD pathology. DMN WMH volume plotted against CSF
$A\beta_{42}$ **(A)** and CSF Tau/$A\beta_{42}$ ratio **(B)**. AD and CVD pathology were not correlated in this CN
sample. All values were log-transformed prior to analyses and are standardized residuals
after regressing out age, sex, and education. The thick dashed lines are the linear best-fits,
and the thin dashed lines are the 95% confidence intervals for the predicted response. R-
and p-values are for the linear best-fit.

References

1.   Zelazo PD, Craik FIM, Booth L. Executive function across the life span. Acta Psychol (Amst). 2004;115(2–3):167–83.

2.   Bopp KL, Verhaeghen P. Aging and Verbal Memory Span: A Meta-Analysis. Journals Gerontol Ser B Psychol Sci Soc Sci. 2005 Sep 1;60(5):P223–33.

3.   Hasher L, Zacks RT. Working Memory, Comprehension, and Aging: A Review and a New View. Psychol Learn Motiv. 1988;22:193–225.

4.   West RL. An application of prefrontal cortex function theory to cognitive aging. Psychol Bull. 1996 Sep;120(2):272–92.

5.   Almkvist O. Neuropsychological features of early Alzheimer's disease: preclinical and clinical stages. Acta Neurol Scand. 1996 Apr 11;94(S165):63–71.

6.   Albert MS, Moss MB, Tanzi R, Jones K. Preclinical prediction of AD using neuropsychological tests. J Int Neuropsychol Soc. Cambridge University Press; 2001 Jul 1;7(5):631–9.

7.   Blacker D, Lee H, Muzikansky A, Martin EC, Tanzi R, McArdle JJ, et al. Neuropsychological measures in normal individuals that predict subsequent cognitive decline. Arch Neurol. American Medical Association; 2007 Jun 1;64(6):862–71.

8.   Pathy MSJ, Sinclair AJ, Morley JE. Principles and practice of geriatric medicine. John Wiley & Sons; 2006.

9.   Bell-McGinty S, Podell K, Franzen M, Baird AD, Williams MJ. Standard measures of executive function in predicting instrumental activities of daily living in older adults. Int J Geriatr Psychiatry. John Wiley & Sons, Ltd.; 2002 Sep;17(9):828–34.

10. Miller EK, Cohen JD. An integrative theory of prefrontal cortex function. Annu Rev Neurosci. Annual Reviews 4139 El Camino Way, P.O. Box 10139, Palo Alto, CA 94303-0139, USA; 2001 Jan 28;24:167–202.

11. Braver TS, Cohen JD, Nystrom LE, Jonides J, Smith EE, Noll DC. A parametric study of prefrontal cortex involvement in human working memory. Neuroimage. 1997 Jan;5(1):49–62.

12. Dove A, Pollmann S, Schubert T, Wiggins CJ, Yves von Cramon D. Prefrontal cortex activation in task switching: an event-related fMRI study. Cogn Brain Res. 2000 Jan;9(1):103–9.

13. Carter CS, Mintun M, Cohen JD. Interference and Facilitation Effects during Selective Attention: An H215O PET Study of Stroop Task Performance. Neuroimage. 1995;2(4):264–72.

14. Salthouse TA. What cognitive abilities are involved in trail-making performance? Intelligence. NIH Public Access; 2011 Jul;39(4):222–32.

15. Gibbons LE, Carle AC, Mackin RS, Harvey D, Mukherjee S, Insel P, et al. A composite score for executive functioning, validated in Alzheimer's Disease Neuroimaging Initiative (ADNI) participants with baseline mild cognitive impairment. Brain Imaging Behav. 2012 Dec;6(4):517–27.

16. Weintraub S, Salmon D, Mercaldo N, Ferris S, Graff-Radford NR, Chui H, et al. The Alzheimer's Disease Centers' Uniform Data Set (UDS): the neuropsychologic test battery. Alzheimer Dis Assoc Disord. Jan;23(2):91–101.

17. Salthouse TA. Selective review of cognitive aging. J Int Neuropsychol Soc. 2010 Sep;16(5):754–60.

18. Kray J, Lindenberger U. Adult age differences in task switching. Psychol Aging. 2000;15(1):126–47.

19. Grady C. The cognitive neuroscience of ageing. Nat Rev Neurosci. Nature Publishing Group, a division of Macmillan Publishers Limited. All Rights Reserved.; 2012 Jul;13(7):491–505.

20. Park DC, Reuter-Lorenz P. The adaptive brain: aging and neurocognitive scaffolding. Annu Rev Psychol. 2009;60:173–96.

21. Nagel IE, Lindenberger U. 6 Adult age differences in working memory. Work Mem ageing. Psychology Press; 2014;129.

22. Braver TS, Reynolds JR, Donaldson DI. Neural Mechanisms of Transient and Sustained Cognitive Control during Task Switching. Neuron. 2003 Aug;39(4):713–26.

23. Owen AM, McMillan KM, Laird AR, Bullmore E. N-back working memory paradigm: A meta-analysis of normative functional neuroimaging studies. Hum Brain Mapp. Wiley Subscription Services, Inc., A Wiley Company; 2005 May;25(1):46–59.

24. Spreng RN, Wojtowicz M, Grady CL. Reliable differences in brain activity between young and old adults: a quantitative meta-analysis across multiple cognitive domains. Neurosci Biobehav Rev. 2010 Jul;34(8):1178–94.

25. Grady CL, Protzner AB, Kovacevic N, Strother SC, Afshin-Pour B, Wojtowicz M, et al. A multivariate analysis of age-related differences in default mode and task-positive networks across multiple cognitive domains. Cereb Cortex. 2010 Jun 1;20(6):1432–47.

26. Burzynska AZ, Garrett DD, Preuschhof C, Nagel IE, Li S-C, Bäckman L, et al. A scaffold for efficiency in the human brain. J Neurosci. 2013 Oct 23;33(43):17150–9.

27. Zhu Z, Johnson NF, Kim C, Gold BT. Reduced frontal cortex efficiency is associated with lower white matter integrity in aging. Cereb Cortex. 2015 Jan 1;25(1):138–46.

28. Stern Y. Cognitive reserve. Neuropsychologia. 2009 Aug;47(10):2015–28.

29. Persson J, Lustig C, Nelson JK, Reuter-Lorenz PA. Age differences in deactivation: a link to cognitive control? J Cogn Neurosci. MIT Press 238 Main St., Suite 500, Cambridge, MA 02142-1046USA journals-info@mit.edu; 2007 Jun 30;19(6):1021–32.

30. Prakash RS, Heo S, Voss MW, Patterson B, Kramer AF. Age-related differences in cortical recruitment and suppression: implications for cognitive performance. Behav Brain Res. 2012 Apr 21;230(1):192–200.

31. Turner GR, Spreng RN. Prefrontal Engagement and Reduced Default Network Suppression Co-occur and Are Dynamically Coupled in Older Adults: The Default-Executive Coupling Hypothesis of Aging. J Cogn Neurosci. 2015 Dec;27(12):2462–76.

32. Raichle ME. A Brief History of Human Functional Brain Mapping. In: Brain Mapping: The Systems. Elsevier; 2000. p. 33–75.

33. Friston KJ, Frith CD, LIddle PF, Frackowiak RSJ. Investigating a network model of word generation with poistron emission tomography. Proc R Soc London B. 1991;244(1310):101–6.

34. Haxby J V, Horwitz B, Ungerleider LG, Maisog JM, Pietrini P, Grady CL. The functional organization of human extrastriate cortex: a PET-rCBF study of selective attention to faces and locations. J Neurosci. 1994 Nov;14(11 Pt 1):6336–53.

35. Shulman GL, Fiez JA, Corbetta M, Buckner RL, Miezin FM, Raichle ME, et al. Common Blood Flow Changes across Visual Tasks: II. Decreases in Cerebral Cortex.

J Cogn Neurosci. MIT Press 238 Main St., Suite 500, Cambridge, MA 02142-1046 USA journals-info@mit.edu; 1997 Jan 7;9(5):648–63.

36.   Raichle ME, Snyder AZ. A default mode of brain function: a brief history of an evolving idea. Neuroimage. 2007 Oct 1;37(4):1083-90-9.

37.   Raichle ME, MacLeod AM, Snyder AZ, Powers WJ, Gusnard DA, Shulman GL. A default mode of brain function. Proc Natl Acad Sci U S A. 2001 Jan 16;98(2):676–82.

38.   Buckner RL, Andrews-Hanna JR, Schacter DL. The brain's default network: anatomy, function, and relevance to disease. Ann N Y Acad Sci. 2008 Mar;1124:1–38.

39.   Vincent JL, Patel GH, Fox MD, Snyder AZ, Baker JT, Van Essen DC, et al. Intrinsic functional architecture in the anaesthetized monkey brain. Nature. Nature Publishing Group; 2007 May 3;447(7140):83–6.

40.   Stafford JM, Jarrett BR, Miranda-Dominguez O, Mills BD, Cain N, Mihalas S, et al. Large-scale topology and the default mode network in the mouse connectome. Proc Natl Acad Sci U S A. National Academy of Sciences; 2014 Dec 30;111(52):18745–50.

41.   Kyathanahally SP, Jia H, Pustovyy OM, Waggoner P, Beyers R, Schumacher J, et al. Anterior–posterior dissociation of the default mode network in dogs. Brain Struct Funct. 2015 Mar 8;220(2):1063–76.

42.   Greicius MD, Supekar K, Menon V, Dougherty RF. Resting-state functional connectivity reflects structural connectivity in the default mode network. Cereb Cortex. 2009 Jan 1;19(1):72–8.

43.   Khalsa S, Mayhew SD, Chechlacz M, Bagary M, Bagshaw AP. The structural and functional connectivity of the posterior cingulate cortex: Comparison between deterministic and probabilistic tractography for the investigation of structure-function

relationships. Neuroimage. 2013 Dec 21;

44. Teipel SJ, Bokde ALW, Meindl T, Amaro E, Soldner J, Reiser MF, et al. White matter microstructure underlying default mode network connectivity in the human brain. Neuroimage. 2010 Feb 1;49(3):2021–32.

45. van den Heuvel MP, Mandl RCW, Kahn RS, Hulshoff Pol HE. Functionally linked resting-state networks reflect the underlying structural connectivity architecture of the human brain. Hum Brain Mapp. 2009 Oct;30(10):3127–41.

46. Bartzokis G, Sultzer D, Lu PH, Nuechterlein KH, Mintz J, Cummings JL. Heterogeneous age-related breakdown of white matter structural integrity: implications for cortical "disconnection" in aging and Alzheimer's disease. Neurobiol Aging. 2004 Aug;25(7):843–51.

47. Glasser MF, Goyal MS, Preuss TM, Raichle ME, Van Essen DC. Trends and properties of human cerebral cortex: correlations with cortical myelin content. Neuroimage. NIH Public Access; 2014 Jun;93 Pt 2:165–75.

48. Lebel C, Gee M, Camicioli R, Wieler M, Martin W, Beaulieu C. Diffusion tensor imaging of white matter tract evolution over the lifespan. Neuroimage. 2012 Mar;60(1):340–52.

49. Roy CS, Sherrington CS. On the Regulation of the Blood-supply of the Brain. J Physiol. 1890 Jan 1;11(1–2):85–158.

50. Fox PT, Miezin FM, Allman JM, Van Essen DC, Raichle ME. Retinotopic organization of human visual cortex mapped with positron- emission tomography. JNeurosci. 1987;7(3):913–22.

51. Fox PT, Mintun MA, Raichle ME, Miezin FM, Allman JM, Van Essen DC. Mapping

human visual cortex with positron emission tomography. Nature. 1986;323(6091):806–9.

52. Ogawa S, Lee TM, Kay AR, Tank DW. Brain magnetic resonance imaging with contrast dependent on blood oxygenation. Proc Natl Acad Sci U S A. 1990 Dec;87(24):9868–72.

53. Fox PT, Raichle ME, Mintun MA, Dence C. Nonoxidative glucose consumption during focal physiologic neural activity. Science. 1988 Jul 22;241(4864):462–4.

54. Lin A-L, Fox PT, Hardies J, Duong TQ, Gao J-H. Nonlinear coupling between cerebral blood flow, oxygen consumption, and ATP production in human visual cortex. Proc Natl Acad Sci U S A. National Academy of Sciences; 2010 May 4;107(18):8446–51.

55. Bandettini PA, Wong EC, Hinks RS, Tikofsky RS, Hyde JS. Time course EPI of human brain function during task activation. Magn Reson Med. Wiley Subscription Services, Inc., A Wiley Company; 1992 Jun;25(2):390–7.

56. Kwong KK, Belliveau JW, Chesler DA, Goldberg IE, Weisskoff RM, Poncelet BP, et al. Dynamic magnetic resonance imaging of human brain activity during primary sensory stimulation. Proc Natl Acad Sci U S A. National Academy of Sciences; 1992 Jun 15;89(12):5675–9.

57. Ogawa S, Tank DW, Menon R, Ellermann JM, Kim SG, Merkle H, et al. Intrinsic signal changes accompanying sensory stimulation: functional brain mapping with magnetic resonance imaging. Proc Natl Acad Sci U S A. 1992 Jul 1;89(13):5951–5.

58. Logothetis NK, Pauls J, Augath M, Trinath T, Oeltermann A. Neurophysiological investigation of the basis of the fMRI signal. Nature. Nature Publishing Group; 2001 Jul 12;412(6843):150–7.

59. Logothetis NK, Wandell BA. Interpreting the BOLD Signal. Annu Rev Physiol. 2004 Mar;66(1):735–69.

60. Bentley WJ, Li JM, Snyder AZ, Raichle ME, Snyder LH. Oxygen Level and LFP in Task-Positive and Task-Negative Areas: Bridging BOLD fMRI and Electrophysiology. Cereb Cortex. 2014 Dec 10;

61. Mazoyer B, Zago L, Mellet E, Bricogne S, Etard O, Houdé O, et al. Cortical networks for working memory and executive functions sustain the conscious resting state in man. Brain Res Bull. 2001 Feb;54(3):287–98.

62. Shulman RG, Hyder F, Rothman DL. Cerebral energetics and the glycogen shunt: neurochemical basis of functional imaging. Proc Natl Acad Sci U S A. National Academy of Sciences; 2001 May 22;98(11):6417–22.

63. Shulman RG, Rothman DL, Behar KL, Hyder F. Energetic basis of brain activity: Implications for neuroimaging. Vol. 27, Trends in Neurosciences. 2004. p. 489–95.

64. Sibson NR, Dhankhar A, Mason GF, Behar KL, Rothman DL, Shulman RG. In vivo 13C NMR measurements of cerebral glutamine synthesis as evidence for glutamate-glutamine cycling. Proc Natl Acad Sci U S A. 1997 Mar 18;94(6):2699–704.

65. Greicius MD, Krasnow B, Reiss AL, Menon V. Functional connectivity in the resting brain: a network analysis of the default mode hypothesis. Proc Natl Acad Sci U S A. 2003 Jan 7;100(1):253–8.

66. Biswal B, Zerrin Yetkin F, Haughton VM, Hyde JS. Functional connectivity in the motor cortex of resting human brain using echo-planar mri. Magn Reson Med. 1995 Oct;34(4):537–41.

67. Montemurro MA, Rasch MJ, Murayama Y, Logothetis NK, Panzeri S. Phase-of-Firing

Coding of Natural Visual Stimuli in Primary Visual Cortex. Curr Biol. 2008 Mar 11;18(5):375–80.

68. Gusnard DA, Raichle ME. Searching for a baseline: functional imaging and the resting human brain. Nat Rev Neurosci. 2001 Oct;2(10):685–94.

69. Vogt BA, Finch DM, Olson CR. Functional Heterogeneity in Cingulate Cortex: The Anterior Executive and Posterior Evaluative Regions. Cereb Cortex. Oxford University Press; 1992;2(6):435–43.

70. Maddock RJ. The retrosplenial cortex and emotion: new insights from functional neuroimaging of the human brain. Trends Neurosci. 1999;22(7):310–6.

71. Simpson JR, Öngür D, Akbudak E, Conturo TE, Ollinger JM, Snyder AZ, et al. The Emotional Modulation of Cognitive Processing: An fMRI Study. J Cogn Neurosci. 2000 Nov;12(supplement 2):157–70.

72. Bechara A, Damasio H, Tranel D, Damasio AR. Deciding Advantageously Before Knowing the Advantageous Strategy. Science (80-). 1997;275(5304).

73. Grossman E, Donnelly M, Price R, Pickens D, Morgan V, Neighbor G, et al. Brain Areas Involved in Perception of Biological Motion. J Cogn Neurosci. MIT Press 238 Main St., Suite 500, Cambridge, MA 02142-1046 USA journals-info@mit.edu ; 2000 Sep;12(5):711–20.

74. Allison T, Puce A, McCarthy G. Social perception from visual cues: role of the STS region. Trends Cogn Sci. 2000;4(7):267–78.

75. Antrobus JS, Singer JL, Goldstein S, Fortgang M. Section of Psychology: MINDWANDERING AND COGNITIVE STRUCTURE*, †. Trans N Y Acad Sci. Blackwell Publishing Ltd; 1970 Feb;32(2 Series II):242–52.

76.   Frith CD, Frith U. Interacting minds--a biological basis. Science. 1999 Nov
        26;286(5445):1692–5.

77.   McGuire PK, Paulesu E, Frackowiak RS, Frith CD. Brain activity during stimulus
        independent thought. Neuroreport. 1996 Sep 2;7(13):2095–9.

78.   SCOVILLE WB, MILNER B. Loss of recent memory after bilateral hippocampal
        lesions. J Neurol Neurosurg Psychiatry. BMJ Publishing Group Ltd; 1957
        Feb;20(1):11–21.

79.   Squire LR, Zola-Morgan S. The medial temporal lobe memory system. Science. 1991
        Sep 20;253(5026):1380–6.

80.   Andrews-Hanna JR, Smallwood J, Spreng RN. The default network and self-
        generated thought: component processes, dynamic control, and clinical relevance.
        Ann N Y Acad Sci. NIH Public Access; 2014 May;1316(1):29–52.

81.   Spreng RN, Mar RA, Kim ASN. The Common Neural Basis of Autobiographical
        Memory, Prospection, Navigation, Theory of Mind, and the Default Mode: A
        Quantitative Meta-analysis. J Cogn Neurosci. MIT Press238 Main St., Suite 500,
        Cambridge, MA 02142-1046, USA journals-info@mit.edu; 2009 Mar;21(3):489–510.

82.   Horovitz SG, Braun AR, Carr WS, Picchioni D, Balkin TJ, Fukunaga M, et al.
        Decoupling of the brain's default mode network during deep sleep. Proc Natl Acad Sci
        U S A. National Academy of Sciences; 2009 Jul 7;106(27):11376–81.

83.   Samann PG, Wehrle R, Hoehn D, Spoormaker VI, Peters H, Tully C, et al.
        Development of the Brain's Default Mode Network from Wakefulness to Slow Wave
        Sleep. Cereb Cortex. Oxford University Press; 2011 Sep 1;21(9):2082–93.

84.   Greicius MD, Kiviniemi V, Tervonen O, Vainionpää V, Alahuhta S, Reiss AL, et al.

Persistent default-mode network connectivity during light sedation. Hum Brain Mapp. Wiley Subscription Services, Inc., A Wiley Company; 2008 Jul;29(7):839–47.

85.   Roquet D, Foucher JR, Froehlig P, Renard F, Pottecher J, Besancenot H, et al. Resting-state networks distinguish locked-in from vegetative state patients. NeuroImage Clin. Elsevier; 2016;12:16–22.

86.   Rosazza C, Andronache A, Sattin D, Bruzzone MG, Marotta G, Nigri A, et al. Multimodal study of default-mode network integrity in disorders of consciousness. Ann Neurol. 2016 May;79(5):841–53.

87.   Vanhaudenhuyse A, Noirhomme Q, Tshibanda LJF, Bruno MA, Boveroux P, Schnakers C, et al. Default network connectivity reflects the level of consciousness in non-communicative brain-damaged patients. Brain. Oxford University Press; 2010 Jan;133(1):161–71.

88.   Fingelkurts AA, Fingelkurts AA, Bagnato S, Boccagni C, Galardi G. The Open Neuroimaging Journal The Chief Role of Frontal Operational Module of the Brain Default Mode Network in the Potential Recovery of Consciousness from the Vegetative State: A Preliminary Comparison of Three Case Reports. Open Neuroimag J. 2016 May 13;10(16):41–51.

89.   Dennis EL, Thompson PM. Functional brain connectivity using fMRI in aging and Alzheimer's disease. Neuropsychol Rev. 2014 Mar;24(1):49–62.

90.   Mevel K, Chételat G, Eustache F, Desgranges B. The default mode network in healthy aging and Alzheimer's disease. Int J Alzheimers Dis. 2011 Jan;2011:535816.

91.   Sheline YI, Raichle ME. Resting state functional connectivity in preclinical Alzheimer's disease. Biol Psychiatry. 2013 Sep 1;74(5):340–7.

92.   Damoiseaux JS, Beckmann CF, Arigita EJS, Barkhof F, Scheltens P, Stam CJ, et al. Reduced resting-state brain activity in the "default network" in normal aging. Cereb Cortex. 2008 Aug 1;18(8):1856–64.

93.   Petrella JR, Sheldon FC, Prince SE, Calhoun VD, Doraiswamy PM. Default mode network connectivity in stable vs progressive mild cognitive impairment. Neurology. 2011 Feb 8;76(6):511–7.

94.   Lustig C, Snyder AZ, Bhakta M, O'Brien KC, McAvoy M, Raichle ME, et al. Functional deactivations: change with age and dementia of the Alzheimer type. Proc Natl Acad Sci U S A. 2003 Nov 25;100(24):14504–9.

95.   Jones DT, Machulda MM, Vemuri P, McDade EM, Zeng G, Senjem ML, et al. Age-related changes in the default mode network are more advanced in Alzheimer disease. Neurology. 2011 Oct 18;77(16):1524–31.

96.   Grady CL, Springer M V, Hongwanishkul D, McIntosh AR, Winocur G. Age-related changes in brain activity across the adult lifespan. J Cogn Neurosci. 2006 Feb;18(2):227–41.

97.   Pihlajamäki M, Sperling RA. Functional MRI assessment of task-induced deactivation of the default mode network in Alzheimer's disease and at-risk older individuals. Behav Neurol. 2009 Jan;21(1):77–91.

98.   Rombouts SARB, Barkhof F, Goekoop R, Stam CJ, Scheltens P. Altered resting state networks in mild cognitive impairment and mild Alzheimer's disease: an fMRI study. Hum Brain Mapp. 2005 Dec;26(4):231–9.

99.   Sperling RA, Laviolette PS, O'Keefe K, O'Brien J, Rentz DM, Pihlajamaki M, et al. Amyloid deposition is associated with impaired default network function in older

persons without dementia. Neuron. 2009 Jul 30;63(2):178–88.

100.   McKiernan KA, Kaufman JN, Kucera-Thompson J, Binder JR. A parametric
       manipulation of factors affecting task-induced deactivation in functional neuroimaging.
       J Cogn Neurosci. MIT Press 238 Main St., Suite 500, Cambridge, MA 02142-1046
       USA journals-info@mit.edu; 2003 Apr 1;15(3):394–408.

101.   Fox MD, Snyder AZ, Vincent JL, Corbetta M, Van Essen DC, Raichle ME. The human
       brain is intrinsically organized into dynamic, anticorrelated functional networks. Proc
       Natl Acad Sci U S A. 2005 Jul 5;102(27):9673–8.

102.   Spreng RN, Schacter DL. Default network modulation and large-scale network
       interactivity in healthy young and old adults. Cereb Cortex. 2012 Nov;22(11):2610–
       21.

103.   Goulden N, Khusnulina A, Davis NJ, Bracewell RM, Bokde AL, McNulty JP, et al. The
       salience network is responsible for switching between the default mode network and
       the central executive network: Replication from DCM. Neuroimage. 2014;99:180–90.

104.   Chen AC, Oathes DJ, Chang C, Bradley T, Zhou Z-W, Williams LM, et al. Causal
       interactions between fronto-parietal central executive and default-mode networks in
       humans. Proc Natl Acad Sci. National Academy of Sciences; 2013 Dec
       3;110(49):19944–9.

105.   Park DC, Polk TA, Hebrank AC, Jenkins LJ. Age differences in default mode activity
       on easy and difficult spatial judgment tasks. Front Hum Neurosci. 2010 Jan;3:75.

106.   Sambataro F, Murty VP, Callicott JH, Tan H-Y, Das S, Weinberger DR, et al. Age-
       related alterations in default mode network: impact on working memory performance.
       Neurobiol Aging. 2010 May;31(5):839–52.

107. Spreng RN. The fallacy of a "task-negative" network. Front Psychol. 2012 Jan;3:145.

108. Kasischke KA, Vishwasrao HD, Fisher PJ, Zipfel WR, Webb WW. Neural Activity Triggers Neuronal Oxidative Metabolism Followed by Astrocytic Glycolysis. Science (80-). 2004 Jul 2;305(5680):99–103.

109. Mintun MA, Vlassenko AG, Rundle MM, Raichle ME. Increased lactate/pyruvate ratio augments blood flow in physiologically activated human brain. Proc Natl Acad Sci U S A. National Academy of Sciences; 2004 Jan 13;101(2):659–64.

110. Bak LK, Schousboe A, Waagepetersen HS. The glutamate/GABA-glutamine cycle: aspects of transport, neurotransmitter homeostasis and ammonia transfer. J Neurochem. Blackwell Publishing Ltd; 2006 Aug;98(3):641–53.

111. Vos M, Lauwers E, Verstreken P. Synaptic mitochondria in synaptic transmission and organization of vesicle pools in health and disease. Front Synaptic Neurosci. Frontiers; 2010;2:139.

112. Verstreken P, Ly C V., Venken KJT, Koh T-W, Zhou Y, Bellen HJ. Synaptic Mitochondria Are Critical for Mobilization of Reserve Pool Vesicles at Drosophila Neuromuscular Junctions. Neuron. 2005;47(3):365–78.

113. Harman D. Free Radical Theory of Aging: Consequences of Mitochondrial Aging. Age (Omaha). Kluwer Academic Publishers; 1983 Jul;6(3):86–94.

114. Beckman KB, Ames BN. Mitochondrial aging: Open questions. In: Annals of the New York Academy of Sciences. Blackwell Publishing Ltd; 1998. p. 118–27.

115. Bernardi P, Petronilli V, Di Lisa F, Forte M. A mitochondrial perspective on cell death. Trends Biochem Sci. 2001 Feb;26(2):112–7.

116. Fukui H, Moraes CT. The mitochondrial impairment, oxidative stress and

neurodegeneration connection: reality or just an attractive hypothesis? Trends Neurosci. NIH Public Access; 2008 May;31(5):251–6.

117. Kroemer G, Reed JC. Mitochondrial control of cell death. Nat Med. 2000 May 1;6(5):513–9.

118. Magistretti PJ, Chatton J-Y. Relationship between L-glutamate-regulated intracellular Na+ dynamics and ATP hydrolysis in astrocytes. J Neural Transm. 2005 Jan 18;112(1):77–85.

119. Vlassenko AG, Raichle ME. Brain aerobic glycolysis functions and Alzheimer's disease. Vol. 3, Clinical and Translational Imaging. NIH Public Access; 2015. p. 27–37.

120. Lunt SY, Vander Heiden MG. Aerobic Glycolysis: Meeting the Metabolic Requirements of Cell Proliferation. Annu Rev Cell Dev Biol. 2011 Nov 10;27(1):441–64.

121. Vaughn AE, Deshmukh M. Glucose metabolism inhibits apoptosis in neurons and cancer cells by redox inactivation of cytochrome c. Nat Cell Biol. NIH Public Access; 2008 Dec;10(12):1477–83.

122. Dastur DK. Cerebral Blood Flow and Metabolism in Normal Human Aging, Pathological Aging, and Senile Dementia. J Cereb Blood Flow Metab. SAGE PublicationsSage UK: London, England; 1985 Mar;5(1):1–9.

123. Brand KA, Hermfisse U. Aerobic glycolysis by proliferating cells: a protective strategy against reactive oxygen species. FASEB J. 1997 Apr;11(5):388–95.

124. Morris JC, Storandt M, McKeel DW, Rubin EH, Price JL, Grant EA, et al. Cerebral amyloid deposition and diffuse plaques in ``normal'' aging: Evidence for

presymptomatic and very mild Alzheimer's disease. Neurology. 1996 Mar 1;46(3):707–19.

125. Price JL, McKeel DW, Buckles VD, Roe CM, Xiong C, Grundman M, et al. Neuropathology of nondemented aging: presumptive evidence for preclinical Alzheimer disease. Neurobiol Aging. 2009 Jul;30(7):1026–36.

126. Sperling RA, Aisen PS, Beckett LA, Bennett DA, Craft S, Fagan AM, et al. Toward defining the preclinical stages of Alzheimer's disease: recommendations from the National Institute on Aging-Alzheimer's Association workgroups on diagnostic guidelines for Alzheimer's disease. Alzheimers Dement. 2011 May;7(3):280–92.

127. Shaw LM, Vanderstichele H, Knapik-Czajka M, Clark CM, Aisen PS, Petersen RC, et al. Cerebrospinal fluid biomarker signature in Alzheimer's disease neuroimaging initiative subjects. Ann Neurol. 2009 Apr;65(4):403–13.

128. Glenner GG, Wong CW. Alzheimer's disease: Initial report of the purification and characterization of a novel cerebrovascular amyloid protein. Biochem Biophys Res Commun. 1984 May;120(3):885–90.

129. Selkoe DJ, Abraham CR, Podlisny MB, Duffy LK. Isolation of Low-Molecular-Weight Proteins from Amyloid Plaque Fibers in Alzheimer's Disease. J Neurochem. 1986 Oct 5;146(6):1820–34.

130. Grundke-Iqbal I, Iqbal K, Tung YC, Quinlan M, Wisniewski HM, Binder LI. Abnormal phosphorylation of the microtubule-associated protein tau (tau) in Alzheimer cytoskeletal pathology. Proc Natl Acad Sci. 1986 Jul 1;83(13):4913–7.

131. NUKINA N, IHARA Y. One of the Antigenic Determinants of Paired Helical Filaments Is Related to Tau Protein. J Biochem. 1986 Apr 1;99(5):1541–4.

132. Nitsch RM, Rebeck GW, Deng M, Richardson UI, Tennis M, Schenk DB, et al. Cerebrospinal fluid levels of amyloid beta-protein in Alzheimer's disease: inverse correlation with severity of dementia and effect of apolipoprotein E genotype. Ann Neurol. 1995 Apr;37(4):512–8.

133. Motter R, Vigo-Pelfrey C, Kholodenko D, Barbour R, Johnson-Wood K, Galasko D, et al. Reduction of beta-amyloid peptide42 in the cerebrospinal fluid of patients with Alzheimer's disease. Ann Neurol. 1995 Oct;38(4):643–8.

134. Vigo-Pelfrey C, Seubert PP, Barbour R, Blomquist C, Lee M, Lee D, et al. Elevation of microtubule-associated protein tau in the cerebrospinal fluid of patients with Alzheimer's disease. Neurology. 1995 Apr 1;45(4):788–93.

135. Andreasen N, Vanmechelen E, Van de Voorde A, Davidsson P, Hesse C, Tarvonen S, et al. Cerebrospinal fluid tau protein as a biochemical marker for Alzheimer's disease: a community based follow up study. J Neurol Neurosurg Psychiatry. 1998 Mar 1;64(3):298–305.

136. Sjogren M. Both total and phosphorylated tau are increased in Alzheimer's disease. J Neurol Neurosurg Psychiatry. 2001 May 1;70(5):624–30.

137. Blennow K, Vanmechelen E, Hampel H. CSF total tau, Abeta42 and phosphorylated tau protein as biomarkers for Alzheimer's disease. Mol Neurobiol. 24(1–3):87–97.

138. Stomrud E, Hansson O, Blennow K, Minthon L, Londos E. Cerebrospinal fluid biomarkers predict decline in subjective cognitive function over 3 years in healthy elderly. Dement Geriatr Cogn Disord. Karger Publishers; 2007 Jan;24(2):118–24.

139. Fagan AM, Roe CM, Xiong C, Mintun MA, Morris JC, Holtzman DM. Cerebrospinal fluid tau/beta-amyloid(42) ratio as a prediction of cognitive decline in nondemented

older adults. Arch Neurol. American Medical Association; 2007 Mar 1;64(3):343–9.

140. De Meyer G, Shapiro F, Vanderstichele H, Vanmechelen E, Engelborghs S, De Deyn PP, et al. Diagnosis-independent Alzheimer disease biomarker signature in cognitively normal elderly people. Arch Neurol. American Medical Association; 2010 Aug 1;67(8):949–56.

141. Vos SJ, Xiong C, Visser PJ, Jasielec MS, Hassenstab J, Grant EA, et al. Preclinical Alzheimer's disease and its outcome: a longitudinal cohort study. Lancet Neurol. 2013 Oct;12(10):957–65.

142. Klunk WE, Engler H, Nordberg A, Wang Y, Blomqvist G, Holt DP, et al. Imaging brain amyloid in Alzheimer's disease with Pittsburgh Compound-B. Ann Neurol. 2004 Mar;55(3):306–19.

143. Villemagne VL, Okamura N. In vivo tau imaging: Obstacles and progress. Alzheimer's Dement. 2014;10(3 SUPPL.):S254–64.

144. Rodrigue KM, Kennedy KM, Devous MD, Rieck JR, Hebrank AC, Diaz-Arrastia R, et al. β-Amyloid burden in healthy aging: regional distribution and cognitive consequences. Neurology. American Academy of Neurology; 2012 Feb 7;78(6):387–95.

145. Mintun MA, Larossa GN, Sheline YI, Dence CS, Lee SY, Mach RH, et al. [11C]PIB in a nondemented population: potential antecedent marker of Alzheimer disease. Neurology. 2006 Aug 8;67(3):446–52.

146. Johnson KA, Schultz A, Betensky RA, Becker JA, Sepulcre J, Rentz D, et al. Tau positron emission tomographic imaging in aging and early Alzheimer disease. Ann Neurol. 2016;

147. Buckner RL, Snyder AZ, Shannon BJ, LaRossa G, Sachs R, Fotenos AF, et al. Molecular, structural, and functional characterization of Alzheimer's disease: evidence for a relationship between default activity, amyloid, and memory. J Neurosci. 2005 Aug 24;25(34):7709–17.

148. Schöll M, Lockhart SN, Schonhaut DR, O'Neil JP, Janabi M, Ossenkoppele R, et al. PET Imaging of Tau Deposition in the Aging Human Brain. Neuron. 2016;89(5).

149. Fagan AM, Mintun MA, Mach RH, Lee S-Y, Dence CS, Shah AR, et al. Inverse relation between in vivo amyloid imaging load and cerebrospinal fluid Abeta42 in humans. Ann Neurol. 2006 Mar;59(3):512–9.

150. Gordon BA, Friedrichsen K, Brier M, Blazey T, Su Y, Christensen J, et al. The relationship between cerebrospinal fluid markers of Alzheimer pathology and positron emission tomography tau imaging. Brain. 2016;139(8):2249–60.

151. Brier MR, Gordon B, Friedrichsen K, McCarthy J, Stern A, Christensen J, et al. Tau and A imaging, CSF measures, and cognition in Alzheimers disease. Sci Transl Med. 2016 May 11;8(338):338ra66-338ra66.

152. Mattsson N, Insel PS, Donohue M, Landau S, Jagust WJ, Shaw LM, et al. Independent information from cerebrospinal fluid amyloid-β and florbetapir imaging in Alzheimer's disease. Brain. 2014 Dec 24;138(3):772–83.

153. Elman JA, Oh H, Madison CM, Baker SL, Vogel JW, Marks SM, et al. Neural compensation in older people with brain amyloid-β deposition. Nat Neurosci. 2014 Oct;17(10):1316–8.

154. Huijbers W, Mormino EC, Wigman SE, Ward AM, Vannini P, McLaren DG, et al. Amyloid deposition is linked to aberrant entorhinal activity among cognitively normal

older adults. J Neurosci. 2014 Apr 9;34(15):5200–10.

155. Sheline YI, Raichle ME, Snyder AZ, Morris JC, Head D, Wang S, et al. Amyloid plaques disrupt resting state default mode network connectivity in cognitively normal elderly. Biol Psychiatry. 2010 Mar 15;67(6):584–7.

156. Hedden T, Van Dijk KRA, Becker JA, Mehta A, Sperling RA, Johnson KA, et al. Disruption of functional connectivity in clinically normal older adults harboring amyloid burden. J Neurosci. 2009 Oct 7;29(40):12686–94.

157. Wang L, Brier MR, Snyder AZ, Thomas JB, Fagan AM, Xiong C, et al. Cerebrospinal fluid Aβ42, phosphorylated Tau181, and resting-state functional connectivity. JAMA Neurol. American Medical Association; 2013 Oct 1;70(10):1242–8.

158. Raz N, Gunning FM, Head D, Dupuis JH, McQuain J, Briggs SD, et al. Selective aging of the human cerebral cortex observed in vivo: differential vulnerability of the prefrontal gray matter. Cereb Cortex. Oxford University Press; 1997 Apr 1;7(3):268–82.

159. Ge Y, Grossman RI, Babb JS, Rabin ML, Mannon LJ, Kolson DL. Age-Related Total Gray Matter and White Matter Changes in Normal Adult Brain. Part I: Volumetric MR Imaging Analysis. Am J Neuroradiol. 2002;23(8).

160. Pfefferbaum A, Sullivan E V, Hedehus M, Lim KO, Adalsteinsson E, Moseley M. Age-related decline in brain white matter anisotropy measured with spatially corrected echo-planar diffusion tensor imaging. Magn Reson Med. 2000 Aug;44(2):259–68.

161. Sullivan E V, Pfefferbaum A. Diffusion tensor imaging and aging. Neurosci Biobehav Rev. 2006 Jan;30(6):749–61.

162. Fjell AM, Walhovd KB, Fennema-Notestine C, McEvoy LK, Hagler DJ, Holland D, et

al. Brain atrophy in healthy aging is related to CSF levels of Aβ1-42. Cereb Cortex. Oxford University Press; 2010 Sep;20(9):2069–79.

163. Fjell AM, McEvoy L, Holland D, Dale AM, Walhovd KB, Alzheimer's Disease Neuroimaging Initiative. What is normal in normal aging? Effects of aging, amyloid and Alzheimer's disease on the cerebral cortex and the hippocampus. Prog Neurobiol. NIH Public Access; 2014 Jun;117:20–40.

164. Threlkeld ZD, Jicha GA, Smith CD, Gold BT. Task deactivation reductions and atrophy within parietal default mode regions are overlapping but only weakly correlated in mild cognitive impairment. J Alzheimers Dis. 2011 Jan;27(2):415–27.

165. Daselaar SM, Iyengar V, Davis SW, Eklund K, Hayes SM, Cabeza RE. Less Wiring, More Firing: Low-Performing Older Adults Compensate for Impaired White Matter with Greater Neural Activity. Cereb Cortex. 2013 Oct 23;bht289-.

166. Basser PJ, Mattiello J, LeBihan D. MR diffusion tensor spectroscopy and imaging. Biophys J. 1994 Jan;66(1):259–67.

167. Pierpaoli C, Jezzard P, Basser PJ, Barnett A, Di Chiro G. Diffusion tensor MR imaging of the human brain. Radiology. American Public Health Association; 1996 Dec 1;201(3):637–48.

168. Beaulieu C. The basis of anisotropic water diffusion in the nervous system - a technical review. NMR Biomed. 2002;15(7–8):435–55.

169. Pierpaoli C, Basser PJ. Toward a quantitative assessment of diffusion anisotropy. Magn Reson Med. 1996 Dec;36(6):893–906.

170. Bartzokis G, Gong JS, Yanagisawa K, Michikawa M, Mayer L, Breitner JC, et al. Age-related myelin breakdown: a developmental model of cognitive decline and

Alzheimer's disease. Neurobiol Aging. Elsevier; 2004 Jan;25(1):5-18-62.

171. Salat DH, Tuch DS, Greve DN, van der Kouwe a JW, Hevelone ND, Zaleta a K, et al. Age-related alterations in white matter microstructure measured by diffusion tensor imaging. Neurobiol Aging. 2005;26(8):1215–27.

172. Song S-K, Yoshino J, Le TQ, Lin S-J, Sun S-W, Cross AH, et al. Demyelination increases radial diffusivity in corpus callosum of mouse brain. Neuroimage. 2005 May 15;26(1):132–40.

173. Sun S-W, Song S-K, Harms MP, Lin S-J, Holtzman DM, Merchant KM, et al. Detection of age-dependent brain injury in a mouse model of brain amyloidosis associated with Alzheimer's disease using magnetic resonance diffusion tensor imaging. Exp Neurol. 2005 Jan;191(1):77–85.

174. Song S-K, Sun S-W, Ju W-K, Lin S-J, Cross AH, Neufeld AH. Diffusion tensor imaging detects and differentiates axon and myelin degeneration in mouse optic nerve after retinal ischemia. Neuroimage. 2003;20(3):1714–22.

175. Marner L, Nyengaard JR, Tang Y, Pakkenberg B. Marked loss of myelinated nerve fibers in the human brain with age. J Comp Neurol. Wiley Subscription Services, Inc., A Wiley Company; 2003 Jul 21;462(2):144–52.

176. Tang Y, Nyengaard JR, Pakkenberg B, Gundersen HJ, Schweizer A, Groot J de. Age-induced white matter changes in the human brain: a stereological investigation. Neurobiol Aging. George Thieme, Leipzig; 1990;18(6):609–15.

177. Peters A, Sethares C. Aging and the myelinated fibers in prefrontal cortex and corpus callosum of the monkey. J Comp Neurol. 2002 Jan 14;442(3):277–91.

178. Peters A. The effects of normal aging on myelin and nerve fibers: A review. J

Neurocytol. Kluwer Academic Publishers; 31(8–9):581–93.

179. Peters A. Structural changes in the normally aging cerebral cortex of primates. Prog Brain Res. 2002 Jan;136:455–65.

180. Breteler MM, van Swieten JC, Bots ML, Grobbee DE, Claus JJ, van den Hout JH, et al. Cerebral white matter lesions, vascular risk factors, and cognitive function in a population-based study: the Rotterdam Study. Neurology. 1994 Jul;44(7):1246–52.

181. de Leeuw F-E. Prevalence of cerebral white matter lesions in elderly people: a population based magnetic resonance imaging study. The Rotterdam Scan Study. J Neurol Neurosurg Psychiatry. 2001 Jan 1;70(1):9–14.

182. Young VG, Halliday GM, Kril JJ. Neuropathologic correlates of white matter hyperintensities. Neurology. 2008 Sep 9;71(11):804–11.

183. Bronge L, Bogdanovic N, Wahlund L-O. Postmortem MRI and histopathology of white matter changes in Alzheimer brains. A quantitative, comparative study. Dement Geriatr Cogn Disord. Karger Publishers; 2002;13(4):205–12.

184. Grafton ST, Sumi SM, Stimac GK, Alvord EC, Shaw CM, Nochlin D. Comparison of postmortem magnetic resonance imaging and neuropathologic findings in the cerebral white matter. Arch Neurol. 1991 Mar;48(3):293–8.

185. Taylor WD, Bae JN, MacFall JR, Payne ME, Provenzale JM, Steffens DC, et al. Widespread Effects of Hyperintense Lesions on Cerebral White Matter Structure. Am J Roentgenol. 2007 Jun;188(6):1695–704.

186. van Norden AGW, de Laat KF, van Dijk EJ, van Uden IWM, van Oudheusden LJB, Gons RAR, et al. Diffusion tensor imaging and cognition in cerebral small vessel disease: The RUN DMC study. Biochim Biophys Acta - Mol Basis Dis.

2012;1822(3):401–7.

187. Debette S, Markus HS. The clinical importance of white matter hyperintensities on brain magnetic resonance imaging: systematic review and meta-analysis. BMJ. 2010;341:c3666.

188. Wen W, Sachdev P. The topography of white matter hyperintensities on brain MRI in healthy 60- to 64-year-old individuals. Neuroimage. 2004;22(1):144–54.

189. Bozzali M. White matter damage in Alzheimer's disease assessed in vivo using diffusion tensor magnetic resonance imaging. J Neurol Neurosurg Psychiatry. 2002 Jun 1;72(6):742–6.

190. Rose SE, McMahon KL, Janke AL, O'Dowd B, de Zubicaray G, Strudwick MW, et al. Diffusion indices on magnetic resonance imaging and neuropsychological performance in amnestic mild cognitive impairment. J Neurol Neurosurg Psychiatry. 2006 Oct 1;77(10):1122–8.

191. Stahl R, Dietrich O, Teipel SJ, Hampel H, Reiser MF, Schoenberg SO. White matter damage in Alzheimer disease and mild cognitive impairment: assessment with diffusion-tensor MR imaging and parallel imaging techniques. Radiology. Radiological Society of North America; 2007 May 1;243(2):483–92.

192. Stricker NH, Schweinsburg BC, Delano-Wood L, Wierenga CE, Bangen KJ, Haaland KY, et al. Decreased white matter integrity in late-myelinating fiber pathways in Alzheimer's disease supports retrogenesis. Neuroimage. 2009 Mar 1;45(1):10–6.

193. Hahn K, Myers N, Prigarin S, Rodenacker K, Kurz A, Förstl H, et al. Selectively and progressively disrupted structural connectivity of functional brain networks in Alzheimer's disease - revealed by a novel framework to analyze edge distributions of

networks detecting disruptions with strong statistical evidence. Neuroimage. 2013 Nov 1;81:96–109.

194. Ringman JM, O'Neill J, Geschwind D, Medina L, Apostolova LG, Rodriguez Y, et al. Diffusion tensor imaging in preclinical and presymptomatic carriers of familial Alzheimer's disease mutations. Brain. 2007 Jul;130(Pt 7):1767–76.

195. Persson J, Lind J, Larsson A, Ingvar M, Cruts M, Van Broeckhoven C, et al. Altered brain white matter integrity in healthy carriers of the APOE epsilon4 allele: a risk for AD? Neurology. 2006 Apr 11;66(7):1029–33.

196. Gold BT, Zhu Z, Brown CA, Andersen AH, LaDu MJ, Tai L, et al. White matter integrity is associated with cerebrospinal fluid markers of Alzheimer's disease in normal adults. Neurobiol Aging. 2014 Oct;35(10):2263–71.

197. Molinuevo JL, Ripolles P, Simó M, Lladó A, Olives J, Balasa M, et al. White matter changes in preclinical Alzheimer's disease: a magnetic resonance imaging-diffusion tensor imaging study on cognitively normal older people with positive amyloid β protein 42 levels. Neurobiol Aging. 2014 Jun 6;

198. Kantarci K, Schwarz CG, Reid RI, Przybelski SA, Lesnick TG, Zuk SM, et al. White matter integrity determined with diffusion tensor imaging in older adults without dementia: influence of amyloid load and neurodegeneration. JAMA Neurol. American Medical Association; 2014 Dec 1;71(12):1547–54.

199. Brown CA, Johnson NF, Anderson-Mooney AJ, Jicha GA, Shaw LM, Trojanowski JQ, et al. Development, validation and application of a new fornix template for studies of aging and preclinical Alzheimer's disease. NeuroImage Clin. 2017;13:106–15.

200. Horiuchi M, Maezawa I, Itoh A, Wakayama K, Jin LW, Itoh T, et al. Amyloid ??1-42

oligomer inhibits myelin sheet formation in vitro. Neurobiol Aging. NIH Public Access; 2012 Mar;33(3):499–509.

201. Xu J, Chen S, Ahmed SH, Chen H, Ku G, Goldberg MP, et al. Amyloid-beta peptides are cytotoxic to oligodendrocytes. J Neurosci. 2001 Jan 1;21(1):RC118.

202. Alonso AC, Zaidi T, Grundke-Iqbal I, Iqbal K. Role of abnormally phosphorylated tau in the breakdown of microtubules in Alzheimer disease. Proc Natl Acad Sci U S A. 1994 Jun 7;91(12):5562–6.

203. Vossel KA, Zhang K, Brodbeck J, Daub AC, Sharma P, Finkbeiner S, et al. Tau reduction prevents Abeta-induced defects in axonal transport. Science (80-). 2010;330(6001):198.

204. DeKosky ST, Scheff SW. Synapse loss in frontal cortex biopsies in Alzheimer's disease: Correlation with cognitive severity. Ann Neurol. 1990 May;27(5):457–64.

205. Davies CA, Mann DMA, Sumpter PQ, Yates PO. A quantitative morphometric analysis of the neuronal and synaptic content of the frontal and temporal cortex in patients with Alzheimer's disease. J Neurol Sci. 1987 Apr;78(2):151–64.

206. Hayes AF. Beyond Baron and Kenny: Statistical Mediation Analysis in the New Millennium. Commun Monogr. Taylor & Francis Group ; 2009 Dec;76(4):408–20.

207. Hayes AF. An introduction to mediation, moderation, and conditional process analysis: A regression-based approach. 3rd ed. New York, NY: Guilford Press; 2013.

208. Baron RM, Kenny DA. The moderator–mediator variable distinction in social psychological research: Conceptual, strategic, and statistical considerations. J Pers Soc Psychol. American Psychological Association; 1986;51(6):1173–82.

209. Preacher KJ, Hayes AF. SPSS and SAS procedures for estimating indirect effects in

simple mediation models. Behav Res Methods, Instruments, Comput. Springer-Verlag; 2004 Nov;36(4):717–31.

210.   Salthouse TA. Neuroanatomical substrates of age-related cognitive decline. Psychol Bull. 2011 Sep;137(5):753–84.

211.   Andrews-Hanna JR, Snyder AZ, Vincent JL, Lustig C, Head D, Raichle ME, et al. Disruption of large-scale brain systems in advanced aging. Neuron. 2007 Dec 6;56(5):924–35.

212.   Vidal-Piñeiro D, Valls-Pedret C, Fernández-Cabello S, Arenaza-Urquijo EM, Sala-Llonch R, Solana E, et al. Decreased Default Mode Network connectivity correlates with age-associated structural and cognitive changes. Front Aging Neurosci. 2014 Jan;6:256.

213.   van Oort ESB, van Cappellen van Walsum AM, Norris DG. An investigation into the functional and structural connectivity of the Default Mode Network. Neuroimage. 2014 Apr 15;90:381–9.

214.   Madden DJ, Spaniol J, Whiting WL, Bucur B, Provenzale JM, Cabeza R, et al. Adult age differences in the functional neuroanatomy of visual attention: a combined fMRI and DTI study. Neurobiol Aging. 2007 Mar;28(3):459–76.

215.   Persson J, Nyberg L, Lind J, Larsson A, Nilsson L-G, Ingvar M, et al. Structure-function correlates of cognitive decline in aging. Cereb Cortex. 2006 Jul 1;16(7):907–15.

216.   Hakun JG, Zhu Z, Brown CA, Johnson NF, Gold BT. Longitudinal alterations to brain function, structure, and cognitive performance in healthy older adults: A fMRI-DTI study. Neuropsychologia. 2015 Apr;71:225–35.

217. Kramer AF, Hahn S, Gopher D. Task coordination and aging: explorations of executive control processes in the task switching paradigm. Acta Psychol (Amst). 1999 Apr;101(2–3):339–78.

218. Cattell RB, Cattell AKS. Handbook for the individual or group culture fair intelligence test. Savoy, IL: Institute for Personality and Ability Testing. 1960.

219. Wechsler D. Wechsler Memory Scale (WMS-III). Psychological corporation; 1997.

220. Hollingshead AB. Two factor index of social position. Unpubl manuscript, Yale Univ New Haven, CT. 1957;

221. Smith SM, Jenkinson M, Woolrich MW, Beckmann CF, Behrens TEJ, Johansen-Berg H, et al. Advances in functional and structural MR image analysis and implementation as FSL. Neuroimage. 2004 Jan;23 Suppl 1:S208-19.

222. Greve DN, Fischl B. Accurate and robust brain image alignment using boundary-based registration. Neuroimage. 2009 Oct 15;48(1):63–72.

223. Andersson J, Jenkinson M, Smith S. Non-linear registration, aka spatial normalisation. FRMIB technical report. 2010.

224. Smith SM, Jenkinson M, Johansen-Berg H, Rueckert D, Nichols TE, Mackay CE, et al. Tract-based spatial statistics: voxelwise analysis of multi-subject diffusion data. Neuroimage. 2006 Jul 15;31(4):1487–505.

225. Johnson NF, Kim C, Clasey JL, Bailey A, Gold BT. Cardiorespiratory fitness is positively correlated with cerebral white matter integrity in healthy seniors. Neuroimage. 2012 Jan 16;59(2):1514–23.

226. Behrens TEJ, Woolrich MW, Jenkinson M, Johansen-Berg H, Nunes RG, Clare S, et al. Characterization and propagation of uncertainty in diffusion-weighted MR imaging.

Magn Reson Med. 2003 Nov;50(5):1077–88.

227. Behrens TEJ, Berg HJ, Jbabdi S, Rushworth MFS, Woolrich MW. Probabilistic diffusion tractography with multiple fibre orientations: What can we gain? Neuroimage. 2007 Jan 1;34(1):144–55.

228. Hakun JG, Zhu Z, Johnson NF, Gold BT. Evidence for reduced efficiency and successful compensation in older adults during task switching. Cortex. 2015 Mar;64:352–62.

229. Persson J, Pudas S, Nilsson L-G, Nyberg L. Longitudinal assessment of default-mode brain function in aging. Neurobiol Aging. 2014 Sep;35(9):2107–17.

230. Cepeda NJ, Kramer AF, Gonzalez de Sather JCM. Changes in executive control across the life span: Examination of task-switching performance. Dev Psychol. American Psychological Association; 2001 Sep 1;37(5):715–30.

231. Weiler M, de Campos BM, Nogueira MH, Pereira Damasceno B, Cendes F, Balthazar MLF. Structural connectivity of the default mode network and cognition in Alzheimer's disease. Psychiatry Res. 2014 Jul 30;223(1):15–22.

232. Healey MK, Hasher L, Campbell KL. The role of suppression in resolving interference: evidence for an age-related deficit. Psychol Aging. 2013 Sep;28(3):721–8.

233. Celone KA, Calhoun VD, Dickerson BC, Atri A, Chua EF, Miller SL, et al. Alterations in memory networks in mild cognitive impairment and Alzheimer's disease: an independent component analysis. J Neurosci. 2006 Oct 4;26(40):10222–31.

234. Hu Y, Chen X, Gu H, Yang Y. Resting-state glutamate and GABA concentrations predict task-induced deactivation in the default mode network. J Neurosci. 2013 Nov 20;33(47):18566–73.

235. He Y, Wang L, Zang Y, Tian L, Zhang X, Li K, et al. Regional coherence changes in the early stages of Alzheimer's disease: a combined structural and resting-state functional MRI study. Neuroimage. 2007 Apr 1;35(2):488–500.

236. Jagust W. Vulnerable Neural Systems and the Borderland of Brain Aging and Neurodegeneration. Neuron. 2013;77(2):219–34.

237. Andreasen N, Blennow K. β-Amyloid (Aβ) protein in cerebrospinal fluid as a biomarker for Alzheimer's disease. Peptides. 2002 Jul;23(7):1205–14.

238. Huijbers W, Mormino EC, Schultz AP, Wigman S, Ward AM, Larvie M, et al. Amyloid-β deposition in mild cognitive impairment is associated with increased hippocampal activity, atrophy and clinical progression. Brain. 2015 Feb 11;138(4):1023–35.

239. Mayda AB V, Westphal A, Carter CS, Decarli C. Late life cognitive control deficits are accentuated by white matter disease burden. Brain. Oxford University Press; 2011 Jun;134(6):1673–83.

240. Hedden T, Van Dijk KRA, Shire EH, Sperling RA, Johnson KA, Buckner RL. Failure to modulate attentional control in advanced aging linked to white matter pathology. Cereb Cortex. Oxford University Press; 2012 May;22(5):1038–51.

241. Le Bihan D, Mangin JF, Poupon C, Clark C a, Pappata S, Molko N, et al. Diffusion tensor imaging: concepts and applications. J Magn Reson Imaging. 2001 Apr;13(4):534–46.

242. Brown C a., Hakun JG, Zhu Z, Johnson NF, Gold BT. White matter microstructure contributes to age-related declines in task-induced deactivation of the default mode network. Front Aging Neurosci. 2015;7.

243. Weiler M, Teixeira CVL, Nogueira MH, de Campos BM, Damasceno BP, Cendes F, et

al. Differences and the relationship in default mode network intrinsic activity and functional connectivity in mild Alzheimer's disease and amnestic mild cognitive impairment. Brain Connect. 2014 Oct;4(8):567–74.

244.   Kane MJ, Engle RW. The role of prefrontal cortex in working-memory capacity, executive attention, and general fluid intelligence: An individual-differences perspective. Psychon Bull Rev. 2002 Dec;9(4):637–71.

245.   Jiang Y. Complementary Neural Mechanisms for Tracking Items in Human Working Memory. Science (80-). American Association for the Advancement of Science; 2000 Jan 28;287(5453):643–6.

246.   Schmitt FA, Nelson PT, Abner E, Scheff S, Jicha GA, Smith C, et al. University of Kentucky Sanders-Brown healthy brain aging volunteers: donor characteristics, procedures and neuropathology. Curr Alzheimer Res. 2012 Jul;9(6):724–33.

247.   Morris JC, Weintraub S, Chui HC, Cummings J, Decarli C, Ferris S, et al. The Uniform Data Set (UDS): clinical and cognitive variables and descriptive data from Alzheimer Disease Centers. Alzheimer Dis Assoc Disord. Jan;20(4):210–6.

248.   Snodgrass JG, Vanderwart M. A standardized set of 260 pictures: norms for name agreement, image agreement, familiarity, and visual complexity. J Exp Psychol Hum Learn. 1980 Mar;6(2):174–215.

249.   Jenkinson M, Beckmann CF, Behrens TEJ, Woolrich MW, Smith SM. FSL. Neuroimage. 2012 Aug 15;62(2):782–90.

250.   Zhang Y, Brady M, Smith S. Segmentation of brain MR images through a hidden Markov random field model and the expectation-maximization algorithm. IEEE Trans Med Imaging. 2001;20(1):45–57.

251.   Smith SM. Fast robust automated brain extraction. Hum Brain Mapp. 2002
        Nov;17(3):143–55.

252.   Jenkinson M, Bannister P, Brady M, Smith S. Improved optimization for the robust
        and accurate linear registration and motion correction of brain images. Neuroimage.
        2002 Oct;17(2):825–41.

253.   Power JD, Barnes KA, Snyder AZ, Schlaggar BL, Petersen SE. Spurious but
        systematic correlations in functional connectivity MRI networks arise from subject
        motion. Neuroimage. 2012 Feb 1;59(3):2142–54.

254.   Beckmann CF, DeLuca M, Devlin JT, Smith SM. Investigations into resting-state
        connectivity using independent component analysis. Philos Trans R Soc Lond B Biol
        Sci. 2005 May 29;360(1457):1001–13.

255.   Andersson JLR, Sotiropoulos SN. An integrated approach to correction for off-
        resonance effects and subject movement in diffusion MR imaging. Neuroimage.
        2016;125:1063–78.

256.   Andersson JLR, Graham MS, Zsoldos E, Sotiropoulos SN. Incorporating outlier
        detection and replacement into a non-parametric framework for movement and
        distortion correction of diffusion MR images. Neuroimage. 2016;141:556–72.

257.   Smith CD, Johnson ES, Van Eldik LJ, Jicha GA, Schmitt FA, Nelson PT, et al.
        Peripheral (deep) but not periventricular MRI white matter hyperintensities are
        increased in clinical vascular dementia compared to Alzheimer's disease. Brain
        Behav. Wiley-Blackwell; 2016 Mar;6(3):e00438.

258.   Fischl B, Salat DH, Busa E, Albert M, Dieterich M, Haselgrove C, et al. Whole Brain
        Segmentation: Automated Labeling of Neuroanatomical Structures in the Human

Brain. Neuron. 2002;33(3):341–55.

259. Dale AM, Fischl B, Sereno MI. Cortical Surface-Based Analysis: I. Segmentation and Surface Reconstruction. Neuroimage. 1999;9(2):179–94.

260. Bartzokis G. Alzheimer's disease as homeostatic responses to age-related myelin breakdown. Neurobiol Aging. 2011 Aug;32(8):1341–71.

261. Barnes CA, McNaughton BL. Physiological compensation for loss of afferent synapses in rat hippocampal granule cells during senescence. J Physiol. 1980 Dec 1;309(1):473–85.

262. Sachdev P, Wen W, Chen X, Brodaty H. Progression of white matter hyperintensities in elderly individuals over 3 years. Neurology. Lippincott Williams & Wilkins; 2007 Jan 16;68(3):214–22.

263. van Norden AGW, de Laat KF, van Dijk EJ, van Uden IWM, van Oudheusden LJB, Gons RAR, et al. Diffusion tensor imaging and cognition in cerebral small vessel disease. Biochim Biophys Acta - Mol Basis Dis. 2012 Mar;1822(3):401–7.

264. Peters A. The effects of normal aging on myelin and nerve fibers: A review. J Neurocytol. Kluwer Academic Publishers; 2002;31(8/9):581–93.

265. Peters A, Sethares C. Is there remyelination during aging of the primate central nervous system? J Comp Neurol. Wiley Subscription Services, Inc., A Wiley Company; 2003 May 26;460(2):238–54.

266. Peters A, Sethares C. Oligodendrocytes, their Progenitors and other Neuroglial Cells in the Aging Primate Cerebral Cortex. Cereb Cortex. Oxford University Press; 2004 Apr 27;14(9):995–1007.

267. Petty MA, Wettstein JG. White matter ischaemia. Brain Res Rev. 1999;31(1):58–64.

268. Pantoni L, Garcia JH. Pathogenesis of Leukoaraiosis A Review. Stroke. 1997;28(3):652–9.

269. JUURLINK BHJ. Response of Glial Cells to Ischemia: Roles of Reactive Oxygen Species and Glutathione. Neurosci Biobehav Rev. 1997;21(2):151–66.

270. Husain J, Juurlink BHJ. Oligodendroglial precursor cell susceptibility to hypoxia is related to poor ability to cope with reactive oxygen species. Brain Res. 1995;698(1–2):86–94.

271. Masliah E, Mallory M, Hansen L, DeTeresa R, Terry RD. Quantitative synaptic alterations in the human neocortex during normal aging. Neurology. 1993 Jan 1;43(1, Part 1):192–192.

272. Lee JT, Xu J, Lee JM, Ku G, Han X, Yang DI, et al. Amyloid-?? peptide induces oligodendrocyte death by activating the neutral sphingomyelinase-ceramide pathway. J Cell Biol. 2004;164(1):123–31.

273. Roher AE, Weiss N, Kokjohn TA, Kuo Y-M, Kalback W, Anthony J, et al. Increased A beta peptides and reduced cholesterol and myelin proteins characterize white matter degeneration in Alzheimer's disease. Biochemistry. 2002 Sep 17;41(37):11080–90.

274. Xia W, Yang T, Shankar G, Smith IM, Shen Y, Walsh DM, et al. A specific enzyme-linked immunosorbent assay for measuring beta-amyloid protein oligomers in human plasma and brain tissue of patients with Alzheimer disease. Arch Neurol. BioMed Central; 2009 Feb 1;66(2):190–9.

275. Vossel KA, Xu JC, Fomenko V, Miyamoto T, Suberbielle E, Knox JA, et al. Tau reduction prevents Aβ-induced axonal transport deficits by blocking activation of GSK3β. J Cell Biol. 2015;209(3):419–33.

276. Cirrito JR, Yamada KA, Finn MB, Sloviter RS, Bales KR, May PC, et al. Synaptic activity regulates interstitial fluid amyloid-beta levels in vivo. Neuron. 2005 Dec 22;48(6):913–22.

277. Bero AW, Yan P, Roh JH, Cirrito JR, Stewart FR, Raichle ME, et al. Neuronal activity regulates the regional vulnerability to amyloid-β deposition. Nat Neurosci. NIH Public Access; 2011 Jun;14(6):750–6.

278. Kryscio RJ, Abner EL, Jicha GA, Nelson PT, Smith CD, Van Eldik LJ, et al. Self-reported memory complaints: a comparison of demented and unimpaired outcomes. J Prev Alzheimer's Dis. 2016 Mar 1;

279. Beckman CF, Smith SM. Probabilistic independent component analysis for function magnetic resonance imaging. IEEE Trans Med Imaging. 2004;23:137–52.

280. Charlton RA, Schiavone F, Barrick TR, Morris RG, Markus HS. Diffusion tensor imaging detects age related white matter change over a 2 year follow-up which is associated with working memory decline. J Neurol Neurosurg Psychiatry. BMJ Publishing Group Ltd; 2010 Jan;81(1):13–9.

281. Ritchie SJ, Bastin ME, Tucker-Drob EM, Maniega SM, Engelhardt LE, Cox SR, et al. Coupled Changes in Brain White Matter Microstructure and Fluid Intelligence in Later Life. J Neurosci. 2015 Jun 3;35(22):8672–82.

282. Barulli D, Stern Y. Efficiency, capacity, compensation, maintenance, plasticity: emerging concepts in cognitive reserve. Trends Cogn Sci. 2013 Oct;17(10):502–9.

283. Cabeza R, Daselaar SM, Dolcos F, Prince SE, Budde M, Nyberg L. Task-independent and task-specific age effects on brain activity during working memory, visual attention and episodic retrieval. Cereb Cortex. 2004 Apr;14(4):364–75.

284. Madden DJ, Turkington TG, Provenzale JM, Denny LL, Hawk TC, Gottlob LR, et al. Adult age differences in the functional neuroanatomy of verbal recognition memory. Hum Brain Mapp. 1999;7(2):115–35.

285. Cabeza R. Hemispheric asymmetry reduction in older adults: the HAROLD model. Psychol Aging. 2002 Mar;17(1):85–100.

286. Reuter-Lorenz PA, Cappell KA. Neurocognitive Aging and the Compensation Hypothesis. Curr Dir Psychol Sci. 2008 Jun 1;17(3):177–82.

287. Rypma B, Berger JS, Genova HM, Rebbechi D, D'Esposito M. Dissociating Age-related Changes in Cognitive Strategy and Neural Efficiency Using Event- related fMRI. Cortex. 2005;41(4):582–94.

288. Oh H, Steffener J, Razlighi QR, Habeck C, Liu D, Gazes Y, et al. Aβ-related hyperactivation in frontoparietal control regions in cognitively normal elderly. Neurobiol Aging. 2015 Dec;36(12):3247–54.

289. Xu J, Chen S, Ahmed SH, Chen H, Ku G, Goldberg MP, et al. Amyloid-β Peptides Are Cytotoxic to Oligodendrocytes. J Neurosci. 2001;21(1).

290. Nitsch RM, Farber SA, Growdon JH, Wurtman RJ. Release of amyloid beta-protein precursor derivatives by electrical depolarization of rat hippocampal slices. Proc Natl Acad Sci. 1993 Jun 1;90(11):5191–3.

291. Vaishnavi SN, Vlassenko AG, Rundle MM, Snyder AZ, Mintun MA, Raichle ME. Regional aerobic glycolysis in the human brain. Proc Natl Acad Sci U S A. National Academy of Sciences; 2010 Oct 12;107(41):17757–62.

292. Reiman EM, Caselli RJ, Yun LS, Chen K, Bandy D, Minoshima S, et al. Preclinical Evidence of Alzheimer's Disease in Persons Homozygous for the ε4 Allele for

Apolipoprotein E. N Engl J Med. Massachusetts Medical Society ; 1996 Mar;334(12):752–8.

293. Reiman EM, Chen K, Alexander GE, Caselli RJ, Bandy D, Osborne D, et al. Functional brain abnormalities in young adults at genetic risk for late-onset Alzheimer's dementia. Proc Natl Acad Sci U S A. 2004 Jan 6;101(1):284–9.

294. Oh H, Madison C, Baker S, Rabinovici G, Jagust W. Dynamic relationships between age, amyloid-β deposition, and glucose metabolism link to the regional vulnerability to Alzheimer's disease. Brain. 2016 May 13;aww108-.

295. Oh H, Habeck C, Madison C, Jagust W. Covarying alterations in Aβ deposition, glucose metabolism, and gray matter volume in cognitively normal elderly. Hum Brain Mapp. 2014 Jan;35(1):297–308.

296. Benzinger TLS, Blazey T, Jack CR, Koeppe RA, Su Y, Xiong C, et al. Regional variability of imaging biomarkers in autosomal dominant Alzheimer's disease. Proc Natl Acad Sci U S A. National Academy of Sciences; 2013 Nov;110(47):E4502-9.

297. Ng KP, Pascoal TA, Mathotaarachchi S, Chung C-O, Benedet AL, Shin M, et al. Neuropsychiatric symptoms predict hypometabolism in preclinical Alzheimer disease. Neurology. Lippincott Williams & Wilkins; 2017 May 9;88(19):1814–21.

298. Vannini P, Hanseeuw B, Munro CE, Amariglio RE, Marshall GA, Rentz DM, et al. Hippocampal hypometabolism in older adults with memory complaints and increased amyloid burden. Neurology. Lippincott Williams & Wilkins; 2017 May 2;88(18):1759–67.

299. Salloway S, Sperling R, Gilman S, Fox NC, Blennow K, Raskind M, et al. A phase 2 multiple ascending dose trial of bapineuzumab in mild to moderate Alzheimer

disease. Neurology. 2009 Dec 15;73(24):2061–70.

300. Sevigny J, Chiao P, Bussière T, Weinreb PH, Williams L, Maier M, et al. The antibody aducanumab reduces Aβ plaques in Alzheimer's disease. Nature. 2016 Aug 31;537(7618):50–6.

301. Doody RS, Thomas RG, Farlow M, Iwatsubo T, Vellas B, Joffe S, et al. Phase 3 Trials of Solanezumab for Mild-to-Moderate Alzheimer's Disease. N Engl J Med. Massachusetts Medical Society; 2014 Jan 23;370(4):311–21.

302. Jack CR, Knopman DS, Jagust WJ, Shaw LM, Aisen PS, Weiner MW, et al. Hypothetical model of dynamic biomarkers of the Alzheimer's pathological cascade. Lancet Neurol. 2010 Jan;9(1):119–28.

303. Abner EL, Kryscio RJ, Schmitt FA, Fardo DW, Moga DC, Ighodaro ET, et al. Outcomes after diagnosis of mild cognitive impairment in a large autopsy series. Ann Neurol. 2017 Feb;

304. Greicius MD, Srivastava G, Reiss AL, Menon V. Default-mode network activity distinguishes Alzheimer's disease from healthy aging: evidence from functional MRI. Proc Natl Acad Sci U S A. 2004 Mar 30;101(13):4637–42.

305. Jones DT, Knopman DS, Gunter JL, Graff-Radford J, Vemuri P, Boeve BF, et al. Cascading network failure across the Alzheimer's disease spectrum. Brain. 2015 Nov 19;139(Pt 2):547–62.

306. Herholz K, Salmon E, Perani D, Baron J-C, Holthoff V, Frölich L, et al. Discrimination between Alzheimer Dementia and Controls by Automated Analysis of Multicenter FDG PET. Neuroimage. 2002;17(1):302–16.

<u>**Vita**</u>

Christopher Alan Brown

Education

Graduate Studies

MD/PhD program at the University of Kentucky College of Medicine, Lexington, KY; August 2012-Present

USMLE Step 1 (June 2014): 250

Baccalaureate Studies

Washington University in St. Louis; St. Louis, MO; August 2007- May 2011
Majors: Biology & Philosophy-Neuroscience-Psychology (BA with Research Emphasis)

Senior Thesis: Validity of a Novel Non-Motor Symptom Scale and [C11]-DTBZ PET-based Measures as Tools for Tracking Disease Severity in MPTP Primates
Academic Awards
Dean's List (Fall 2007, Fall 2009-Spring 2011)
Missouri Boy's State Academic Scholarship (2007-2011)

Research Experience:
Graduate Research Assistant, July 2014-Present
Dr. Brian Gold, Department of Neuroscience, University of Kentucky College of Medicine

Summer Research Fellow, June 2013-July 2013
Dr. Brian Gold, Department of Neuroscience, University of Kentucky College of Medicine

Summer Research Fellow, July 2012
Dr. Luke Bradley, Department of Neuroscience, University of Kentucky College of Medicine

Research Technician II, July 2011-June 2012
Dr. Joel Perlmutter, Department of Neurology, Washington University School of Medicine

Undergraduate Research Student, June 2008-May 2011
Dr. Joel Perlmutter, Department of Neurology, Washington University School of Medicine

Professional Positions:
University of Kentucky MD/PhD Program Internal Advisory Committee, July 2014-May 2017
Teaching Assistant, Principles of Human Anatomy (ANA 209), Department of Anatomy and Neurobiology, University of Kentucky, Fall 2015 & Spring 2016 Semesters

Awards and Honors:
Parkinson's Disease Foundation Summer Undergraduate Fellow, 2008

Summer Undergraduate Research Fellow funded by HHMI, 2010
ASCI/AAP Joint Meeting Travel Award, April 2015
University of Kentucky CCTS Predoctoral Fellowship, NCATS TL1TR00015, May 2015-May 2017
Burroughs-Wellcome Fund Travel Award, April 2017

Memberships in Professional Societies:
American Medical Association
American Physician Scientist Association
Society for Neuroscience
American Academy of Neurology

Scientific Publications:

Brown CA, Johnson NF, Anderson-Mooney AJ, Jicha GA, Shaw LM, Trojanowski JQ, Van Eldik LJ, Schmitt FA, Smith CD, Gold BT. Development, validation and application of a new fornix template for studies of aging and preclinical Alzheimer's disease. NeuroImage Clin. 2017;13:106–115.

Brown CA, Hakun JG, Zhu Z, Johnson NF, Gold BT. White matter microstructure contributes to age-related declines in task-induced deactivation of the default mode network. Front Aging Neurosci. 2015;7. PMID: 26500549

Hakun JG, Zhu Z, **Brown CA**, Johnson NF, Gold BT. Longitudinal alterations to brain function, structure, and cognitive performance in healthy older adults: A fMRI-DTI study. Neuropsychologia. 2015 Apr;71:225–235. PMID: 25862416

Gold BT, Zhu Z, **Brown CA**, Andersen AH, LaDu MJ, Tai L, Jicha GA, Kryscio RJ, Estus S, Nelson PT, Scheff SW, Abner E, Schmitt FA, Van Eldik LJ, Smith CD. White matter integrity is associated with cerebrospinal fluid markers of Alzheimer's disease in normal adults. Neurobiol Aging. 2014 Oct;35(10):2263–71. PMID: 24866404

Dugan LL, Tian L, Quick KL, Hardt JI, Karimi M, **Brown C**, Loftin S, Flores H, Moerlein SM, Polich J, Tabbal SD, Mink JW, Perlmutter JS. Carboxyfullerene neuroprotection postinjury in Parkinsonian nonhuman primates. Ann Neurol. 2014 Jul 8; PMID: 25043598

Tian L, Karimi M, **Brown CA**, Loftin SK, Perlmutter JS. In vivo measures of nigrostriatal neuronal response to unilateral MPTP treatment. Brain Res. 2014 Jul 7;1571:49–60. PMID: 24845719

Brown CA, Karimi MK, Tian L, Flores H, Su Y, Tabbal SD, Loftin SK, Moerlein SM, Perlmutter JS. Validation of midbrain positron emission tomography measures for nigrostriatal neurons in macaques. Ann Neurol. 2013 Oct;74(4):602–10. PMID: 23686841

Karimi M, Tian L, **Brown CA**, Flores HP, Loftin SK, Videen TO, Moerlein SM, Perlmutter JS. Validation of nigrostriatal positron emission tomography measures: critical limits. Ann Neurol. 2013 Mar;73(3):390–6. PMID: 23423933

Tabbal SD, Tian L, Karimi M, **Brown CA**, Loftin SK, Perlmutter JS. Low nigrostriatal reserve for motor parkinsonism in nonhuman primates. Exp Neurol. 2012 Oct;237(2):355–62. PMID: 22836146

Brown CA, Campbell MC, Karimi M, Tabbal SD, Loftin SK, Tian LL, Moerlein SM, Perlmutter JS. Dopamine pathway loss in nucleus accumbens and ventral tegmental area predicts apathetic behavior in MPTP-lesioned monkeys. Exp Neurol. Elsevier Inc.; 2012 Jul;236(1):190–7. PMID: 22579525

Tian L, Karimi M, Loftin SK, **Brown CA**, Xia H, Xu J, Mach RH, Perlmutter JS. No differential regulation of dopamine transporter (DAT) and vesicular monoamine transporter 2 (VMAT2) binding in a primate model of Parkinson disease. Ulrich H, editor. PLoS One. Public Library of Science; 2012 Jan;7(2):e31439. PMID: 22359591

Conference Abstracts and Presentations:

Brown CA; Smith CD; Schmitt FA; Gold BT. White matter microstructure in the DMN mediates the effects of aging, Alzheimer's, and cerebrovascular pathology on executive function. Poster presented at American Academy of Neurology 69th Annual Meeting; 2017 April 24; Boston, MA

Brown CA; Smith CD; Schmitt FA; Gold BT. White matter microstructure in the DMN mediates the effects of aging, Alzheimer's, and cerebrovascular pathology on executive function. Poster presented at Translational Science 2017. 2017 April 20; Washington D.C.

Brown CA; Smith CD; Schmitt FA; Gold BT. White matter microstructure mediates the negative effects of amyloid on DMN function and executive performance. Poster session presented at Human Cognition: Aging II. Society for Neuroscience 2016 Annual Meeting; 2016 November 15; San Diego, CA

Brown CA; Smith CD; Schmitt FA; Gold BT. The effects of preclinical AD pathology on default-mode function and executive performance are mediated by declining white matter microstructure. Oral Presentation presented at CCTS Scholars Presentations: 2016 Annual Center for Clinical and Translational Science Spring Conference; 2016 April 20; Lexington, KY

Brown, CA; Anderson-Mooney, AJ; Jicha, GA; Schmitt, FA; Van Eldik, L; Smith, CD; Gold, BT. White matter microstructure in a tractography-derived fornix template is associated with neuropathological markers of Alzheimer's disease. Poster session presented at: Trainnee Poster Session. Translational Science 2016. 2016 April 14; Washington D.C.

Brown, CA; Anderson-Mooney, AJ; Jicha, GA; Schmitt, FA; Van Eldik, L; Smith, CD; Gold, BT. White matter microstructure in a tractography-derived fornix template is associated with neuropathological markers of Alzheimer's disease. Poster session presented at: Alzheimer's Disease: Clinical Detection and Biomarkers. Society for Neuroscience 2015 Annual Meeting; 2015 October 21; Chicago, IL

Brown, CA; Hakun, JG; Zhu, Z; Johnson, NF; Gold, BT. White matter microstructure contributes to age-related changes in default-mode network deactivation Poster

session presented at: APSA poster session. 2015 ASCI/AAP Joint Meeting; 2015 April 24-26; Chicago, IL

Perlmutter, JS; Tian LL; Quick K; Hardt J; Karimi M; **Brown CA**; Moerlein SM; Polich, J; Mink, JW; Dugan, LL. Carboxyfullerene rescue of MPTP-induced nigrostriatal injury in non-human primates. Mov. Disord. 2014 May; 29:S259.

Perlmutter, JS; **Brown, CA**; Karimi, MK; Flores, H; Su, Y; Tabbal, SD; Loftin, S; Moerlein, SM. Validation of PET measures of midbrain uptake of VMAT2 & DAT tracers for nigrostriatal neurons. Mov. Disord. 2013 June; 28: S51.

Karimi, MK; Tian LL; Brown, CA; Flores HB; Loftin, SK; Videen, TO; Moerlein, SM; Perlmutter, JS. Comparison of In Vivo PET with In Vitro Measures of Pre-Synaptic Nigrostriatal Neurons. Annals Neurol. 2012 Jan; 72:S98-S99.

Brown CA; Perlmutter JS. Validity of a Novel Non-Motor Symptom Scale and [C11]-DTBZ Pet-based Measures as Tools for Tracking Disease Severity in MPTP Primates. Poster presented at Mid-states Math & Science Consortium Undergraduate Research Symposium. 2010 November 7; Chicago, IL